INFORMATION TO USERS

This manuscript has been reproduced from the microfilm master. UMI films the text directly from the original or copy submitted. Thus, some thesis and dissertation copies are in typewriter face, while others may be from any type of computer printer.

The quality of this reproduction is dependent upon the quality of the copy submitted. Broken or indistinct print, colored or poor quality illustrations and photographs, print bleedthrough, substandard margins, and improper alignment can adversely affect reproduction.

In the unlikely event that the author did not send UMI a complete manuscript and there are missing pages, these will be noted. Also, if unauthorized copyright material had to be removed, a note will indicate the deletion.

Oversize materials (e.g., maps, drawings, charts) are reproduced by sectioning the original, beginning at the upper left-hand corner and continuing from left to right in equal sections with small overlaps.

Photographs included in the original manuscript have been reproduced xerographically in this copy. Higher quality 6" x 9" black and white photographic prints are available for any photographs or illustrations appearing in this copy for an additional charge. Contact UMI directly to order.

ProQuest Information and Learning
300 North Zeeb Road, Ann Arbor, MI 48106-1346 USA
800-521-0600

Effect of Intermetallic Phases on Corrosion of Aluminum-Silicon Carbide (Al-SiC_p) Composites

BY

Adeyinka Hakeem Adeleke

A Thesis Presented to the

DEANSHIP OF GRADUATE STUDIES

KING FAHD UNIVERSITY OF PETROLEUM & MINERALS

DHAHRAN, SAUDI ARABIA

In Partial Fulfillment of the
Requirements for the Degree of

MASTER OF SCIENCE

In

MECHANICAL ENGINEERING

January, 2001

UMI Number: 1406103

UMI Microform 1406103

Bell & Howell Information and Learning Company
300 North Zeeb Road
P.O. Box 1346
Ann Arbor, MI 48106-1346

KING FAHD UNIVERSITY OF PETROLEUM AND MINERALS

DHAHAN 31261, SAUDI ARABIA

DEANSHIP OF GRADUATE STUDIES

This thesis, written by **ADEYINKA HAKEEM ADELEKE** under the direction of his Thesis Advisor and approved by his Committee, has been presented to and accepted by the Dean of Graduate Studies, in partial fulfillment of the requirements for the degree of **MASTER OF SCIENCE DEGREE IN MECHANICAL ENGINEERING.**

Thesis Committee

Dr. Zaki Ahmad (Thesis Advisor)

Dr. Ibrahim Allam (Member)

Dr. Zuhair Gassem (Member)

Dr. Anwar Hamid (Member)

Mr. Abdul Aleem B.J (Member)

Department Chairman

Dean of Graduate Studies

28 / 5 / 2001

Date

عمادة الدراسات العليا
DEANSHIP OF GRADUATE STUDIES

ACKNOWLEDGEMENTS

First and foremost, all praises and thanks are to Allah, *subhanahu-wa-ta'ala*, the Almighty, the Lord of *Alamin* (mankind, jinn, and all that exists), who gave me an opportunity, courage and patience to carry out this work. I feel privilege to glorify His name in the sincerest way through this small accomplishment. I seek His mercy, favor, and forgiveness. And I ask Him to accept my little effort. May He, *subhanahuwa-ta-Aaala*, guide us and the whole humanity to the right path (Aameen).

Acknowledgement is due to King Fahd University of Petroleum & Minerals for providing support to this research work.

I wish to express my profound gratitude to my advisor, Dr. Zaki Ahmad for his cooperation, advice, support and encouragement throughout the entire period of my M.Sc program at King Fahd University of Petroleum & Minerals,Saudi Arabia . Working with him was indeed a learning experience. My appreciation also goes to other member of my thesis Committee, Dr. Ibrahim Allam, Dr. Zuhair Gaseem, Dr. Anwarul Hamid and Mr. Abdul Aleem B.J for their deep interest, constructive criticism and stimulating discussions during the course of this work.

The valuable assistance rendered by Corrosion & Materials Lab Engineers, Mr. Abbas Saleh, Mr. Reyaz and Mr. Lateef, is highly appreciated. I also wish to express my thanks to Prof. C.A Loto of Research Institute, for his fatherly assistance, support and sincere criticism in putting me through any professional difficulties. The help provided by Mr. Rasheed, also of Research Institute, is highly appreciated. I thank each and everyone of them for their indefatigable assistance and immeasurable contribution toward the success of my research work.

I am thankful to the department chairman, Dr. Abdulghani Al-Farayedhi and other faculty members for their cooperation.

I am thankful to my fellow graduate students and all my friends on campus especially Dr. Kamorudeen Abidogun, Sirajudeen Adedotun Adewusi, AbdulLameed Olabode Babalola, Abdul-Kareem Modupe Melaiye, Taofeek Ayinde, Iyanda Sulyman, Lekan Fawumi, Shaibu Abdul-Basit, Adamu Bashir, Ruchan Yin, Salman Oloriegbe, Taofeek Abiola, Yunus Umar, Jimoh Tijani, Danjuma, Rasheed Gidado, Alpha Bangura, Saliu Moshood, Rufai Raheem , Muazu, Saidu & others and to my friends abroad Adediran Aderinkomi, Adetayo Adedokun, Oyewole Ogunnaike and Jide Akinlade. They all provided a wonderful company. I am also thankful to the following families: Adejumo (Lagos), Oladejo (Lagos), Oloyedes, Adedokun, Raji and Aderinkomi,

Last but not the least, thanks are due to the members of my family for their emotional and moral support throughout my academic career. No personal development could ever take place without the proper guidance of parents. They taught me the fundamental concept of life. There is popular adage that says "tough times never last, but tough people do". I acknowledge with gratitude, the affection and encouragement of my sisters - Mrs. Olanike Ogundiran, Miss Adeyoola Adeleke, my brothers - Aderemi, Adebisi, Adegbola, and Ademola Adeleke. I am greatly indebted to my darling wife, Adenike Arike Adeleke, who provides a steady flame for my candle in the wind. I sincerely appreciate her patience and understanding. True love, I believe, never grows old. Thanks are also due to my in-laws, my uncles and my aunts for their love and support.

Dedicated to

- my mother, my first teacher, ***Mrs. Aderounke Ebe Jimoh-Adeleke***, who breathed her last in the course of Allah's wish and in the light of her unalloyed love for the "seeds" Allah has bestowed upon her. May her gentle soul rest in perfect peace (Aameen). *"Though I have solaced myself under God's protection and favor but no single second passes without feeling the pain on the scar face. I miss you Mum".*

- my father, ***Prince Ayodeji Adeleke***, who has been providing me constant inspiration, guidance, support and motivation since the beginning of my life on earth. May Allah protect him and make him live long to reap the fruit of his sweat (Aameen).

Table of Contents

CHAPTER 3

CHAPTER 4

METHODOLOGY

LIST OF FIGURES

LIST OF TABLES

الخلاصة

تستخدم التولينا المكونة من الفلزات والمعززة بجسيمات من اللافلزات في التطبيقات التي تتطلب قدرة ميكانيكية عالية يتميز هذه التوليفات بخواص لاتتوافر في المواد الأحاديةة مثل الصلابه العالية ، معامل تمدد حراري منخفض ، مقاومة عالية للبلى ، وكثافة منخفضة مما يجعلها مناسبة لبعض الصناعات مثل صناعة مراكب الفضاء والسيارات والبناء التآكل الموضعي في هذا النوع من التوليفات يمثل أحد العوائق الرئيسة في استخدامها على نطاق واسع ويمكن الحمن هذا العائق من خلال التصميم الأولي ومن خلال تعديل عملية التصنيع للمولفات ٠

لقد تم دراسة تاثير التآكل في أربعة أنواع من سبائك الألمنيوم وهي (F3k.00S,F3S.00S) و (F3k.20S,F3S.20S) المعززة بنسبة ٢٠ % من الحجم بواسطة(SiC) تمت دراسة مقاومة هذه السبائك للتآكل بالطرق التالية فقدان الوزن وقياسات الممانعة الكهروكيميائية في محلول مائي يحتوي على ٥ر٣ % من كلوريد الصوديوم،استخدم المجهر الضوئي والألكتروني الماسح وحيود الأشعة السينية والفحص الفلوري للأشعة السينية لتقييم دور المركبات الفلزية ، عينات متآكلة وعينات غير متكاملة من السبائك المعنية في هذه الدراسة ٠

أظهرت النتائج أن السبائك المعززة لها قابلية عالية للتآكل مقارنة بالسبائك الغير معززة ٠ كما أنه لوحظ أن عمليات النقر في هذه السبائك اتخذت أشكال مختلفة ٠بعض المركبات الفلزية في هذه السبائك لها دور ملحوظ في تكون التآكل المتمركز ٠

Abstract

Particulate-reinforced metal-matrix composites (MMC) have been used in several applications where high mechanical performance and other related properties are paramount requirements. High specific modulus, low thermal expansion coefficient, good wear resistance, low density and low cost are the major attractive characteristics of this class of materials in aerospace, automobile and construction industries. Localized corrosion, in these alloys, is usually insidious and may lead to catastrophic service failures. This can only be minimized by incorporating corrosion control at the design stage and by modifying the processing routes.

The corrosion behavior of four different types of aluminum alloy was studied. Two of these alloys *(F3K.20S and F3S.20S)* are reinforced with 20% by vol. SiC while the remaining two samples *(F3S.00S, and F3K.00S)* are not reinforced. Weight loss, potentiodynamic and cyclic polarization techniques were used to study their corrosion behavior in 3.5%wt. NaCl solution. Micro-analytical studies such as optical micrography, scanning electron micrography (SEM), X-ray diffraction, X-ray fluorescence (XRF) were utilized to analyze the role of intermetallic phases in both corroded and non-corroded samples of these mentioned alloys.

The results showed that un-reinforced alloys have higher corrosion resistance as compared to their reinforced counterparts. Pits observed in all the alloys show different shapes and structures. Some intermetallic phases in the reinforced alloys were suspected to have contributed to the formation of localized corrosion.

Chapter 1

1.1 General Introduction

Metal matrix composites are the focus of attention of automotive, electronic, and aerospace industries because of their high temperature strength, stiffness, and dimension stability on thermal recycling. Interest in the application of metal matrix composites in marine environment is rapidly expanding. Aluminum alloys, mainly 2024, 5052, 6061 and 7071 have been widely used as matrix materials with silicon carbide (particles) as their major reinforcing agent.

Although sufficient knowledge on the mechanical and physical properties of metal matrix composites has accumulated in recent years, existing knowledge on their corrosion behavior is meager. Investigations on the corrosion behavior have been focused on Al 6061/SiC in recent years. Parallel investigations on alloy 6013, with 20% vol. SiC, have been recently reported. The above investigations have shown that secondary phases containing major alloying elements are the preferred sites for localized corrosion. Investigation on whether the silicon carbide particles are the sites for localized corrosion or not needs more experimental evidence. It has been established that Al/SiC composites suffer more localized corrosion than their monolithic counterparts [1,2]. The preferential localized attack has been ascribed to factors, such as a reactive silicon carbide matrix, presence of crevices and pores, processing routes, presence of secondary phases and the volume percentage of reinforcement (SiC).

The most intriguing fact is that a greater number of smaller intermetallic precipitate forms on the composite compared to the alloy. This indicates the possibility of a greater number of secondary phases being stimulated by silicon carbide. A higher volume fraction is also known to have increased localized corrosion. In the latest work on alloy 6013-20 SiC, the preponderance of localized corrosion on secondary phases has been shown [2]. The key factor would be to establish the role of secondary phases in relation to silicon carbide particles and microstructures in the localized corrosion processes involved in localized corrosion. It would be possible to incorporate corrosion control in design and make these alloys more viable for technological applications.

The challenge to realize application of composites, in particular Al 6061/SiC composite, has increased by a sharp focus on service life and resistance to environmental degradation. The challenge can only be realized successfully by a complete understanding of the corrosion processes, in particular intriguing nature of silicon carbide particles and their influence on the secondary phases and microstructure.

1.2 Present State of the problem

Aluminum alloy 6061, 2024 and 7075 reinforced with SiC have been the focus of attention because of their application potential in a wide range of demanding applications; such as automotive, aerospace and defense. There are many other applications, which involve exposure of the composites to potential corrosive environment. Despite the great risk of corrosion, most of the work on composites

is concentrated on its mechanical properties and processing routes[3-5], and there are only relatively few investigative studies addressing the corrosion behavior of aluminum metal matrix composites [3]. Because of the duplex nature of the composites, they are prone to accelerated corrosion compared to their monolithic counter-part [6-9]. Corrosion of the composites not only limits their service life but also lead to deterioration of their unique mechanical properties for which it is designed.

There has been a recent interest in the corrosion behavior of advanced aluminum alloys prepared by techniques, such as rapid solidification processing, laser surface melting, and surface modification by ion beam technique [10-14]. By this technique the solid solubility of alloying element is increased.

It has been observed that localized corrosion degrades physical and mechanical properties. A 50% degradation in the transverse strength of B/Al composite was observed after it was immersed in 3.5 wt% NaCl for six hours [15]. The magnitude of pitting corrosion observed on Al 6061/ SiC was greater compared to corresponding unreinforced alloys [16,17]. The pits on Al 6061 reinforced with SiC reinforcement were observed to be shallower and more numerous than on the unreinforced alloy [18]. The silicon carbide/Al interface has been suggested to be the preferred sites for pits initiation[19]. Corrosion damage in extruded composite was observed to be lesser due to the absence of defects like gas pores, and a more homogeneous distribution of particles[20] compared to the unreinforced alloys. The presence of SiC is reported to alter the growth of corrosion pits [21]. Al 6061/SiC has been most widely used host material for

corrosion investigation in recent years because of its market potential. Following is the summary of corrosion investigations conducted by several workers.

- Studies both on Al 6061/SiC and Al 6013/SiC have shown that SiC is not a preferred site for attack [18-22].
- Large number of pits is formed in the composite compared to the wrought alloys. Composites corrode faster than the base alloy even though the attack is confined to the interface. The pits are, however, shallower on the composite. It has been established by studies on Al 6061/SiC.
- The effect of SiC reinforcement o localized corrosion is not clearly understood. Some investigators suggest that pits initiate at SiC particles, whereas others suggest that SiC is not a preferred site for pit nucleation. There is also evidence to suggest that SiC introduces micro structural changes in the matrix, which affect the corrosion process [18-23]. The microstructure plays a pivotal role in the corrosion behavior of Al/SiC composites.
- Alloys 6061 in T6 temper exhibits shallow intergranular corrosion whereas in T4 temper Al 6013 exhibits only pitting [24], which shows the role of micro structural changes and processing routes on the corrosion behavior.
- Aging time appears to strongly influence the corrosion behavior as indicated by preliminary investigations on Al 2124/SiC [19].
- The degree of corrosion of Al/SiC composites increases with increasing SiC (P) contents. The film breakdown was related to the volume percentage of SiC (P) [19].

- It has been a considered opinion that processing variables play an important role in the corrosion behavior of metal matrix composites and a high extrusion ratio and an appropriate heat treatment can significantly enhance corrosion resistance [26].

It has been shown in recent years that, pits in Al 5456/SiC initiate at micro structural secondary phases within the metal matrix [17]. Energy dispersive analysis of a pit in Al-5456 showed the presence of intermetallic precipitate comprising of major alloying elements of the alloy Mg, Cr, Al, Mn and Fe as impurity. What was revealing was that the composites (Al 5456/Al-SiC0 contained a greater number of smaller intermetallic precipitates than the wrought alloy [26]. It has already been mentioned above that a large number of pits form on the composites than on their respective wrought alloys. The composites corrode faster than the wrought alloys, however, the localized attack is confined to the interface in composites resulting in crevice or pits. The greater susceptibility of composite to corrosion is consistent with the inherent tendency of duplex system to corrode faster. Therefore, controlling the number of suspected sites of localized corrosion can possibly minimize corrosion of composites.

1.3 Nature of Aluminum Reinforcement

Generally, composite materials are made up of a bulk material, called the matrix, and a filler or reinforcement material such as fibers, whiskers, or metal wires. The reinforcement materials or agents consist of high-strength materials in

continuos fiber, whiskers, particulates, or fabric form. These reinforcement materials usually carry the major stresses and loads, while the matrix material holds the reinforcement materials together. Figure 1.2 shows how a composite material is selected and created [27].

There are four major categories of composite reinforcements:

- Continuous fibers
- Whiskers
- Particulates
- Wires or fabric

Table 1.1 shows the variety and complexity of different types of reinforcement materials.

Aluminum, Titanium, Magnesium, and copper alloys are the most important metals that

can be used to produce metal matrix composites.

Aluminum matrix composites are reinforced with continuous fibers such as Boron, silicon carbide, alumina, and graphite; discontinuous fibers such as alumina and alumina-silica; silicon carbide whiskers; or particulates of silicon carbide and boron carbide.

1.4 Classification of Aluminum-Based Alloys

Aluminum-based alloys are usually classified as:

- Wrought Aluminum alloys
- Cast Aluminum alloys

These alloys in each of the two categories can be further classified according to whether they respond to heat treatment or not. In this classification, the term 'heat treatment' refers to a strengthening heat treatment, and does not include annealing, which is a softening heat treatment [28].

Wrought Aluminum alloys are manufactured in the form of sheet, tube, forgings, wire, and extruded sections. They can be classified as work-hardening alloys (will not respond to heat treatment) or heat-treatable alloys (can be strengthened by precipitation heat treatment).

When high ductility and corrosion resistance is required, commercially pure aluminum is used with addition of a small amount of silicon or magnesium. Cast aluminum alloys can be grouped as 'As Cast' Aluminum Alloys (derive no benefit from heat treatment) and Heat-treatable casting aluminum alloys (other alloying elements, apart from silicon, are usually added). Figure 1.1 illustrates the various forms of aluminum alloys.

Table 1.2 shows the designations and nominal compositions of common aluminum alloys used for casting. Table 1.3 shows the characteristics of common aluminum alloys used in sand and permanent mold casting. In Table 1.4, typical tensile properties of common aluminum casting alloys are shown.

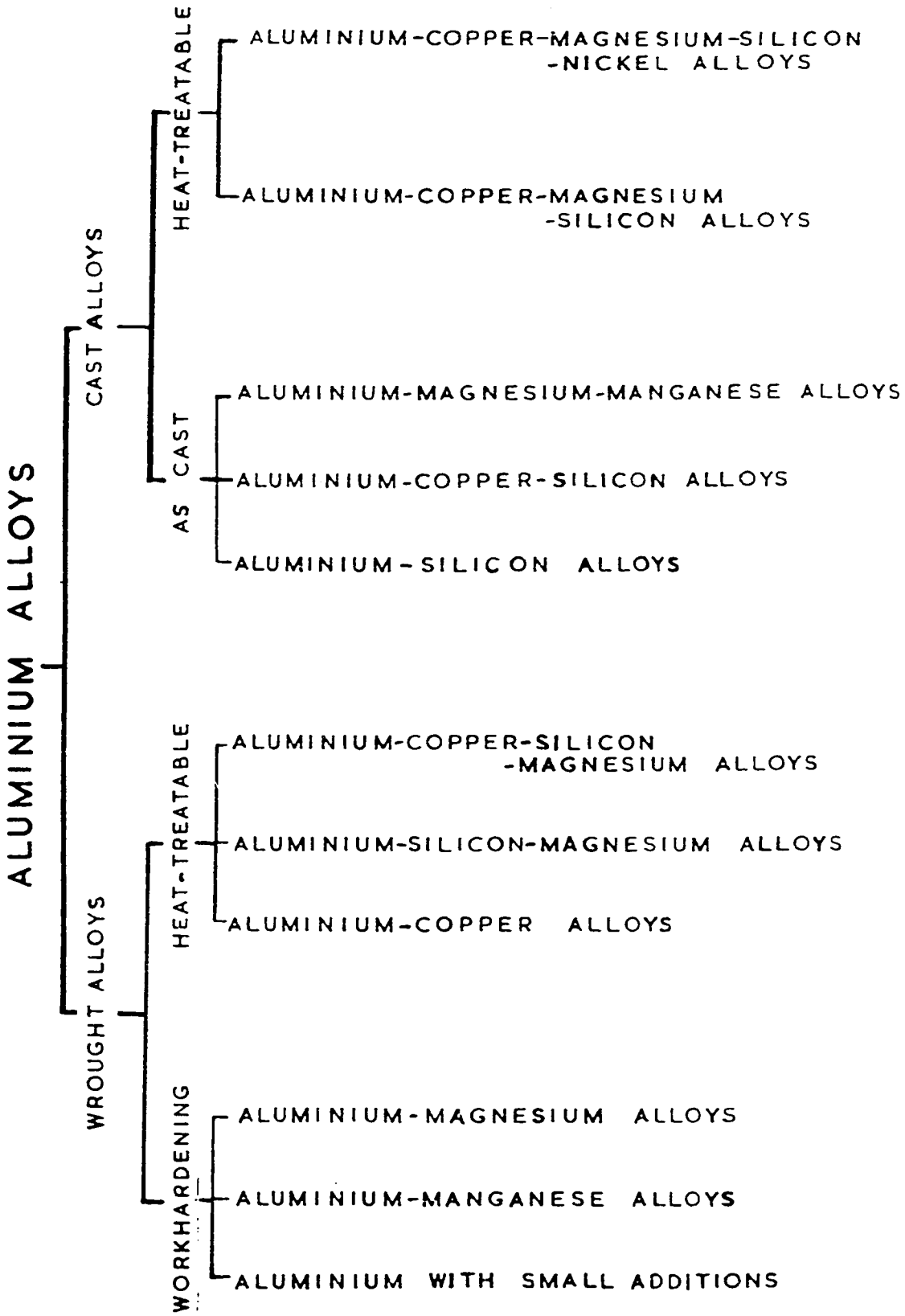

Figure1.1: Aluminum Alloys [28]

Table 1.1: Types of Reinforcement Materials for Composite Materials

REINFORCING AGENTS	
CONTINUOUS FIBERS	PARTICULATES (including flakes)
BORON (B)	TUNGSTEN (W)
GRAPHITE (C)	MOLYBDENUM (Mo)
ALUMINA (Al_2O_3)	CHROMIUM (Cr)
SILICON CARBIDE (SiC)	SILICON CARBIDE (SiC)
BORON CARBIDE (B_4C)	BORON CARBIDE (B_4C)
BORON NITRIDE (BN)	TITANIUM CARBIDE (TiC)
SILICA (SiO_2)	ALUMINUM DODECABORIDE (AlB_{12})
TITANIUM DIBORIDE (TiB_2)	TUNGSTEN CARBIDE (WC)
ALUMINA-BORIA-SILICA ("NEXTEL")	CHROMIUM CARBIDE (Cr_3C_2)
	SILICA (SiO_3)
WHISKERS	ALUMINA (Al_2O_3)
	MOLYBDENUM DISILICIDE ($MoSi_2$)
OVER 100 MATERIALS PRODUCED	
	METAL WIRES
METAL REINFORCEMENTS	
IRON (Fe)	TUNGSTEN (W)
NICKEL (Ni)	TITANIUM (Ti)
COPPER (Cu)	MOLYBDENUM (Mo)
NICKEL ALUMINIDE ($NiAl_3$)	BERYLLIUM (Be)
ALUMINUM OXIDE-ALUMINA-SAPPHIRE (Al_2O_3)	STAINLESS STEEL
	NIOBIUM-TIN (NbSn) - SUPERCONDUCTOR
SILICON CARBIDE (SiC)	
GRAPHITE (C)	NIOBIUM-TITANIUM (NbTi) - SUPERCONDUCTOR
SILICON NITRIDE (Si_3N_4)	

Table 1.2: Designation and nominal compositions of common aluminum alloys [85]

Alloys				Composition, %				
AA number	Former AA designation	Former ASTM number	Product(a)	Cu	Mg	Mn	Si	Others
201.0	...	...	S	4.6	0.35	0.35	...	0.7 Ag, 0.25 Ti
206.0	...	...	S or P	4.6	0.25	0.35	0.10(b)	0.22 Ti, 0.15 Fe(b)
A206.0	...	...	S or P	4.6	0.25	0.35	0.05(b)	0.22 Ti, 0.10 Fe(b)
208.0	108	CS43A	S	4.0	...	...	3.0	...
242.0	142	CN42A	S or P	4.0	1.5	...	...	2.0 Ni
295.0	195	C4A	S	4.5	...	...	0.8	...
296.0	B295.0, B195	...	P	4.5	...	...	2.5	...
308.0	A108	SC64A	S or P	4.5	...	...	5.5	...
319.0	319, Allcast	SC64D	S or P	3.5	...	...	6.0	...
336.0	A332.0, A132	SN122A	P	1.0	1.0	...	12.0	2.5 Ni
354.0	354	SC92A	P	1.8	0.50	...	9.0	...
355.0	355	SC51A	S or P	1.2	0.50	0.50(b)	5.0	0.6 Fe(b), 0.35 Zn(b)
C355.0	C355	SC51B	S or P	1.2	0.50	0.10(b)	5.0	0.20 Fe(b), 0.10 Zn(b)
356.0	356	SG70A	S or P	0.25(b)	0.32	0.35(b)	7.0	0.6 Fe(b), 0.35 Zn(b)
A356.0	A356	SG70B	S or P	0.20(b)	0.35	0.10(b)	7.0	0.20 Fe(b), 0.10 Zn(b)
357.0	357	...	S or P	...	0.50	...	7.0	...
A357.0	A357	...	S or P	...	0.6	...	7.0	0.15 Ti, 0.005 Be
359.0	359	SG91A	S or P	...	0.6	...	9.0	...
360.0	360	SG100B	D	...	0.50	...	9.5	2.0 Fe(b)
A360.0	A360	SG100A	D	...	0.50	...	9.5	1.3 Fe(b)
380.0	380	SC84B	D	3.5	...	...	8.5	2.0 Fe(b)
A380.0	A380	SC84A	D	3.5	...	...	8.5	1.3 Fe(b)
383.0	...	SC102A	D	2.5	...	...	10.5	...
384.0	384	SC114A	D	3.8	...	...	11.2	3.0 Zn(b)
A384.0	384	SC114A	D	3.8	...	...	11.2	1.0 Zn(b)
390.0	390	...	D	4.5	0.6	...	17.0	1.3 Zn(b)
A390.0	A390	...	S or P	4.5	0.6	...	17.0	0.5 Zn(b)
413.0	13	S12B	D	...	...	...	12.0	2.0 Fe(b)
A413.0	A13	S12A	D	...	...	...	12.0	1.3 Fe(b)
4430	43	S5B	S	0.6(b)	...	...	5.2	...
A443.0	43	...	S	0.30(b)	...	...	5.2	...
B443.0	43	S5A	S or P	0.15(b)	...	...	5.2	...
C443.0	A43	S5C	D	0.6(b)	...	...	5.2	2.0 Fe(b)
514.0	214	G4A	S	...	4.0	...	...	...
518.0	218	G8A	D	...	8.0	...	...	...
520.0	220	G10A	S	...	10.0	...	...	...
535.0	Almag 35	GM70B	S	...	6.8	0.18	...	0.18 Ti
A535.0	A218	...	S	...	7.0	0.18	...	...
B535.0	B218	...	S	...	7.0	...	...	0.18 Ti
712.0	D712.0, D612, 40E	ZG61A	S or P	...	0.6	...	...	5.8 Zn, 0.5 Cr, 0.20 Ti
713.0	613, Tenzaloy	ZC81A,B	S or P	0.7	0.35	...	...	7.5 Zn, 0.7 Cu
771.0	Precedent 71A	ZG71B	S	...	0.9	...	...	7.0 Zn, 0.13 Cr, 0.15 Ti
850.0	750	...	S or P	1.0	...	...	...	6.2 Sn, 1.0 Ni

(a) S = sand casting, P = permanent mold casting, D = die casting. (b) Maximum.

Table 1.3: Characteristics of common aluminum alloys [85]

Alloy	Type of mold(c)	Fluidity	Resistance to hot cracking	Pressure tightness	Heat treatment	Strength at elevated temperatures	General corrosion resistance	Machining	Polishing	Anodizing Appearance	Weldability
208.0 ...	S	2	2	2	Optional	3	4	3	3	3	2
213.0 ...	P	2	3	3	No	3	4	2	2	3	3
222.0 ...	S or P	3	3	3	Yes	1	4	1	2	3	3
242.0 ...	S or P	3	4	4	Yes	1	4	2	2	3	4
295.0 ...	S	3	4	4	Yes	3	4	2	2	2	3
296.0 ...	P	3	4	3	Yes	2	4	3	2	3	3
308.0 ...	P	2	2	2	No	3	3	3	3	4	2
319.0 ...	S or P	2	2	2	Optional	3	3	3	4	4	2
328.0 ...	S	1	1	2	Optional	2	3	3	3	4	1
332.0 ...	P	1	2	2	Yes	1	3	4	4	4	2
333.0 ...	P	1	2	2	Yes	2	3	3	3	4	3
336.0 ...	P	1	2	2	Yes	1	3	4	4	4	3
354.0 ...	P	1	1	1	Yes	2	3	4	4	4	3
355.0 ...	S or P	1	1	1	Yes	2	3	3	3	4	1
C355.0 ...	S or P	1	1	1	Yes	2	3	3	3	4	1
356.0 ...	S or P	1	1	1	Yes	3	2	3	4	4	1
A356.0 ...	S or P	1	1	1	Yes	3	2	3	4	4	1
357.0 ...	S or P	1	1	1	Yes	3	2	3	4	4	1
A357.0 ...	S or P	1	1	1	Yes	2	2	3	4	4	1
359.0 ...	S or P	1	2	2	Yes	2	2	4	4	4	1
B443.0 ...	S or P	1	1	1	No	4	2	5	4	4	1
512.0 ...	S	3	3	4	No	3	1	2	2	2	3
513.0 ...	P	4	4	4	No	3	1	1	1	1	3
514.0 ...	S	4	4	5	No	3	1	1	1	1	3
520.0 ...	S	4	4	5	Yes	5	1	1	1	1	4
535.0 ...	S	5	4	5	Optional	3	1	1	1	1	4
705.0 ...	S or P	4	4	4	No	4	2	1	2	2	4
707.0 ...	S or P	4	4	4	No	4	2	1	2	2	4
710.0 ...	S	4	5	4	No	4	4	1	2	2	4
711.0 ...	S	3	5	4	No	4	3	1	2	2	4
713.0 ...	S or P	3	4	4	No	4	3	1	1	1	4
771.0 ...	S	3	4	4	Yes	4	3	1	1	1	4
850.0 ...	S or P	4	5	5	Yes	5	4	1	3	...	5
851.0 ...	S or P	4	5	5	Yes	5	4	1	3	...	5
852.0 ...	S or P	4	5	5	Yes	5	4	1	3	...	5

(a) From Standards for Aluminum Sand and Permanent Mold Castings, The Aluminum Association, 1977. (b) Characteristics are comparatively rated from 1 to 5; 1 is the highest or best possible rating. (c) S = sand; P = permanent.

Table 1.4: Typical Tensile Properties of Common Aluminum Casting Alloys [85]

Alloy	Product(a)	Temper	Tensile strength MPa	Tensile strength ksi	Yield strength(b) MPa	Yield strength(b) ksi	Elongation(c), %
201.0	S	T4	365	53	215	31	20
	S	T6	485	70	435	63	7
	S	T7	460	67	415	60	4.5
206.0, A206.0	S	T7	435	63	345	50	11.7
208.0	S	F	145	21	97	14	2.5
242.0	S	T21	185	27	125	18	1.0
	S	T571	220	32	205	30	0.5
	S	T77	205	30	160	23	2.0
	P	T571	275	40	235	34	1.0
	P	T61	325	47	290	42	0.5
295.0	S	T4	220	32	110	16	8.5
	S	T6	250	36	165	24	5.0
	S	T62	285	41	220	32	2.0
296.0	P	T4	255	37	130	19	9.0
	P	T6	275	40	180	26	5.0
	P	T7	270	39	140	20	4.5
308.0	P	F	195	28	110	16	2.0
319.0	S	F	185	27	125	18	2.0
	S	T6	250	36	165	24	2.0
	P	F	235	34	130	19	2.5
	P	T6	280	40	185	27	3.0
336.0	P	T551	250	36	195	28	0.5
	P	T65	325	47	295	43	0.5
354.0	P	T61	380	55	285	41	6.0
355.0	S	T51	195	28	160	23	1.5
	S	T6	240	35	175	25	3.0
	S	T61	270	39	240	35	1.0
	S	T7	265	38	250	36	0.5
	S	T71	175	35	200	29	1.5
	P	T51	210	30	165	24	2.0
	P	T6	290	42	190	27	4.0
	P	T62	310	45	280	40	1.5
	P	T7	280	40	210	30	2.0
	P	T71	250	36	215	31	3.0

Table 1.4: Typical Tensile Properties of Common Aluminum Casting Alloys [85] (contd)

356.0	S	T51	175	25	140	20	2.0
	S	T6	230	33	165	24	3.5
	S	T7	235	34	210	30	2.0
	S	T71	195	28	145	21	3.5
	P	T6	265	38	185	27	5.0
	P	T7	220	32	165	24	6.0
357.0, A357.0	S	T62	360	52	290	42	8.0
359.0	P	T61	330	48	255	37	6.0
		T62	345	50	290	42	5.5
360.0	D	F	325	47	170	25	3.0
A360.0	D	F	320	46	165	24	5.0
380.0	D	F	330	48	165	24	3.0
383.0	D	F	310	45	150	22	3.5
384.0, A384.0	D	F	330	48	165	24	2.5
390.0	D	F	280	41	240	35	1.0
	D	T5	300	43	260	38	1.0
A390.0	S	F, T5	180	26	180	26	<1.0
	S	T6	280	40	280	40	<1.0
	S	T7	250	36	250	36	<1.0
	P	F, T5	200	29	200	29	1.0
	P	T6	310	45	310	45	<1.0
	P	T7	260	38	260	38	<1.0
413.0	D	F	300	43	140	21	2.5
A413.0	D	F	290	42	130	19	3.5

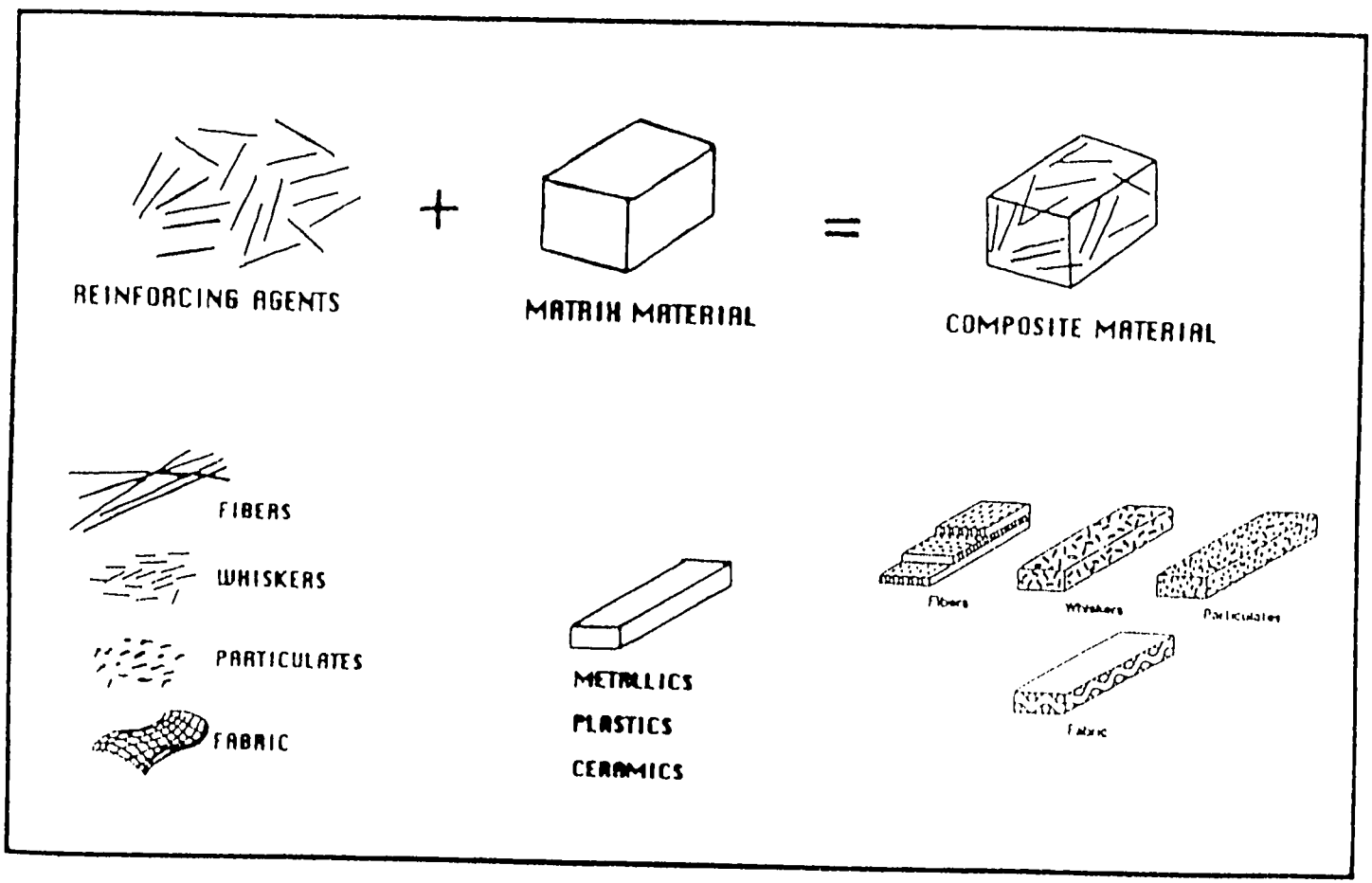

Figure1.2: Schematic Diagram of Composite Materials [28]

Chapter 2

LITERATURE REVIEW

2.1 Effect of Manufacturing Processes on Mechanical Properties of Al-SiC_p

Defects in the matrix produced during manufacturing of the composite material can have adverse effect on mechanical properties as well as corrosion behavior of such material. Therefore, the influence of reinforcing particles and the manufacturing process on the corrosion behavior of MMCs required adequate study [29].

Styles et al [30] reported that particulate silicon carbide (SiC_p) reinforced aluminum alloys has been observed to posses improved specific strength and stiffness over those of equivalent monolithic materials while maintaining good secondary formability and isotropic properties. Investigations of short fiber, whisker, or particle-reinforced alloys were carried out with the purpose of reducing fabrication cost and obtaining materials, which are easy to use, and with improved mechanical properties [31-33].

Metal Matrix Composites (MMCs) reinforced with discontinuous fibers, whiskers or particulates of silicon carbide have become materials of interest for few years back. These composites are potential candidate materials for a variety of applications in the fields of aerospace, automotive, industrial and leisure goods. The importance of these composites could be attributed to their high stiffness,

superior room and elevated temperature strength, improved wear resistance and low coefficient of thermal expansion [34-35].

Divecha et al [36] discussed several processing routes in production of aluminum matrix composites reinforced with SiC whiskers and particulates. Casting route seems to be most attractive out of these methods. Several variants of casting route namely compocasting, liquid pressure forming, spray casting and squeeze casting have been tried successfully to fabricate Al-SiC_p, Al-SiC_w and Al-SiC_f composite [37].

2.1.1 Processing Route

Vasudevan et al [38] carried out research on fabrication and properties of Al matrix composites reinforced with SiC particles. They were able to prepare Aluminum matrix composites reinforced with SiC particles by a process, which involved pre-treatment aluminum ingot and SiC particles. This was followed by addition of particles into an impeller-agitated melt. They found out that presence of SiC particles appreciably improved the hardness, elastic modulus, tensile strength and compressive strength. Ductility and fracture toughness were significantly less than that of reinforced matrices.

Buhrmaster et al [39] developed a new process for producing near-net-shape aluminum and Al/SiC composite components. This process uses an apparatus which is basically a modified gas metal arc (GMA) welding torch, where aluminum wire feed stock is melted and can be considered with SiC particles or whiskers entrained in inert gas. Upon striking a substrate or mold, the mixture of

aluminum and SiC solidifies into a composite structure. The structures obtained are shown in Figure 2.1 and Figure 2.2. Mechanical properties obtained in unreinforced materials using this process are similar to those found in conventionally produced versions of the same alloys.

Aluminum silicon composite produced by hot isostatically press has been observed to possess about 2.5% higher degree of densification than extruded counterpart [40]. This difference did not result in an improvement in UTS for the hot isostatically press (HIP) samples but transmission electron microscopy (TEM) results show severe deformation of SiC particulates by neighboring particulates in the HIP samples. This resulted to reduction in strain at fracture from 2.8% to 0.7% in HIP samples.

Vacuum hot pressing technique was used by Tweed [41] to manufacture 2014 aluminum reinforced with SiC particulate. He observed that for hot pressing at the solidus temperature, under identical applied and transferred load conditions, increase in the SiC content from 0 to 20 vol. % leads to a reduction in average densification rate by about a factor of 2 over the range from 85% to 90% of full density.

Usually, aluminum based composites have a higher hot strength than the unreinforced monolithic alloy because of the increased dislocation density caused by the reinforcements [42]. Ko et al [43] discussed the hot deformation behavior of 2024 aluminum alloy composites, reinforced with various sizes of SiC_{pp}. They found out that the composite reinforced with 8μm SiC_p showed the highest flow stress (256MPa) at 320°C and the highest failure strain (3.65) at 480°C under a

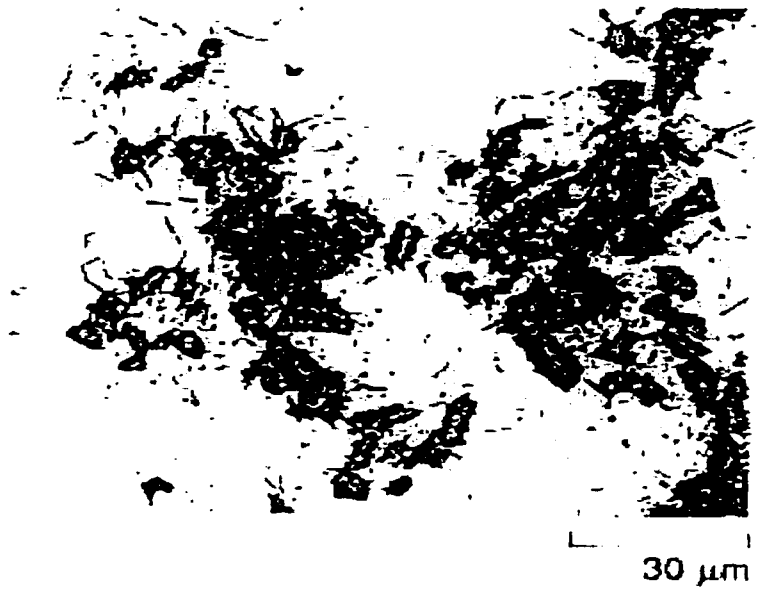

Figure 2.1: SiC particulate produced by spraying casting process

Figure 2.2 : SiC Whiskers produced by spray casting process

strain rate of $1.0s^{-1}$; while composite reinforced with 1μm SiC_p showed the highest strain rate sensitivity (0.36) at 480°C.

Milliere and Surey [31] studied the fabrication and properties of metal matrix composites based on SiC fiber reinforced aluminum alloys. He discovered that Al-Si alloys containing up to 15% Nicalon SiC fiber can be produced successfully with a macroscopically homogeneous distribution of the fibers by the combined processing route of compocasting followed by squeeze casting. He observed that, at room temperature, SiC fibers appreciably improve hardness, wear resistance, and compressive strength of the matrix at room temperature but these fibers are efficient for reinforcement of Al-SiC alloys, at high temperature, up to 300°C.

Powder-Metallurgy Aluminum matrix composites can also be produced [44]. Reinforcements obtained from powder metallurgy are shown in Figure 2.3 and properties of some selected ceramics used in reinforcement are also shown in Table 3.1.

2.2 Role of Secondary Phase Particles

Intermetallics in aluminum alloys are either intentionally developed to obtain the desired mechanical properties or are present in the alloys as natural impurities. Depending on types of alloy, different second-phase particles are present [45]. For example, 1xxx alloys contain Al_6Fe and Al_3Fe and 3xxx alloys contain AlMg and AlMnMg secondary phase particles. There are intermetallics which when present

in alloy decrease significantly the resistance to localized corrosion (such as particles with Cu and Fe in 2xxx and 1xxx alloys, respectively) and particles, which seem to not adversely affect corrosion resistance. The behavior of the intermetallics depends mainly on the potential difference between the particles and the matrix in a solution. The phases, which are more electrochemically noble than the matrix, play the role of cathodes while to the inclusions matrix undergoes anodic dissolution [47].

Buchheit [46] collected the corrosion potential values for intermetallic phases (mainly in NaCl solutions) common in aluminum alloys, which can help to predict the galvanic cell formation in aluminum alloys. Nisancioglu (48) studied the electrochemical behavior of Al_3Fe, α Al (Fe, Mn) Si and δ AlFeSi in NaOH solutions. He used alkaline solution for his measurement because of high PH is established around intermetallics acting as the cathode for oxygen evolution.

Nisancioglu [48] obtained similar result of Golubev and Ronzhin [49] when he found that near the corrosion potential the Al_3Fe undergoes a selective dissolution of Al and the surface of the Al_3Fe crystals becomes richer in Fe. Enrichment with Fe is detrimental to cathodic behavior. Oxidation of Fe into a protective Fe_3O_4 occurs at more anodic potentials. A formation of iron oxide inhibits the aluminum dissolution. The presence of Mn or Si in the phase reduces the effect of Fe on both the anodic and cathodic reaction rates.

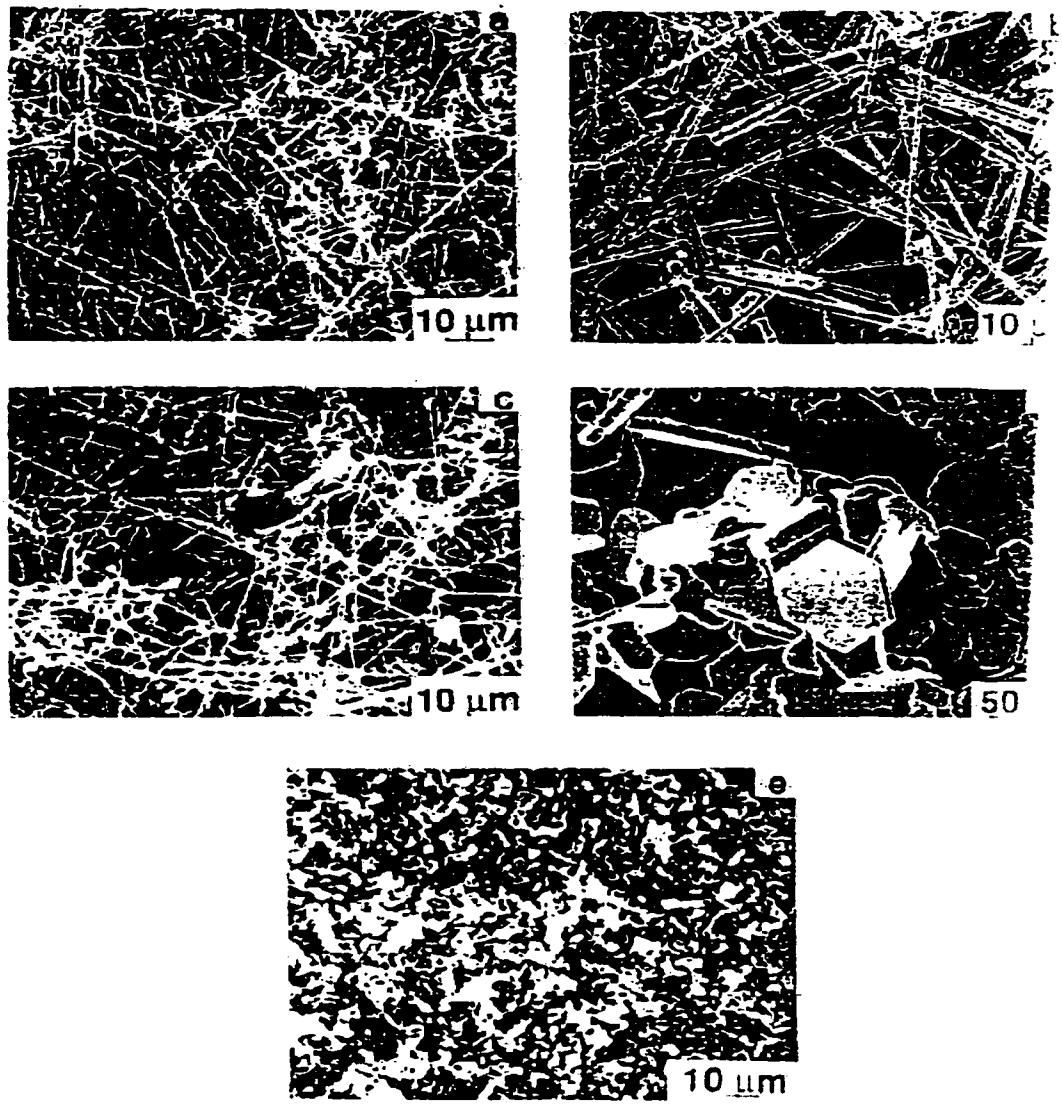

Figure 2.3: SEM of Discontinuous SiC Reinforcement

(a) ACMC Whisker, (b) AMMATRIX Whiskers, (c) Tokai Whiskers, (d) AMMATRIX Oblate Platelets, and (e) Particulates.

Table 2.1: Properties of Selected Carbide Reinforcement

Ceramic	Coefficient of Expansion (10^{-6}/°F)	Strength (ksi)	Elastic Modulus (mpsi)
BeO	4.1	3.5(2000°F)	27.5(2000°F)
MgO	6.45	6.0(2000°F)	22.0(2000°F)
ThO_2	5.3	28.0(2000°F)	29.0(2000°F)
UO_2	5.3	-	25.0(2000°F)
ZrO_2	6.67	12.0(2000°F)	19.2(2000°F)
CeO_2	6.9	85.4(75°F)	26.8(75°F)
Al_2O_3	4.4	32.0(2000°F)	55.0(2000°F)
$TaSi_2$	6.0	-	49.0(2300°F)
$MoSi_2$	4.85	40.0(2000°F)	40.0(2300°F)
WSi_2	5.0	-	36.0(2000°F)
TiB_2	4.6	-	60.0(2000°F)
ZrB_2	4.5	-	73.0(75 o F)
TiC	4.22	8.0(2000°F)	39.0(75°F)
ZrC	3.7	13.0(2000°F)	52.0(75°F)
HfC	3.7	-	46.0(75°F)
VC	3.98	-	63.0(75°F)
NbC	3.8	-	49.0(75°F)
TaC	3.59	-	53.0(75°F)
Mo_2C	3.23	-	33.0(75°F)
WC	2.83	-	97.0(75°F)
B_4C	3.38	400.0(75°F)	65.0(75°F)
SiC	3.00	1210.0(75°F)	47.0(2000°F)
AlN	2.69	300.0(75°F)	45.0(2000°F)

Mazurkiewics and Piotrowski [50,51] studied the behavior of Al_2Cu at the open circuit potential and under anodic polarization in the sulfate solutions and found dissolution of this intermetallic with the formation of Al^{3+} and Cu^{2+}.

Chemical composition of the particles in AA2024- T3 was determined by Buchheit et al [52]. They studied its behavior in 0.1M NaCl at pH 4.2. Four main types of particles were found: 60% were AlCuMg (second phase), 12% were Al (Cu, Fe, Mn), AlCuFe and (Al, Cu) Mn. The s-phase occupied 2.7% of the total surface area. This phase was active and Mg and Al selectively dissolved, leaving a pit where the particle was present. The s-phase dealloying left Cu-rich particle remnants, which were cathodic to the matrix and therefore caused the peripheral formation of pits around the particle.

Buchheit and Moran [53] studied the localized corrosion behavior of AA2090. Two types of pitting were found. The first type was attributed to the dissolution of the subgrain boundary phase (Al_2CuLi). A direct correlation between increased subgrain boundary precipitation and increased subgrain boundary pitting was noted. The second type of pitting involved anenhanced local galvanic attack of the matrix material surrounding the AlCuFe constituents, which occurred randomly throughout the plate.

Zamin [54] studied the role of Mn in the corrosion behavior of Al-Mn alloys. He found out that the positive effect of an increase of manganese in a solid solution results in the shift potential of the matrix in the cathodic direction whereas an increase in the Mn/Fe ratio in the intermetallic shifts their potential in the

anodic direction. In effect, the potential difference between the matrix and the intermetallic decreases.

Blanc et al [55] suggested that the geometry of the intermetallic influence the susceptibility to pitting. The differences in the pitting behavior of 6056 and 2024 alloys were explained by the differences in the behavior of the coarse particles in the alloys.

Iron was found to be a common impurity in Al-Si casting alloys which readily forms the ternary intermetallic phases α-AlFeSi (Al_8Fe_2Si) and β-AlFeSi (Al_5FeSi) [56]. Their chemical compositions vary widely depending on the conditions under which they form and the presence of other alloying additions [57]. Tables 3.2, 3.3, 3.4 [56] show some phases, which are usually, present in aluminum alloys. Further investigation was carried out by Tang and Sritharan [58] on the morphology of β-AlFeSi intermetallics in Al-7Si alloy castings. They found that by increasing the iron level and decreasing the cooling rate encouraged the β platelets to crystallize independently of silicon. The size of the β platelets increased with increase in iron level and with decrease in cooling rate.

2.3 Corrosion Behavior of Aluminum Silicon Carbide

Many previous workers have noted that the pitting potentials of SiC-reinforced MMCs and the corresponding plain alloy are very similar. However, the presence of the SiC phase affects the growth of corrosion pits. The pits in MMCs are greater in number, smaller in size and shallow in penetration depth. Some

researchers [59-60] have attributed this difference to the greater number of intermetallic phases found in the composite when compared with the plain alloy. The smaller size of pits established on the composite surfaces suggests that the SiC reinforcement might interfere with or decrease the metal dissolution rate.

Trowsdale et al [62] studied the influence of silicon carbide reinforcement on the pitting behavior of Aluminum. They observed that addition of SiC particulates reinforcement to 1050 aluminum alloy produces a small but reproducible increase in susceptibility to pitting attack. These pitting zones were attributed to arise from the presence of voids and crevices at the reinforcement/ matrix interface. In their conclusion, they noticed that reaction between aluminum and silicon carbide to produce aluminum carbide and elemental silicon appears to have little detrimental influence on pitting susceptibility.

When corrosion behavior of 2024 T351 aluminum alloy (usually used in aircraft industry) was studied in chloride solution by Valerie Guillaumin and Mankowski [63], both pitting and intergranular corrosion were found to have developed. The grain boundaries are more susceptible to preferential dissolution because they are more anodic in comparison to the rest of the matrix and the dissolution of the intergranular precipitates makes them fragile.

Similar research was carried out by Ahmad Zaki and Aleem [82] to study the effect of temper on seawater corrosion of an aluminum-silicon carbide composite alloy. It was reported that T4 temper alloy has higher corrosion resistance than F and O temper alloy. This was attributed to formation of finer and more homogeneously distributed precipitates in T4 temper alloy.

Table 2.2 : Phases formed in Aluminum-Copper Alloys [56]

Cu	*Cu<2%* in solid solution	*Cu<2%* $CuAl_2$	*Fe>Si* Cu_2FeAl_7 or $(CuFe)Al_6$	*Mg>1/2Si* $CuMgAl_2$ or $CuMg_4Al_6$	*Mn>Fe* $Cu_2Mn_3Al_{20}$ or $(CuFeMn)Al_6$	*Mg<Si* $Cu_2Mg_8Si_6Al_5$ $(CuFeMn)_3Si_2Al_{15}$	*Ni>0.1%* Cu_4NiAl_7, or $(CuNi)_2Al_3$ or $Cu_2(FeNi)Al_7$ or $(CuFeNi)Al_6$
Fe	*Si>2Mg* Fe_2SiAl_8 or $FeSiAl_5$	*Fe>Si* Cu_2FeAl_7 or $(CuFe)Al_6$, $FeAl_3$	*Mn>0.1%* $(CuFeMn)Al_6$ or $(CuFeMn)_3Si_2Al_{15}$	*Ni>0.1%* $FeNiAl_9$ or $(CuFeNi)Al_6$	$(CuFeNi)_2Al_3$, $Cu_2(FeNi)Al_7$		
Si	*Si>Fe* $FeSiAl_5$	*Si<Fe,Mg>Si* Mg_2Si	*Mg~Si* $Cu_2Mg_8Si_6Al_5$	*Mn>0.1%* $(CuFeMn)_3Si_2Al_{15}$	*Si>Mg + Fe* *Si*		
Mg	*Mg<0.2%* in solid soln.	*Si<0.6Mg<Mg* Mg_2Si	*Si~Mg* $Cu_2Mg_8Si_6Al_5$	*Si<0.6Mg* $CuMgAl_2$	*Cu<Mg* $CuMg_4Al_6$		
Mn	*Mn<0.2%* in solid soln.	*Fe>Si* $(FeMn)Al_6$	*Fe<Si* $(CuFeMn)_3Si_2Al_{15}$	*Fe,Si<Mn* $Cu_2Mn_3Al_{20}$	*Ni>0.1%* Mn_3NiAl_{16}		
Zn	*Zn<2%* in solid soln.	*Zn>2%* $Cu_5Zn_2Al_3$					
Ni	*Cu>Fe* Cu_4NiAl_7	*Cu<2Fe,Fe>Si* $FeNiAl_9$, or $(CuFeNi)_2Al_3$	*Mn>0.1%* Mn_3NiAl_{16}				
Pb	*Mg,Pb<0.1%* Pb	*Bi<0.1Pb, and* Mg_2Pb	*Mg>1.7Si*	*Bi>0.1Pb* $BiPb_3$			
Bi	*Pb>0.2Bi* $BiPb_3$	*Bi<0.1Pb, and* Bi_2Mg_3	*Mg>1.7Si*				
Sn	*Mg<1.7Si* Sn	*Mg>1.7Si* Mg_2Sn					
Cd	Cd						
Ti	$TiAl_3$						
Ag	*Ag<0.3%* in solid soln.	*Ag>0.3%* Ag_2Al	*Mg>1.7Si* $(AgCuAl)_{49}Mg_{32}$	or AgMg			

Table 2.3 : Phases formed in Aluminum-Silicon Alloys [56]

Si	*Si<12%* eutectic	*Si>12%* eutectic & primary	*Mg>0.2%* Mg_2Si	*Fe>0.05%* $FeSiAl_5$	*Mn>0.1%* $(FeMn)_3Si_2Al_{15}$	*Cr>0.1%* $(CrFe)_4Si_4Al_{13}$	*Fe>Mg* $FeMg_3Si_6Al_8$	*Mg>2Cu* $Cu_2Mg_8Si_6Al_5$
Na	*Na<0.01%* dispersed	*Na>0.01%* $(NaAl)Si_2$						
P	*Si<12%* dispersed	*Si>12%,* AlP, often	*P>0.01%* inside Si crystals					
Fe	*Fe<0.7%* $FeSiAl_5$ eutectic	*Fe>0.7%* $FeSiAl_5$ primary	*Co>0.1%* $(CoFe)_2Al_9$	*Cr>0.1%* $(CrFe)_4Si_4Al_{13}$, $(CrFe)_5Si_8Al_2$	*Mn>0.2%* $(FeMn)_3Si_2Al_{15}$	*Mo>0.1%* AlFeMo	*Ni>0.01%* $FeNiAl_9$	*Mg<Fe* $FeMg_3Si_6Al_8$
Mg	*Mg<0.2%* in solid solution	*Mg>0.2%, Cu<0.2%* Fe<Mg Mg_2Si	*Cu<1/2Mg* $Cu_2Mg_8Si_6Al_5$	*Fe>Mg* $FeMg_3Si_6Al_8$				
Cu	*Cu<1%* in solid solution	*Cu>1%,* Mg<0.2%, Fe<0.3% $CuAl_2$	*Cu>1%,* Mg>2Cu $Cu_2Mg_8Si_6Al_5$					
Co	$(CoFe)_2Al_9$							
Cr	$(CrFe)_4Si_4Al_{13}$ or $(CrFe)_5Si_8Al_2$							
Mn	$(FeMn)_3Si_2Al_{15}$							
Zn	In solid soln.							

Table 2.4 : Phases formed in Aluminum-Magnesium Alloys [56]

Mg	*Mg<2%* in solid soln.	*Mg>2%* Mg_5Al_8	*Si>0.05%* Mg_2Si	*Cu>0.2%* $CuMg_4Al_6$			
Si	*Fe<0.3%* Mg_2Si	*Fe>0.3%, Mg<2%* Fe_2SiAl_8	*Fe>0.3%, Mg<2%, Mn or Cr>0.1%* $(FeMn)_3Si_2Al_{15}$ or $(CrFe)_4Si_4Al_{13}$				
Fe	*Si<0.3%* *Mg>2%* $FeAl_3$	*Si>0.3%* *Mg<2%* Fe_2SiAl_8	*Si>0.3%* *Mg<2%* *Mn>0.1%* $(FeMn)_3Si_2Al_{15}$	*Si<0.3%* *Mg>2%* Mn>Fe $(FeMn)Al_6$	*Si>0.3%* *Mg<2%* *Cr>0.1%* $(CrFe)_4Si_4Al_{13}$	*Si<0.3%* *Mg>2%* *Cr>0.1%* $(CrFe)Al_7$	*Si<2%* *Fe>0.3%* *Cu>1%* Cu_2FeAl_7
Mn	*Si<Mg* $(FeMn)Al_6$	*Si>2Mg* $(FeMn)_3Si_2Al_{15}$					
Cr	*Si<Mg* $(CrFe)Al_7$	*Si>2Mg* $(CrFe)_4Si_4Al_{13}$					
Cu	*Fe<Cu* $CuMg_4Al_6$	*Fe>Cu,* Mg<2% Cu_2FeAl_7					
Zn	*Zn<2%* in solid soln.	*Zn>2%* Mg_3ZnAl_2					

In 1997, Blanc and Mankowski [64] worked on susceptibility of 6065 T6 Aluminum Alloys (French equivalent of the 6013 T6 Alloy) to pitting corrosion. It was discovered that regardless of the potential used, there was no significant dissolution of the coarse particles, no deposition of alloying elements and no alloying enrichment of the passive film for the 6065 alloys as compared to 2024 alloy that is being used for the same application.

A year later, 1998, Blanc et al [65] introduced another approach by which behavior of coarse intermetallic particles in 6065 Aluminum alloy can be determined. The study they carried out in 1997 was basically based on scanning electron microscopy (SEM) observations only. The new approach involved the use of phase shifting interferometric microscopy. The specimens were immersed in a sulphate solution before carrying out the study. Their results show that AlMg-Si-containing particles largely dissolved in the overaged alloy whereas the dissolution of this compound was very low for the 6065 T6 alloy.

Grigoris et al [66] investigated the pitting behavior of AA 2024/SiC_p composites using variable fraction of SiC particles. They found out that pitting potential is unaffected by the presence and volume fraction of SiC particles in AA2024/ SiC_p composites. They also observed that the SiC_p/ aluminum alloy matrix interface is not a preferential passive film breakdown site. Failure of the protective oxide film occurs rather in copper depleted areas, which serves as local anodes in the microstructure of the materials.

Behavior of localized corrosion of 6065 T6 aluminum alloy in chloride media was investigated by Valerie Guillaumin and Georges Mankowski [67].

Their results, concerning pit formation, agreed quite well with what Szkarska obtained in 1999 but formation of intergranular form of corrosion was also noticed. They observed that these two forms of corrosion seem tobe dependent on each other since intergranular corrosion starts on pit walls. It was also understood that coarse intermetallic Al-Si-Mg containing particles were strongly reactive in 1M NaCl solution and seem to be nucleation sites for pits and consequently for intergranular corrosion. They concluded that intergranular corrosion mechanism of 6065 T6 alloy consists of preferential dissolution of the anodic Cu and Si depleted zone along grain boundaries whereas Si-Mg-Cu rich intergranular precipitates function as local cathodes and stimulate the electrochemical attack of this depleted zone.

Ahmad Zaki et al [84] studied the mechanism of localized corrosion of aluminum-silicon carbide composites in a chloride-containing environment. They found that SiC/Al 6013 interface is the preferred site for breakdown of protective film of α-AlOOH and α-$Al(OH)_3$ and increased dislocation generation at this interface contributes significantly to increased surface activity.

Modi et al [68] carried out a research on the role of alloy matrix on corrosion behavior of cast Aluminum alloy composites. They reported that corrosion loss of the composites was higher than that of the corresponding matrix alloys. They observed that graphitic aluminum alloy showed higher material loss than the composite containing SiC.

Behavior of pit in Aluminum Alloy 2024 was studied by Liao et al [69]. This is necessary to understand clearly the importance of intermetallic constituent

particles in pit formation of Aluminum alloys. They reported that pitting corrosion is promoted by galvanic coupling between the alloy matrix constituent particles. Two categories of particles-induced pitting corrosion were clearly identified general pitting (occurs at isolated surface particles) and severe pitting (developsat subsurface particle clusters). Particles are therefore contributed not only to pit initiation but also to pit growth.

It was established by Sato et al [70] that the barrier film formed on Al or Al alloys is of a duplex nature. It consists of an inner layer of adherent, compact, closed, and very stable oxide film covered with an outer porous and less stable layer that is more susceptible to corrosion.

It was reported by Chen and Mansfeld [71], in a research on corrosion protection of Al 6092/SiC_p metal matrix composite, that the failure of several corrosion and new environmentally acceptable methods of protection is most likely due to interfaces created during manufacture of the Al 6092/SiC_p MMC. These areas are highly susceptible to localized corrosion.

Trzaskoma et al [72], examined the effect of silicon carbide (whiskers), SiC_w, on the corrosion behavior of three SiC_w – aluminum (Al) composites in 0.1M sodium chloride (NaCl). They found out that pit initiation susceptibility was the same for the SiC_w – Al 6061 (UNS A96061) and SiC_w – Al 5456 (UNS A95456) composites as for their corresponding base matrices. However, SiC_w – Al2024 composite (UNS A92024) showed a greater propensity to pit initiation than wrought Al alloy.

In a later study, Trzaskoma reported that pits initiated at the secondary phases such as intermetallic compounds in SiC_w Al 5456 [73]. Whisker reinforcement enhanced precipitation of the intermetallics, and more pits nucleated on the composite. Trzaskoma reported that the interfacial regions were not preferred sites for pitting but Aylor and Moran [74] found preferential attack at the matrix-reinforcement interface.

Sun et al [75] investigated the effect of reinforcement volume fraction on the corrosion behavior of SiC particulate (SiC_p) – Al 6061. The authors pointed out that, although the extent of pitting in SiC_p increased with increasing SiC_p, the amount of pitting was not commensurate with the volume fraction of intermetallic compounds. This finding suggested the presence of secondary phases was not the only factor in the increased corrosion susceptibility of discontinuously reinforced metal-matrix composites.

Experiments on the corrosion behavior of as-cast, silicon carbide particulates, aluminum alloy metal-matrix composite were conducted by Buazaiga and Thorpe [76] using pit propagation rate (PPR) technique. They found out that the most susceptible pitting site determined by PPR testing on the unreinforced alloy occurred at the Al-$FeMg_3Si_6Al_8$ interface as a result of the formation of a local galvanic cell. In composite alloy, the most susceptible pitting sites determined by PPR testing occurred at the SiC-Si, SiC-Al, and Al-$FeSiAl_5$ interfaces. The change in microstructure caused by the addition of SiC particulate reinforcement produced a change in the pitting corrosion mechanism.

Griffiths and Turnbull [77] investigated the electrochemical polarization behavior of 6061 Aluminum metal matrix composites. They found out that there is no galvanic interaction between the SiC and Al alloy in a SiC/ 6061 Al. They concluded by saying that there is no apparent general effect of SiC reinforcement on the electrochemical polarization behavior of 6061 Al. The effect of reinforcement is a specific function of the environmental conditions and the processing route.

As reported by Garrard [78], corrosion behavior of boron, graphite, aluminum oxide and silicon carbide containing aluminum composites has been investigated by many researchers. Boron composites were found to suffer from interfacial attack at the matrix-matrix interface due to crevice and galvanic corrosion. Severe galvanic corrosion was observed in aluminum – graphite composites as a result of large potential difference established between the graphite and the matrix, whereas segregation of magnesium near the fibers in aluminum –aluminum oxide composites caused attack to occur at the interface. In silicon carbide composites, pitting was the primary type of attack.

Garrard [78] in his own experimental work on the corrosion behavior of Aluminum silicon carbide composite in aerated 3.5% NaCl provided another contribution to the previous researches. He observed that exposure of SiC fibers in 6061-SiC enhanced the corrosion rate of the composite relative to the matrix material (aluminum alloy 6061). Pitting was found to occur on the 6061 alloys, while for the composite preferential crevice and pitting attack occurred around the fibers or crevice corrosion took place in the voids or fractures.

Aylor and Moran [74] studied the 6061 –silicon carbide composite and the 6061 alloy and concluded that: (1) processing forms and heat treatments did not affect the polarization behavior of the composite or matrix alloy, (2) silicon carbide did not increase the pitting susceptibility of the composite and (3) pitting morphology differed between the composite and the matrix. They observed that the formation of aluminum carbide during processing lead to the marked corrosion susceptibility of this composite rather than galvanic coupling.

CHAPTER 3

3. MATERIALS AND TESTING ENVIRONMENT

3.1 Material

Four different types of Aluminum metal matrix composite were used as experimental materials. The compositions of these alloys are shown in Table 3.2. Two of these alloys were reinforced with SiC particles. In each case, the reinforcement has chemical composition of at least 98% SiC with particle size distribution of 12.8μm ± 1.0μm.

3.2 Mechanical Properties of the Materials Used

Mechanical properties of five different alloys used are shown in Table 3.1. Properties considered include Ultimate Tensile strength, Modulus of Elasticity, Yield strength, and percentage elongation. Condition used during the manufacturing process for each material is also indicated.

Table 3.1: Mechanical Properties of Materials used

Alloy Identification	Ultimate Tensile Strength (MPa)	Modulus of Elasticity (GPa)	Yield Strength (MPa)	Elongation %	Temper
F3S.00S	324	87	262	0.6	T6
F3S.20S	359	98.6	338	0.4	T6
F3K.00S	240	94	172	0.3	T5
F3K.20S	283	101	269	0.2	T5

T5: Artificially aged only
T6: Solution heat treated and artificially aged

Table 3.2: Composition of the alloys used

Alloy Identification	% Composition											
	Si	Fe	Cu	Mn	Ni	Ti	Zn	Sr	Pb	Others	Al	SiC
F3S.00S	9.5-10.5	0.8-1.0	3.0-3.5	0.5-0.8	1.0-1.5	0.2max	0.03	0.005-0.015	.	0.1	Remain	
F3S.20S	9.5-10.5	0.8-1.0	3.0-3.5	0.5-0.8	1.0-1.5	0.2max	0.03	0.005-0.015	.	0.1	Remain	19.0-22.0
F3K.00S	9.5-10.5	0.2max	2.8-3.2	0.8-1.2	1.0-1.5	0.20max	0.05	.	.	0.1	Remain	.
F3K.20S	9.5-10.5	0.2max	2.8-3.2	0.8-1.2	1.0-1.5	0.20max	0.05	.	.	0.1	Remain	18.0-22.0

3.3 Testing Environment

3.5wt % NaCl solution in deareated condition was used throughout the experiment. De-aration was carried out by passing nitrogen, (N_2), through the solution. This continued until the solution became saturated with 99.5%.

3.4 Sample Dimensions

For weight loss study, square sample of 20mm x 20mm were used from each material-type being analyzed. The exposed area was 9.6cm^2. Potentiodynamic and cyclic polarization studies were performed on circular samples of 16mm diameter. The exposed area of the sample was 1cm^2. The same sample dimension was used for micrograph analyses (Optical Micrography, X-Ray Diffraction (XRD), X-Ray Fluorescence (XRF), Scanning Electron Micrograph, SEM).

CHAPTER 4

4. METHODOLOGY

4.1 Weight Loss Studies in Static Condition

4.1.1 Introduction

Effect of corrosion on the alloys was evaluated by weight-loss method. The amount of metal removed is determined by weighing the specimen before and after exposure. The corrosion rate is calculated from the weight-loss and exposure time data. The alloys used were exposed to 3.5wt % NaCl solution. The experiment was carried out according to the ASTM standard G31-72 [85].

4.1.2 Experimental Procedure

4.1.2.1 Apparatus

The specimens were suspended in 3 liters PVC containers by fluorocarbon plastic strings. The vessels were covered to prevent contamination and also to minimize liquid loss due to evaporation. The set-up is illustrated in Figure 4.1. The vessels were positioned in a wooden shelf at room temperature.

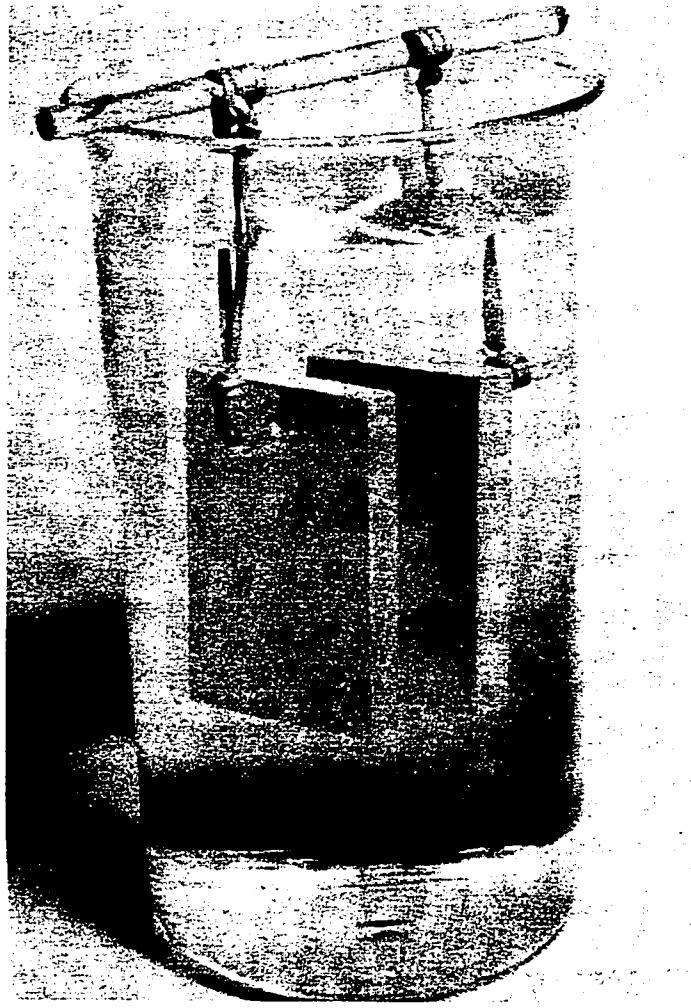

Figure 4.1: Experimental Set-up for weight loss study

4.1.2.2 Test Specimen

Duplicate samples from each alloy measuring 20mm x 20mm were used. The exposed surface area of the specimen was calculated with an accuracy of ±1%. Grinding and polishing processes were performed on all the specimens to remove some minor scratches present on the surfaces.

4.1.2.3 Specimen Preparation

The samples were washed in a hot detergent for five minutes and then rinsed with distilled water. The samples were then exposed to solution containing potassium dichromate, 28ml of phosphoric acid and de-mineralized water to make 1 liter of solution and then degreased. Cleaning was performed in ultrasonic cleaner in distilled water.

The samples were then dried in desiccator for 24 hours after cleaning. The dried samples were weighted in an analytical balance with an accuracy of± 0.5 mg. After each test period, the corroded samples were treated with the same solution of potassium dichromate and phosphoric acid to remove corrosion products without damaging the surface in accordance with ASTM standard G5-72 [85]. The samples were ultrasonically cleaned. The samples were dried in a desiccator for 24 hours and the dried samples were weighed in an analytical balance.

4.1.2.4 Test Conditions

The samples were tested at room temperature within an accuracy of $\pm 3^{\circ}$C. The test solution level was kept above the samples, and evaporation losses compensated by periodically adding fresh solution. Weight loss was determined after every 200hours of exposure, and once taken out, the samples were not re-exposed. The maximum period of exposure was 1600 hours. As recommended by ASTM standard (G31-72) [85], the experiments were performed under static condition in de-aerated solution.

4.1.2.5 Evaluation of Corrosion Rate

The rate of corrosion (CR) was calculated by utilizing the following equation:

$$Corrosion\ Rate\ (CR) = {}^{(K*W)}\!/_{(A*t)}$$

Where:

K = Constant, and its value varies with the unit used for calculating corrosion rate. Different values of K are given in Table 4.1.

W = Weight Loss in grams

A = Exposed surface area of the specimen in cm^2

t = Time of exposure in hours

4.2 Electrochemical Test

4.2.1 Pitting Corrosion

Pitting is usually defined as localized corrosion of a metal surface, confined to a point or small area and takes the form of cavities. It is a serious problem for metals that show passivity. Pitting is one of the most important parameters by which performance of an alloy in seawater and similar environment is evaluated. Generally, corrosion process consists of a set of redox reactions, which are electrochemical in nature. Aluminum is oxidized at anodic sites and some species are reduced at cathodic sites. The following chemical equations show anodic and cathodic reactions:

Anodic Reaction:

$$Al \rightarrow Al^{+++} + 3e$$
$$Al + 3H^{+} + OH^{-} \rightarrow Al(OH)_3 3H^{+}$$

Cathodic Reaction:

$$O_2 + H_2O + 4e^{-} \rightarrow 4OH^{-} \quad \text{(in neutral solution)}$$

$$O_2 + 4H^{+} + 4e^{-} \rightarrow H_2O \quad \text{(in acid solution)}$$

Pits are formed at the anodic sites. Within a pit, oxygen is depleted due to restricted convection and metal dissolution continues to take place by creating acidic conditions. The process of anodic dissolution shown in Figure produces an excess of positive ions (metal ions). In order to neutralize charge, migration of anions (Cl^{-}, Br^{-}, I^{-}) take place in the interior pit, which results in the

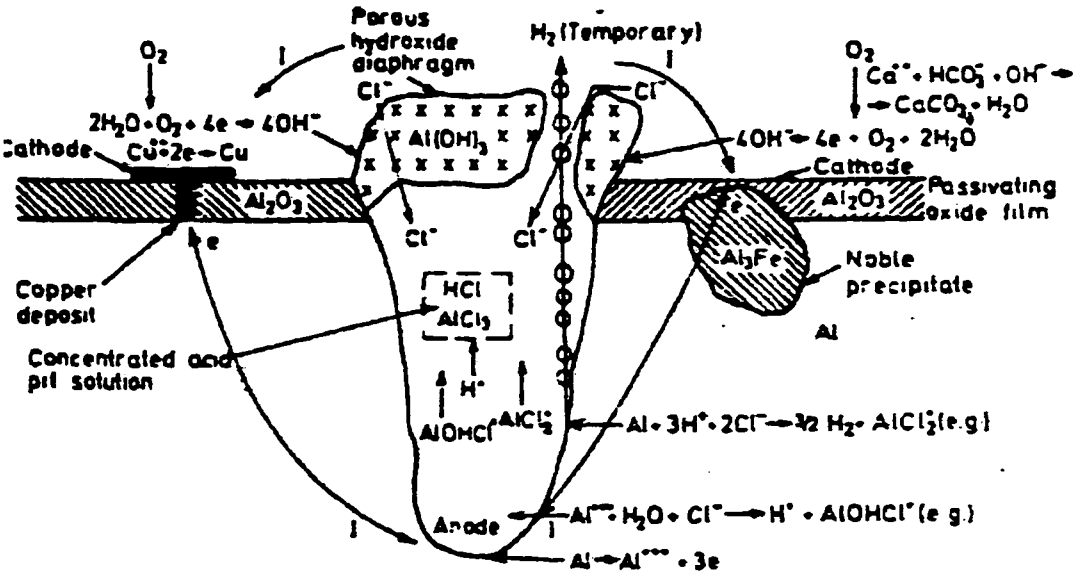

Figure 4.2: Process of Anodic Dissolution

formation of metal chlorides (M^+Cl^-). As shown in the equation, hydrolysis process is sequentially obtained.

$$M^+Cl^- + H^+|H^+OH^- \rightarrow MOH + H^+ + Cl^-$$

The production of H^+ and Cl^- accelerates the process of dissolution. In this process the solution becomes acidic and the pit continues to grow. In spite of depletion of oxygen, the process of dissolution continues within the pit. The pitting process, is therefore, termed as "autocatalytic", that is, once started it continues till the metal is perforated. In the process many new pits are inactivated because the inward migration of chloride ionizes insufficiently to offset the loss of corrosion products by diffusion and convection.

The outer surfaces of the pit are protected because of the migration of electrons from the pit interior. This is one reason why the surface of the metal adjacent to the pit does not corrode. Electrochemical techniques such as polarization curves and pitting scans are frequently used to evaluate and analyze pitting.

4.2.1.1 Potentiodynamic Polarization

The potentiodynamic Polarization technique is generally used to produce a qualitative picture or "fingerprint" of a substance in a given solution. It also detects any tendency of the substance to passivate. The potential range used to

produce the curve is often broad, ranging from -250mV (SCE) with respect to E_{corr} to +1.5 or more. Both Tafel and polarization analyses can be estimated based the selected potential regions and calculation performed on the data. Thus it is possible to get both qualitative and quantitative results from a single Potentiodynamic plot. Scan rate of about 2.5mV/s or slower is usually recommended in order to achieve current measurements that are close to steady state at each potential. Slow scans also ensure accumulation of enough data points for a high-resolution curve.

4.2.1.2 Cyclic Polarization

A Cyclic Polarization scan provides a qualitative view of pitting corrosion mechanisms. More specifically, a "pitting scan" (another name for the technique) can determine the tendency of a material to undergo surface pitting or crevicing when placed in a specific corrosive environment. The technique is particularly useful in the development of alloys that require a high degree of pit resistance.

The Cyclic polarization setup has much in common with the Potentiodynamic, Tafel Plot, and Polarization Resistance setups, except that it has the Apex (vertex) potential parameter to specify where you want the scan to reverse. Cyclic Polarization focuses on the behavior of a material in the vicinity of the critical anodic current density, that is, the point where the current begins to increase very rapidly as applied potential increases. The forward scan is followed

by a reverse scan back to the final potential, generally located between the apex potential and E_{corr}.

The resulting current-potential plot shows how readily the material will pit. If the reverse scan traces the same path as the forward scan in the region beyond the critical anodic current density, the material has little tendency to pit. If the current beyond the knee is lower on the forward scan, the material will be likely to pit. Repassivation of the pits may occur during the reverse scan, causing a lower current at each potential point than during the forward scan. The function traces a hysteris loop; the shape and position of the loop may indicate the material's pitting characteristics. A typical polarization plot is shown in Figure 4.3.

4.2.1.3 Experimental set-up

A potentiostat Model EG and G 273 A, interfaced with Pentium II computer was used to evaluate the pitting resistance of the alloys being investigated. A polarization cell consisting of a reference, auxiliary and working electrode was connected to the potentiostat, as shown in Figure 4.4. All potentials were measured with respect to a saturated calomel electrode (SCE). A high-density graphite electrode was used as a counter electrode. The working electrode comprised of the specimen holder, mounting rod and the electrode holder, as shown in Figure 4.4.

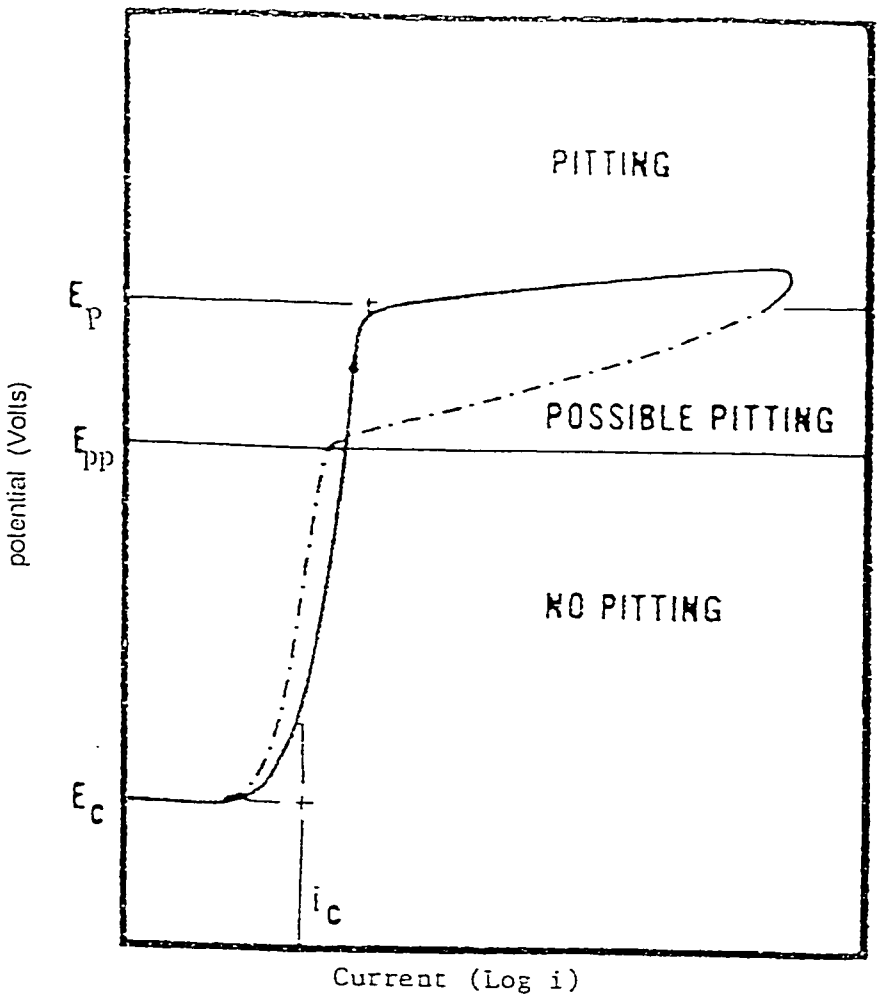

Figure 4.3: Typical Polarization Curve

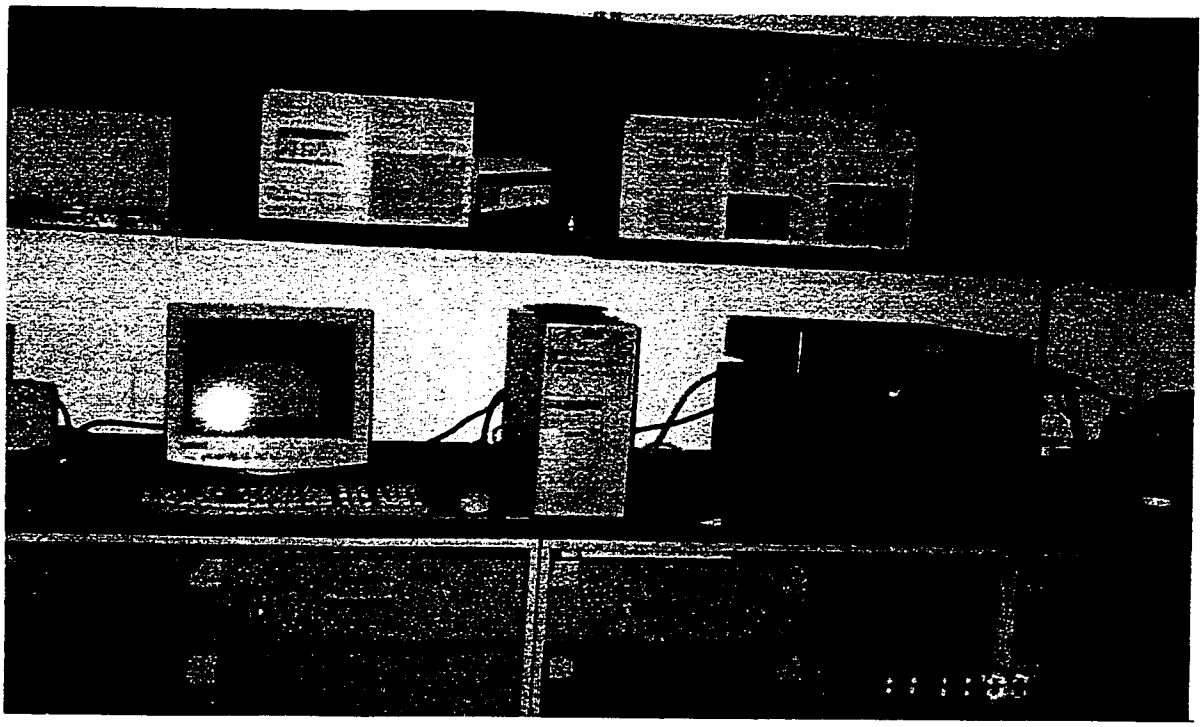

Figure 4.4: Experimental set-up for potentiodynamic and cyclic polarization

4.2.1.4 Specimen Preparation

Circular disk specimens of about 16mm from each of the alloys were grounded with a 320, 400 and 600 grit silicon carbide, in sequential order, to remove the coarse scratches. Polishing was carried out with a 0.3 micron, silicon carbide abrasive particles and final polishing was done with 0.05-micron abrasive particles. The specimens were then treated with boiling benzene and 5% acetic acid for five to ten minutes, rinsed in acetone, washed with demineralized water, air dried and stored in a desiccator for 24 hours prior to the commencement of experiment.

4.2.1.5 Polarization Procedure

Both potentiodynamic and cyclic polarization analyses were carried out under the same experimental conditions. Corrosion cell was filled with 35%wt of NaCl solution and the electrodes were connected accordingly to potentiostat (see figure 4.5). After maintaining a constant open circuit potential, experiment began. Initial potential, for potentiodynamic, was fixed at -0.25mV (SCE) with scan rate of about 0.5mV/s. Final potential was equally fixed at 0.8mV(SCE). For cyclic polarization analysis, forward scan was fixed from –0.5V to 1.5V (SCE) with scan rate of 5mV/s and reverse scan was fixed from 1.5V to -0.8V (SCE) with scan rate of 2.5mV/s. The pitting potential (Ep), in each case, was determined by the extrapolation of polarization curve. In cyclic polarization, the protection potential

(Epp) is represented by the intersection of the reverse polarization curve with forward anodic polarization curve.

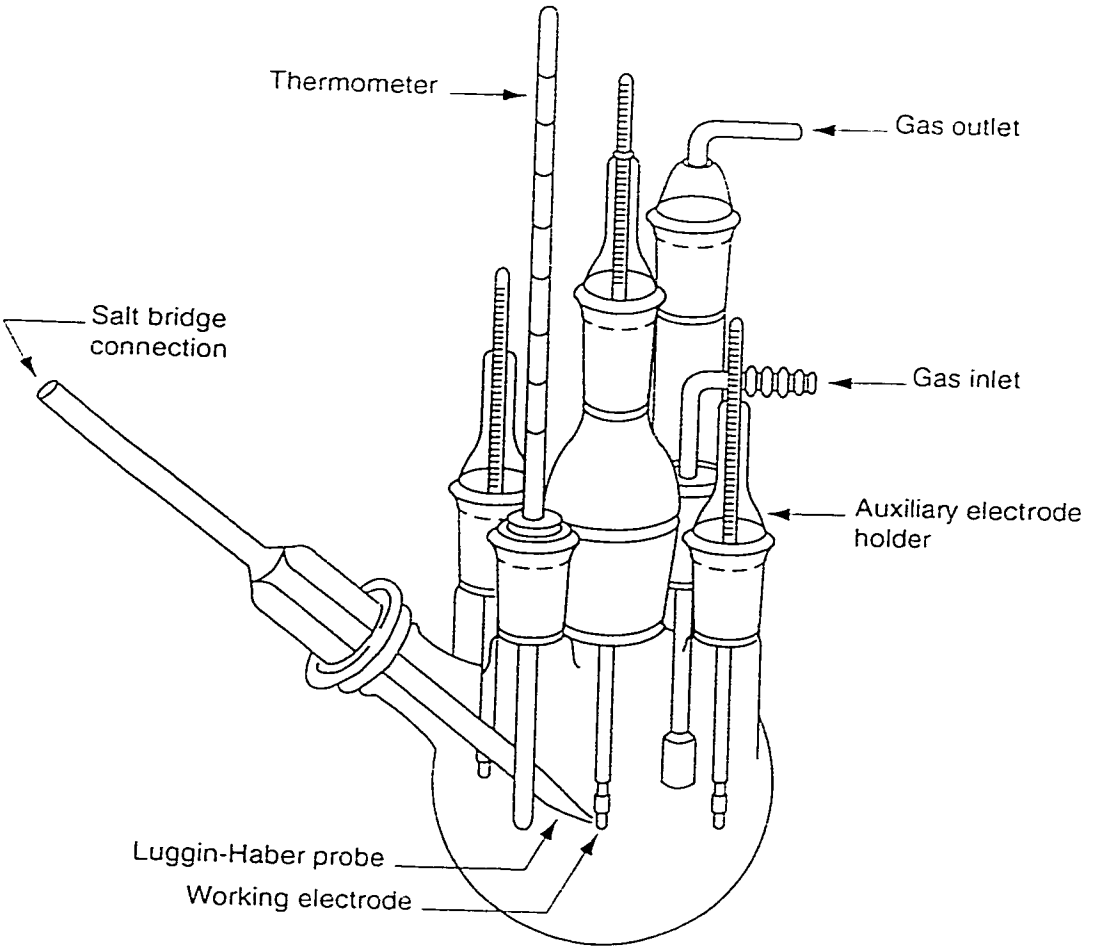

Figure 4.5: Corrosion Cell

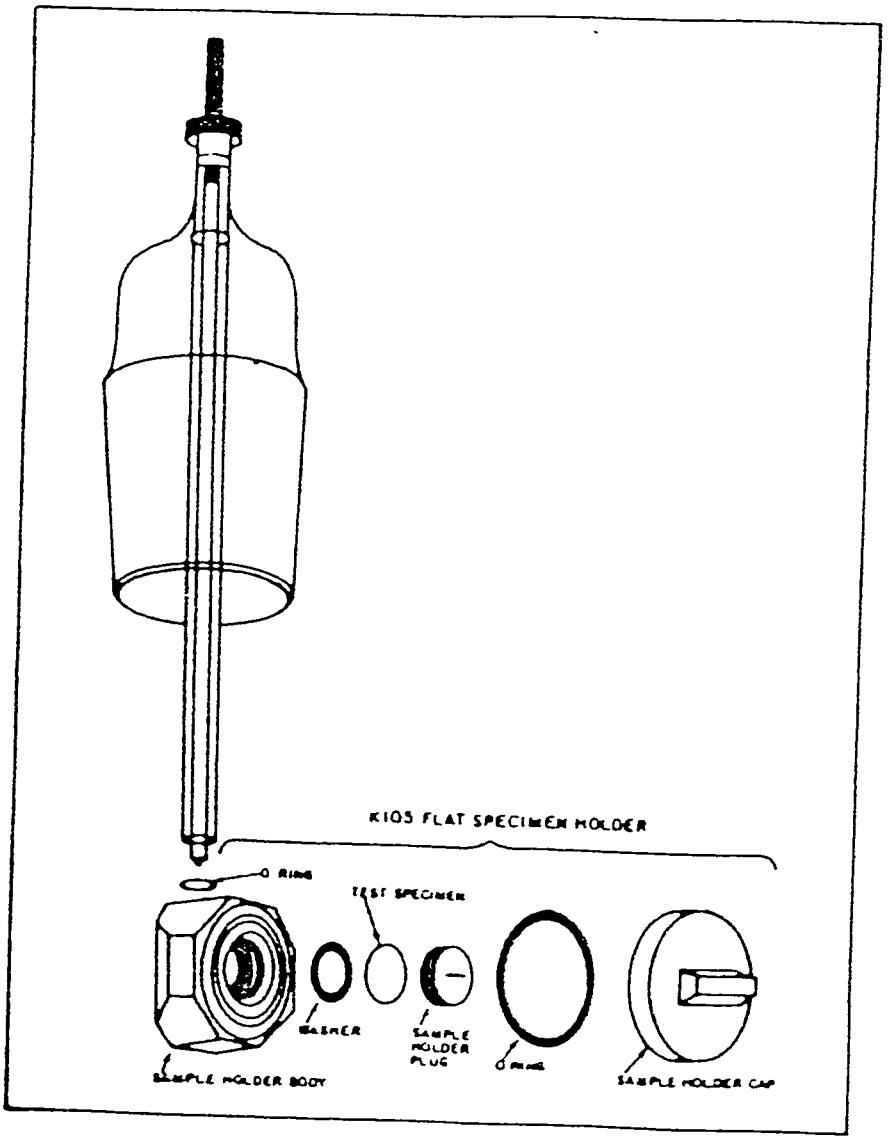

Figure 4.6: Working Electrode Diagram

CHAPTER 5

5. RESULTS AND DISCUSSION

Results obtained are sub-sectioned into three parts. The first part illustrates the results from weight-loss experiment while the second section analyses results from electrochemical studies. Micro-analytical studies are thoroughly presented and discussed in the third section of this chapter.

5.1 Results from Weight-Loss Experiment

The variation of corrosion rates as a function of exposure time in aerated condition in 3.5wt % sodium chloride solution for the four alloys used, F3S.20S, F3S.00S, F3K.20S and F3K.00S, are shown in figures 5.1 to 5.9. The results are summarized in Table 5.1 to 5.4.

By visualizing the shapes of the curves obtained, it was observed that all curves show an initial increase in corrosion rate with respect to time. At certain period of time, these curves attain their peak level after which there is sudden decrease in corrosion rate with respect to time. The later section of the curve shows a substantial, constant corrosion rates over a specified period of time. The initial behavior of this process can be attributed to the gradual response of aluminum alloy constituents to sodium chloride environment. This is necessary, especially for those alloys that show passivity, to counter the aggressive effect of

the environment. The oxide film does form at once but gradually on the surface, which explains the initial increase in corrosion rate with respect to time.

As soon as the protective film is formed, corrosion rate ceases to increase further. At certain stage, the protective oxide film undergoes frequent rupture, which leads to relatively constant corrosion rate with respect to time. This rupture phenomenon is assumed to have occurred due to residual tensile stresses created between the oxide film layer and aluminum matrix.

By simple interpretation of the result, F3S.20S alloy was found to have its maximum corrosion rate of about 2.0797mpy after 800hrs of exposure. On the other hand, F3S.00S alloy had maximum corrosion rate of 1.4639mpy after 1400hrs. These results show that F3S.00S alloy forms a protective layer of oxide earlier than its reinforced counterpart. The same trend of results was observed in F3K.00S and F3K.20S alloys. Here, F3K.20S alloy had its maximum corrosion rate of 3.898mpy after 1000hrs and F3K.00S alloy had its maximum corrosion rate of 2.565mpy after 600hrs. With these results, F3K.00S alloy forms protective film earlier enough before F3K.20S alloy.

In order to fulfill one of the main objectives of this research work, adequate comparison was made between unreinforced alloys, F3S.00S and F3K.00S, and their respective reinforced counterparts, F3S.20S and F3K.20S alloys. It is believed that alloy with least corrosion rate will definitely be the alloy with highest corrosion resistance. By comparing the four alloys used, F3S.00S has the least corrosion rate, which makes it an alloy with highest corrosion resistance (figure). For this reason, it is the most suitable alloy that can be used, among the four alloys

used, in sodium chloride environment. In another form of comparison, reinforced alloys (F3S.20S and F3K.20S) possess less corrosion resistance characteristics when compared to their respective unreinforced counterparts, F3S.00S and F3K.00S alloys (Figures 5.7 and 5.8). Based on these observations, it is also agreed, with what other researchers have previously investigated, that alloys reinforced with SiC show less corrosion resistance, though higher strength, than unreinforced alloys of the same material.

Table 5.1: Weight Loss Result for F3S.20S Alloy

Sample	Initial Weight *(gm)*	Final Weight *(gm)*	Exposure Time *(Hours)*	Weight Loss *gm*	Weight Loss Average*(gm)*	Corrosion Rate	
						mpy	*mm/yr*
1a	2.2513	2.2491	200	0.0023	0.00185	1.2312	0.03126
1b	2.1521	2.1507	200	0.0014			
2a	2.3312	2.3276	400	0.0036	0.004	1.331	0.033796
2b	2.0386	2.0342	400	0.0044			
3a	2.2622	2.2549	600	0.0073	0.008	1.7747	0.04506
3b	2.2082	2.1995	600	0.0087			
4a	2.288	2.2818	800	0.0118	0.0125	2.0797	0.0528
4b	2.037	2.0302	800	0.0132			
5a	2.1145	2.1065	1000	0.008	0.0108	1.4442	0.03667
5b	1.9568	1.9431	1000	0.0137			
6a	1.6444	1.6334	1200	0.0138	0.0126	1.3976	0.03549
6b	2.1081	2.0967	1200	0.0114			
7a	2.0485	2.041	1400	0.0143	0.0142	1.35	0.03428
7b	2.0203	2.0103	1400	0.0141			
8a	1.6958	1.654	1600	0.0104	0.01575	1.31022	0.03327
8b	2.1166	2.0955	1600	0.0211			

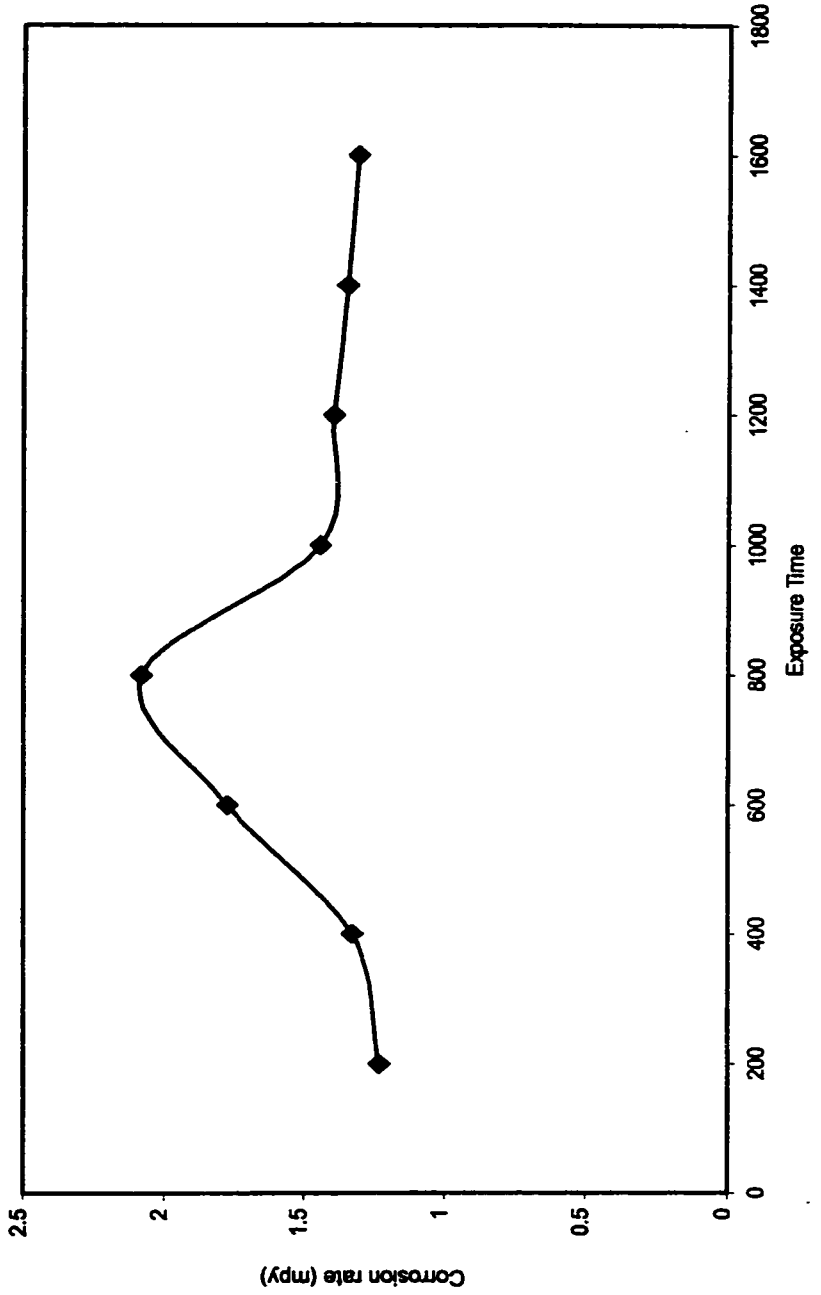

Figure 5.1: Graph of Corrosion Rate vs Exposure Time for F3S.20S Alloy

Table 5.2: Weight Loss Result for F3S.00S Alloy

Sample	Initial Weight *(gm)*	Final Weight *(gm)*	Exposure Time *(Hours)*	Weight Loss *gm*	Weight Loss Average*(gm)*	Corrosion Rate	
						mpy	*mm/yr*
1a	2.3056	2.3050	200	0.0003	0.0002	0.1331	0.0034
1b	2.5214	2.3521	200	0.0001			
2a	2.5926	2.5922	400	0.0004	0.0006	0.1997	0.0052
2b	2.4326	2.4318	400	0.0008			
3a	2.3178	2.3138	600	0.0004	0.0014	0.3105	0.0078
3b	2.2581	2.5557	600	0.0024			
4a	2.3889	2.3871	800	0.0018	0.0033	0.5488	0.0139
4b	2.6414	2.6366	800	0.0048			
5a	2.4413	2.4350	1000	0.0063	0.0084	1.1180	0.0284
5b	2.3340	2.3235	1000	0.0105			
6a	2.6640	2.6515	1200	0.0125	0.0132	1.4639	0.0372
6b	2.5322	2.5183	1200	0.0139			
7a	2.5627	2.5539	1400	0.0088	0.0097	0.9220	0.0234
7b	2.4482	2.4376	1400	0.0106			
8a	2.3244	2.3176	1600	0.0063	0.0072	0.5990	0.0152
8b	2.4148	2.4067	1600	0.0081			

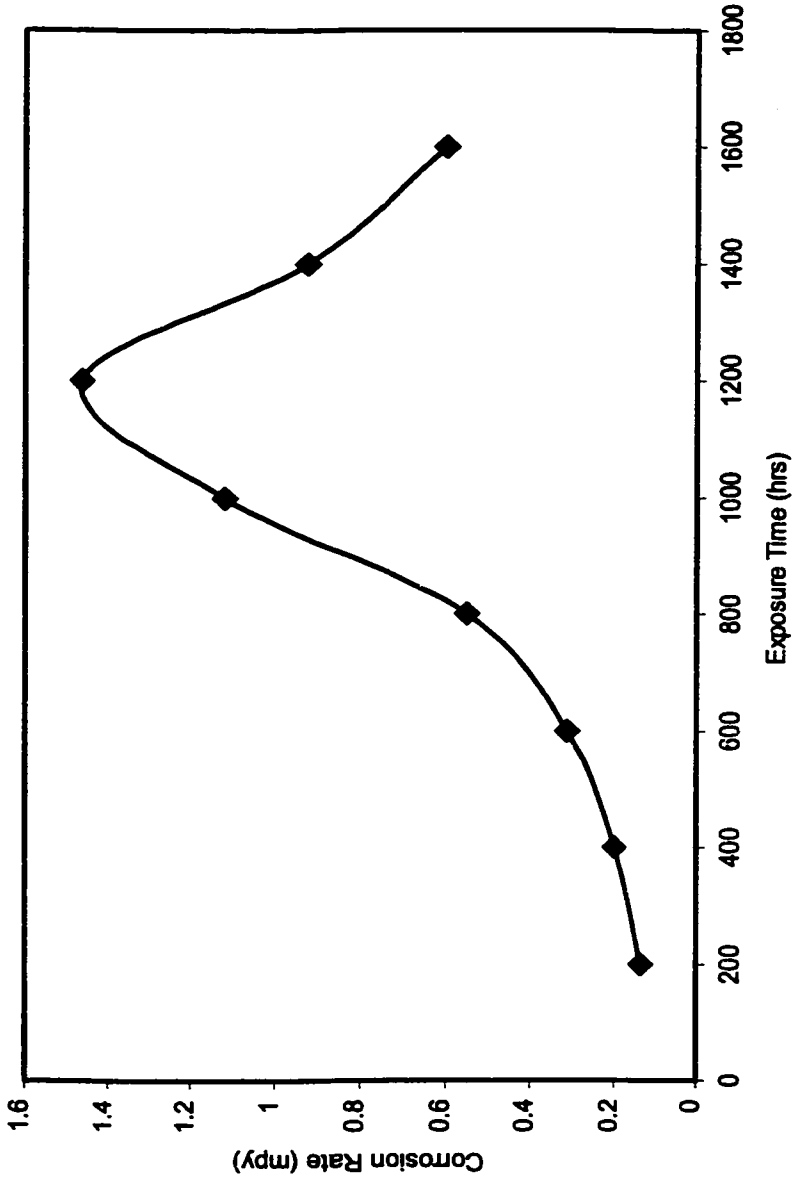

Figure 5.2: Graph of Corrosion Rate vs Exposure Time for F3S.00S Alloy

Table 5.3: Weight Loss Result for F3K.20S Alloy

Sample Identification	Initial Weight *(gm)*	Final Weight *(gm)*	Exposure Time *(Hours)*	Weight Loss *gm*	Weight Loss Average*(gm)*	Corrosion Rate	
						mpy	*mm/yr*
1a	3.7818	3.7776	200	0.0042	0.0038	1.3289	0.0338
1b	3.7624	3.7590	200	0.0034			
2a	3.8186	3.8176	400	0.0010	0.0045	1.4974	0.0380
2b	3.4351	3.4271	400	0.0080			
3a	3.7098	3.7046	600	0.0052	0.0062	1.5752	0.0400
3b	3.6782	3.6710	600	0.0072			
4a	3.8286	3.8095	800	0.0191	0.0184	2.0599	0.0523
4b	3.7230	3.7053	800	0.0177			
5a	3.6633	3.6177	1000	0.0456	0.0368	3.8981	0.0990
5b	3.5787	3.5507	1000	0.0280			
6a	3.7466	3.7142	1200	0.0324	0.0232	1.5728	0.0399
6b	3.7924	3.7784	1200	0.0140			
7a	3.6782	3.6620	1400	0.0162	0.0128	1.2169	0.0309
7b	3.6446	3.6352	1400	0.0094			
8a	3.5896	3.5774	1600	0.0122	0.0106	0.8818	0.0224
8b	3.7248	3.7158	1600	0.0090			

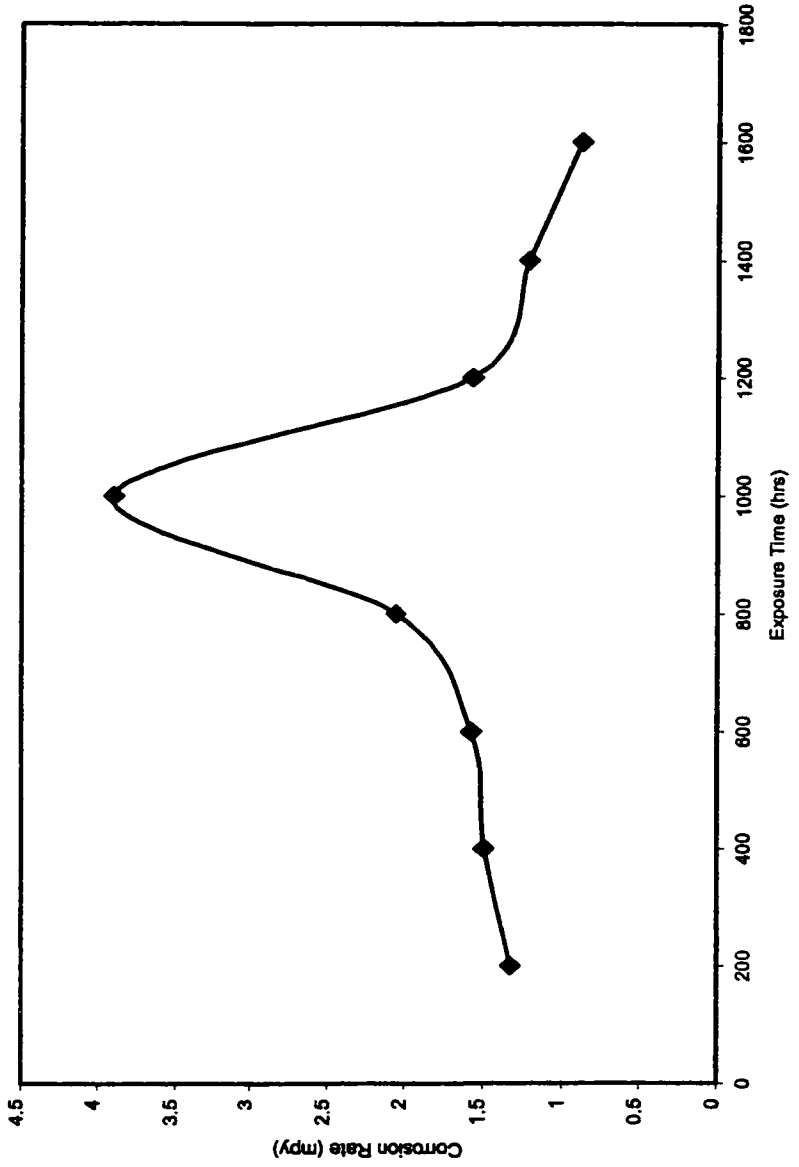

Figure 5.3: Graph of Corrosion Rate vs Exposure Time for F3K.20S Alloy

Table 5.4: Weight Loss Result for F3K.00S Alloy

Sample Identification	Initial Weight *(gm)*	Final Weight *(gm)*	Exposure Time *(Hours)*	Weight Loss *gm*	Weight Loss Average*(gm)*	Corrosion Rate	
						mpy	*mm/yr*
1a	3.8864	3.8831	200	0.0033	0.0019	0.2454	0.0062
1b	3.6789	3.6784	200	0.0005			
2a	3.9477	3.9468	400	0.0009	0.0052	0.7303	0.0185
2b	3.8280	3.8185	400	0.0095			
3a	3.7843	3.7798	600	0.0482	0.0296	2.5653	0.0651
3b	3.8346	3.8236	600	0.0110			
4a	4.1475	4.1306	800	0.0169	0.0312	2.1886	0.0556
4b	3.7898	3.7442	800	0.0456			
5a	3.8175	3.8073	1000	0.0102	0.0092	0.4224	0.0107
5b	3.9210	3.9128	1000	0.0082			
6a	4.0978	4.0892	1200	0.0086	0.0064	0.3985	0.0101
6b	4.1064	4.1022	1200	0.0042			
7a	3.9089	3.9025	1400	0.0064	0.0050	0.2456	0.0062
7b	4.0960	4.0924	1400	0.0036			
8a	3.7520	3.7488	1600	0.0032	0.0041	0.2325	0.0059
8b	3.8820	3.8770	1600	0.0050			

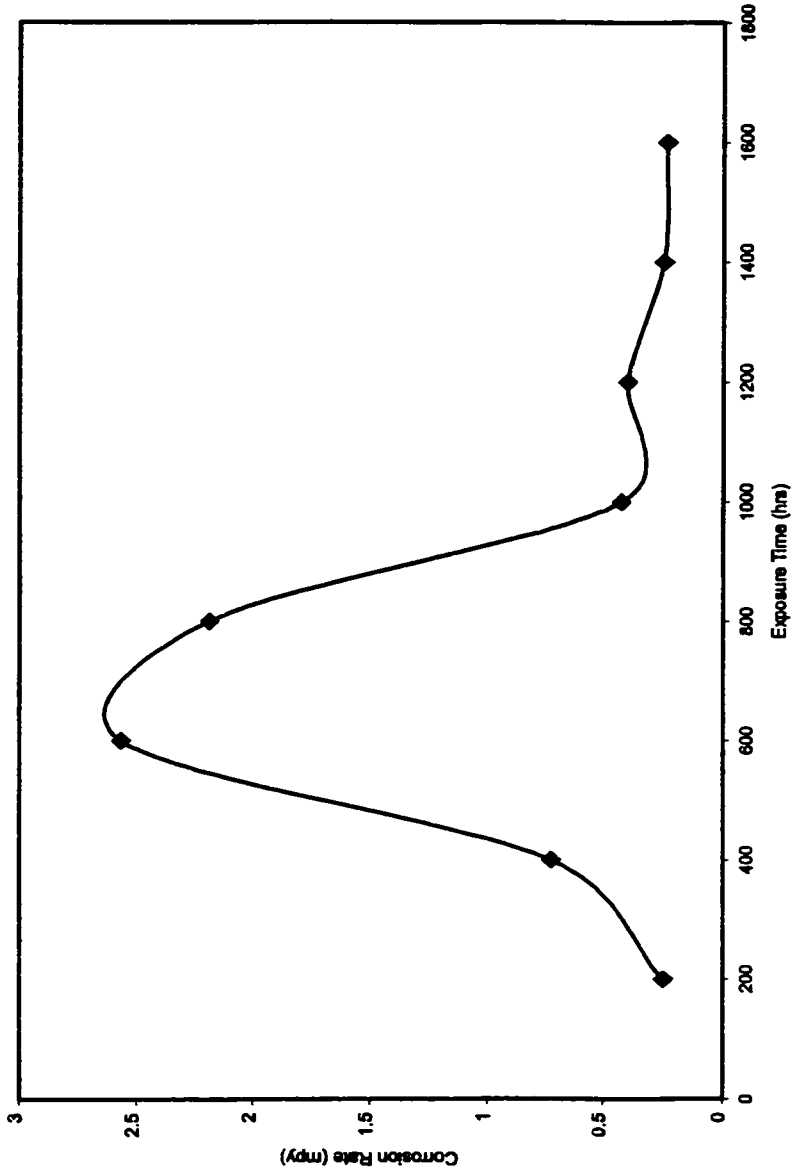

Figure 5.4: Graph of Corrosion Rate vs Exposure Time for F3K.20S Alloy

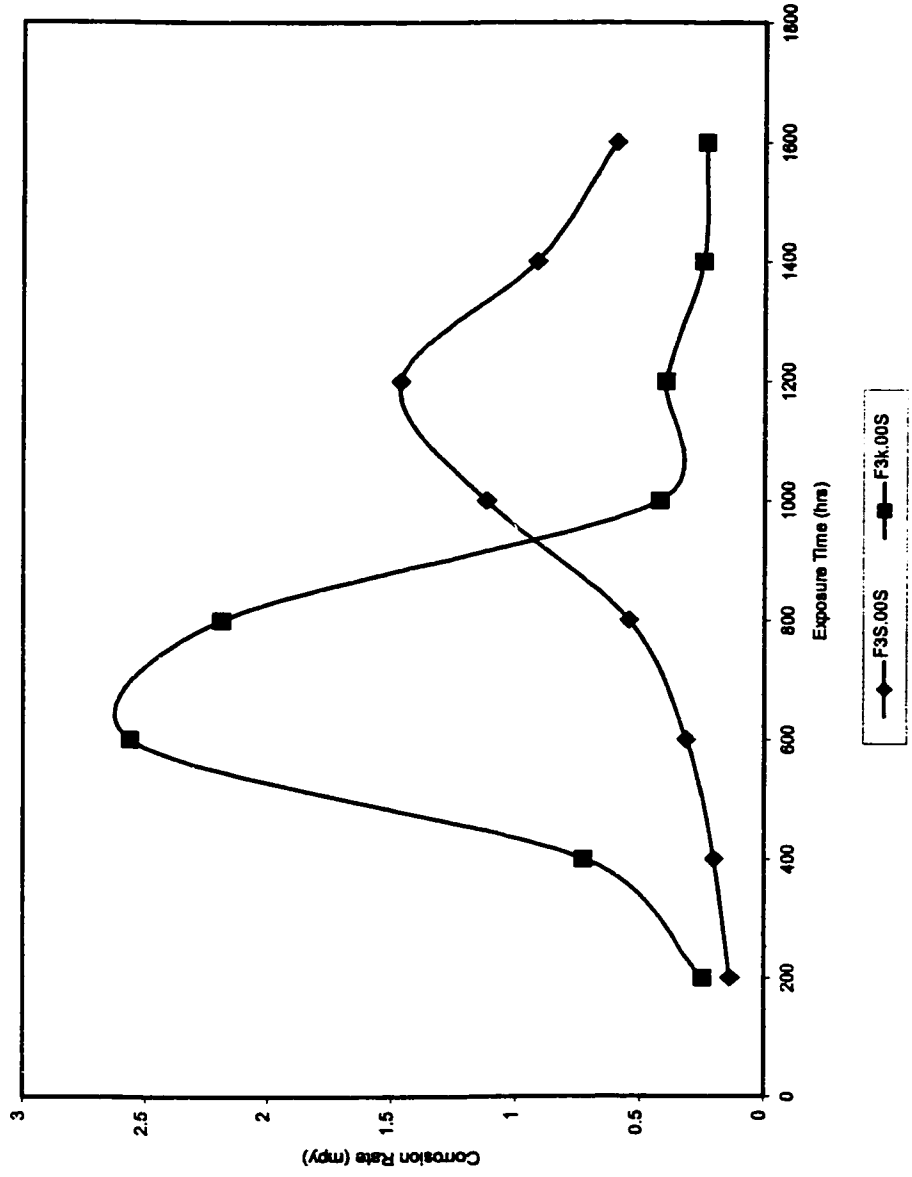

Figure 5.5: Comparison of Corrosion rate vs Exposure Time graphs for F3S.00S and F3K.00S

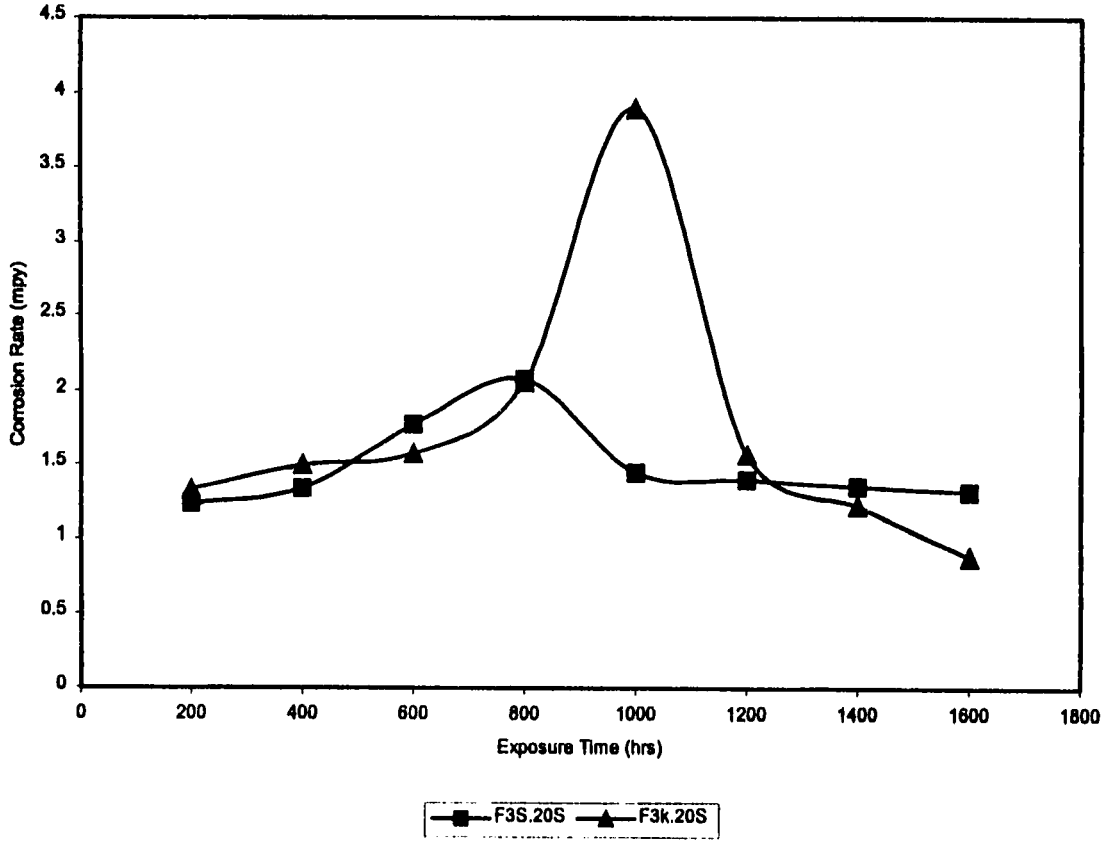

Figure 5.6: Comparison of Corrosion Rate vs Exposure Time graphs for F3S.20S and F3K.20S

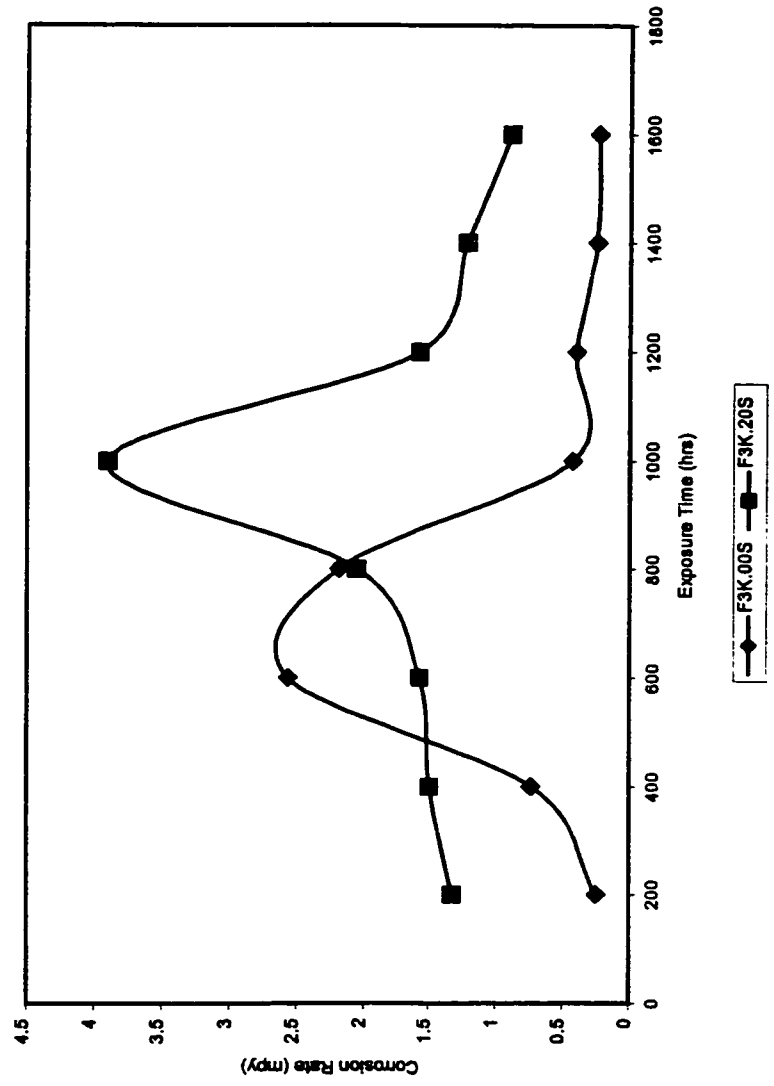

Figure 5.7: Comparison of Corrosion rate vs Exposure Time graphs for F3K.00S and F3K.20S

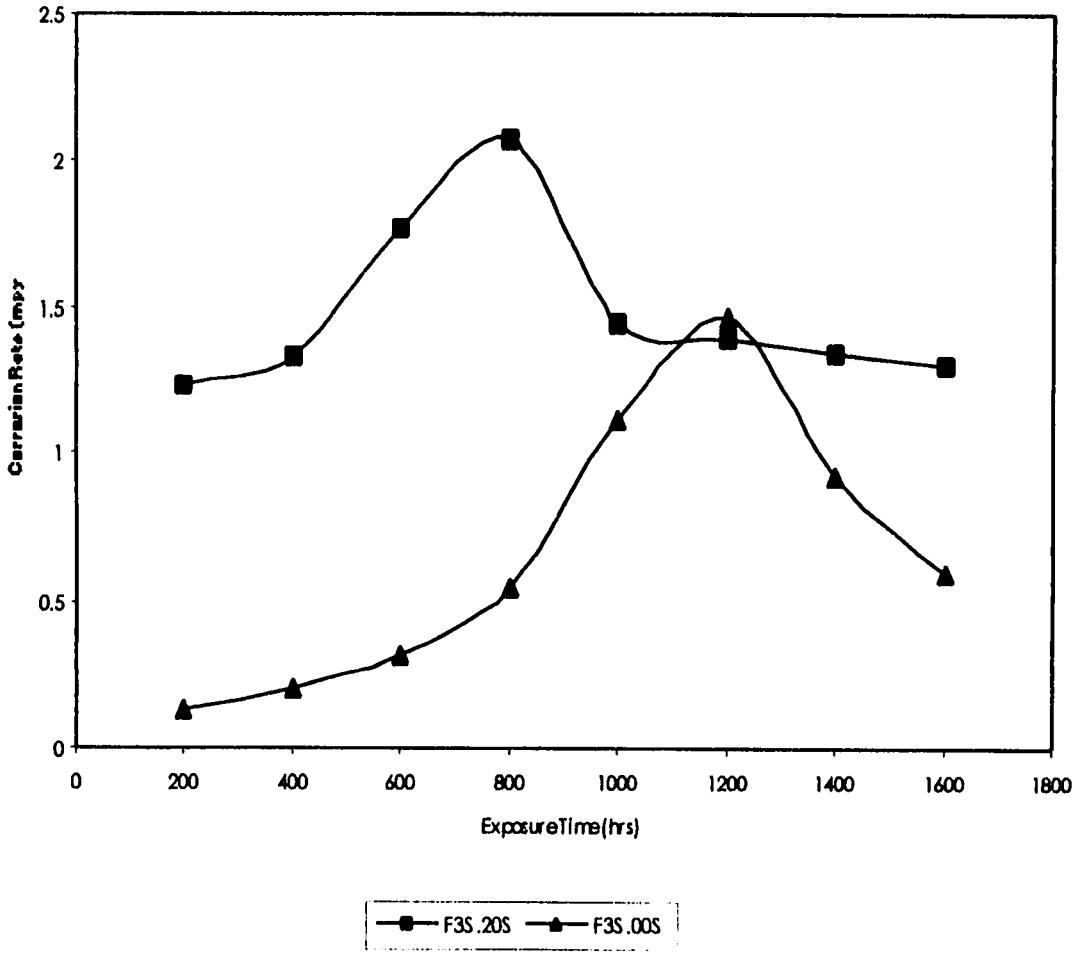

Figure 5.8: Comparison of Corrosion rate vs Exposure Time graphs for F3S.00S and F3S.20S

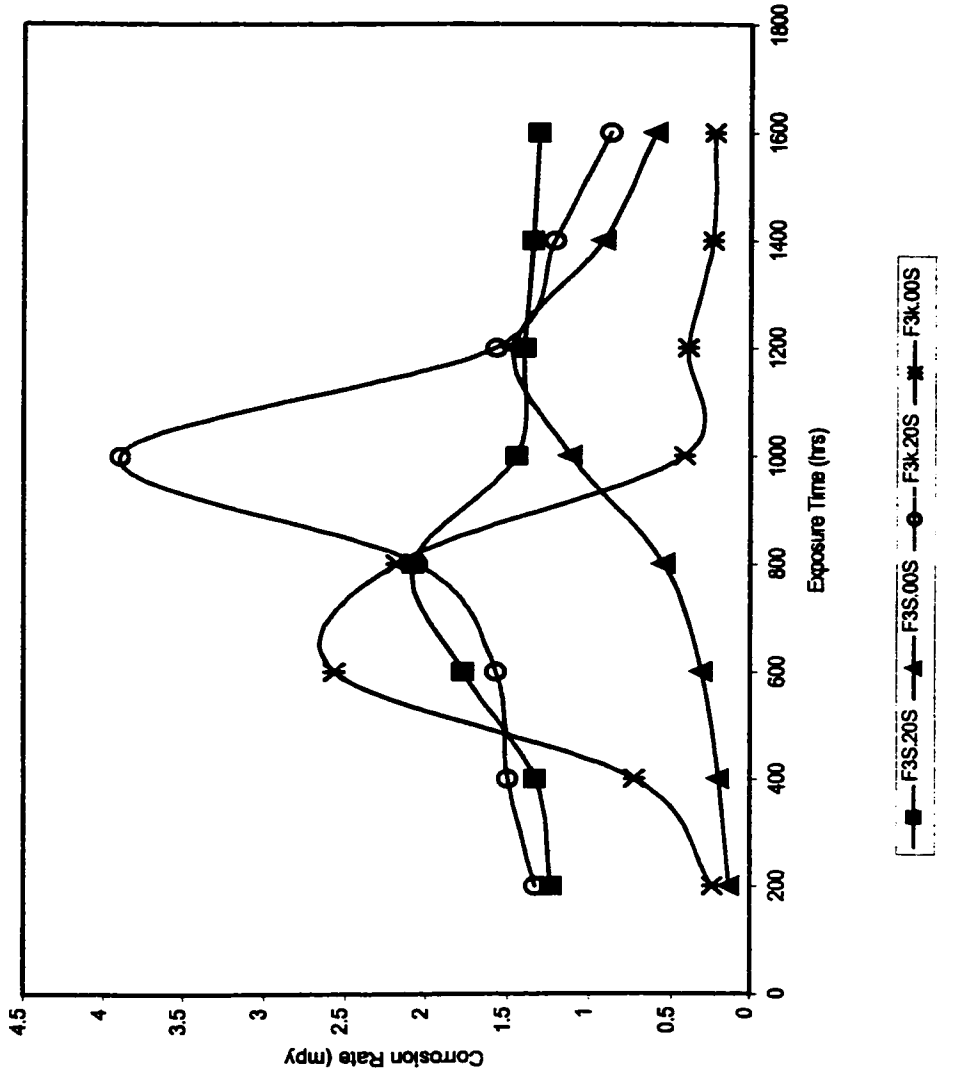

Figure 5.9: Comparison of Corrosion rate vs Exposure time graphs for the Four alloys used

5.2 Electrochemical Studies: *Potentiodynamic and Cyclic Polarization Techniques*

Summary of the results obtained in electrochemical studies is illustrated in subsequent pages. The results obtained by potentiodynamic method in dearated condition are summarized in Tables 5.10 to 5.14. From cyclic polarization test, the results obtained are summarized in Table 5.9 and hysteris loops obtained from respective techniques, potentiodynamic and cyclic polarization, are shown in figures 5.10 to 5.26.

5.2.1 Potentiodynamic Technique

In potentiodynamic polarization studies, three different experiments are run for each of the alloys at room temperature. This is necessary to achieve reproducibility of the results under the same experimental conditions. Open circuit potential (OCP), representing the point at which the rate of oxidation equals the rate of reduction, was found to be in the range of -0.500V and –0.557V for F3S.00S alloy. This range indicates the stability region of corrosion potential of this particular alloy. Open circuit potential was ranged between –0.683V and –0.765V for F3S.20S. It was also found to be in the range of -0.483V to –0.549V and –0.497V to –0.564V in F3K.00S and F3K.20S respectively.

Under potentiodynamic studies, two important approaches were used to estimate the corrosion rate of each of the alloys used. These methods include Tafel

and Polarization resistance. For convenience sake, only two units for corrosion rate were used in its computation. In contribution to the results obtained in weight-loss studies, F3S.00S alloy shows least corrosion rate (0.762mpy) as compared to other three alloys used, by using Tafel approach (Table 5.6). This is sequentially followed by F3K.00S (with corrosion rate of 0.936mpy), F3K.20S (with corrosion rate of 1.489mpy) and F3S.20S (with corrosion rate of 1.688mpy). Similar trend of result was observed with the use of polarization resistance technique. This result shows that F3S.00S alloy has the highest corrosion resistance capability while lowest magnitude of corrosion resistance is found in its reinforced counterpart, F3S.20S alloy.

5.1.1 Cyclic Polarization Technique

For cyclic polarization studies, the difference between the pitting potential (Ep) and open circuit/corrosion potential (Ecorr) was computed for each alloy sample (Table 5.9). The greater the difference between these two values, the higher the pitting resistance of the respective alloy. This difference, Ecorr – Ep, is particularly used to determine the service performance of aluminum alloy in sodium chloride environment. Three sets of experiment were conducted on each of alloy and average of Ecorr – Ep values was computed. F3S.20S alloy has the greatest value of Ecorr – Ep among the four alloys used (0.1550V). F3K.00S, F3S.20S, and F3K.20S have respective Ecorr – Ep values of 0.1527V, 0.1386V and 0.1236V.

As long as this Ecorr – Ep value is used to determine service performance of aluminum alloys, F3S.00S alloy has demonstrated superior pitting resistance in sodium chloride environment when compared to other three alloys used. It is, sequentially followed, in superiority in terms of corrosion resistance by F3K.00S, F3K.20S and F3S.20S alloys.

Table 5.5: Potentiodynamic Result for F3S.20S using Tafel and Polarization Resistance (R_P) Calculations

Sample Identification	Temperature (degree Celcius)	Corrosion Current Icorr (uA)	OCP (Volt)	Beta Anodic (Volt/decade)	Beta Cathodic (Volt/decade)	TAFELCALCULATIONS: Corrosion Rate	
						(mpy)	(mm/yr)
1C-1	Room Temp.	0.6202	-0.683	60.31E-3	99.4E-3	0.347	0.009
1C-2	Room Temp.	0.5314	-0.721	68.90E-3	146.8E-3	0.886	0.022
1C-3	Room Temp.	0.9029	-0.763	65.42E-3	97.4E-3	1.688	0.043

Sample Identification	Temperature (degree Celcius)	Corrosion Current Icorr (uA)	OCP (Volt)	Beta Anodic (Volt/decade)	Beta Cathodic (Volt/decade)	R_P CALCULATIONS: Corrosion Rate	
						(mpy)	(mm/yr)
1C-1	Room Temp.	0.5321	-0.687	0.1	0.1	1.700	0.044
1C-2	Room Temp.	1.235	-0.725	0.1	0.1	3.341	0.087
1C-3	Room Temp.	1.356	-0.765	0.1	0.1	2.688	0.070

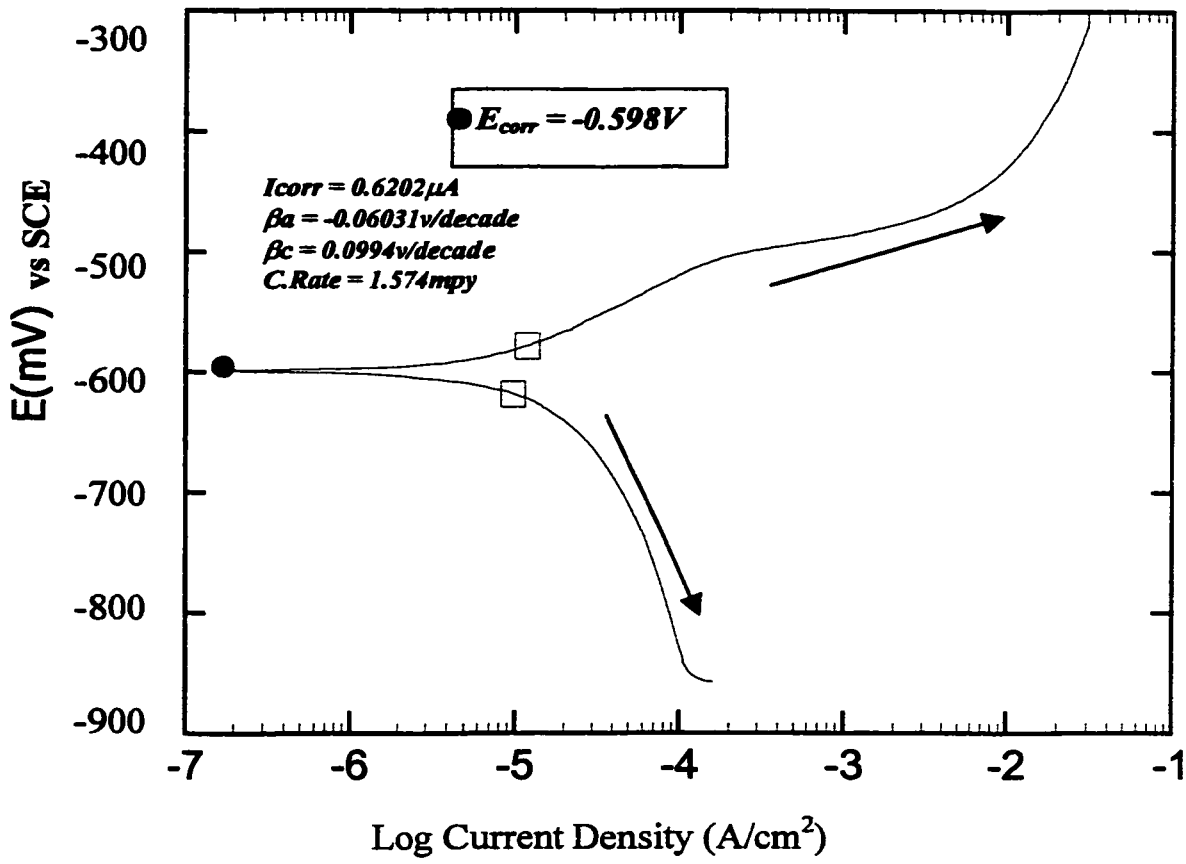

Figure 5.10: Potentiodynamic Curve for F3S.20S Alloy

Table 5.6: Potentiodynamic Result for F3S.00S using Tafel and Polarization Resistance (R_P) Calculations

Sample Identification	Temperature (degree Celcius)	Corrosion Current Icorr (uA)	OCP (Volt)	Beta Anodic (Volt/decade)	Beta Cathodic (Volt/decade)	TAFEL CALCULATIONS: Corrosion Rate	
						(mpy)	(mm/yr)
1B-1	Room Temp.	0.8476	-0.500	123.6E-3	249.5E-3	0.762	0.019
1B-2	Room Temp.	0.6214	-0.553	116.2E-3	383.9E-3	0.234	0.006
1B-3	Room Temp.	0.4299	-0.539	110.7E-3	361.6E-3	0.523	0.018

Sample Identification	Temperature (degree Celcius)	Corrosion Current Icorr (uA)	OCP (Volt)	Beta Anodic (Volt/decade)	Beta Cathodic (Volt/decade)	R_P CALCULATIONS: Corrosion Rate	
						(mpy)	(mm/yr)
1B-1	Room Temp.	1.777	-0.510	0.1	0.1	3.734	0.097
1B-2	Room Temp.	3.811	-0.557	0.1	0.1	1.123	0.029
1B-3	Room Temp.	4.179	-0.542	0.1	0.1	2.510	0.065

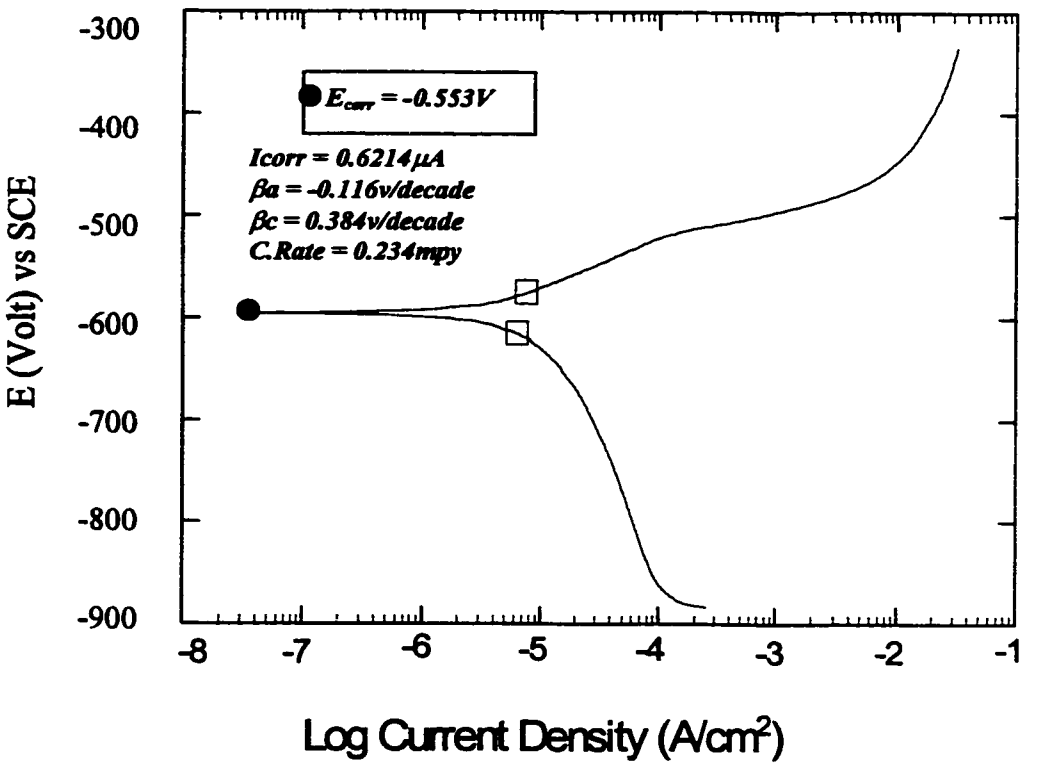

Figure 5.11: Potentiodynamic Curve for F3S.00S Alloy

Table 5.7: Potentiodynamic Result for F3K.20S using Tafel and Polarization Resistance Calculations

Sample Identification	Temperature (degree Celcius)	Corrosion Current Icorr (uA)	OCP (Volt)	Beta Anodic (Volt/decade)	Beta Cathodic (Volt/decade)	TAFEL CALCULATIONS: Corrosion Rate	
						(mpy)	(mm/yr)
1B-1	Room Temp.	0.4476	-0.524	184.2E-3	257.8E-3	1.489	0.038
1B-2	Room Temp.	0.6722	-0.496	200.0E-3	195.2E-3	0.781	0.020
1B-3	Room Temp.	0.9541	-0.560	224.2E-3	195.0E-3	1.286	0.033

Sample Identification	Temperature (degree Celcius)	Corrosion Current Icorr (uA)	OCP (Volt)	Beta Anodic (Volt/decade)	Beta Cathodic (Volt/decade)	R_P CALCULATIONS: Corrosion Rate	
						(mpy)	(mm/yr)
1B-1	Room Temp.	3.467	-0.532	0.1	0.1	3.742	0.097
1B-2	Room Temp.	1.673	-0.497	0.1	0.1	2.749	0.073
1B-3	Room Temp.	2.994	-0.564	0.1	0.1	3.503	0.091

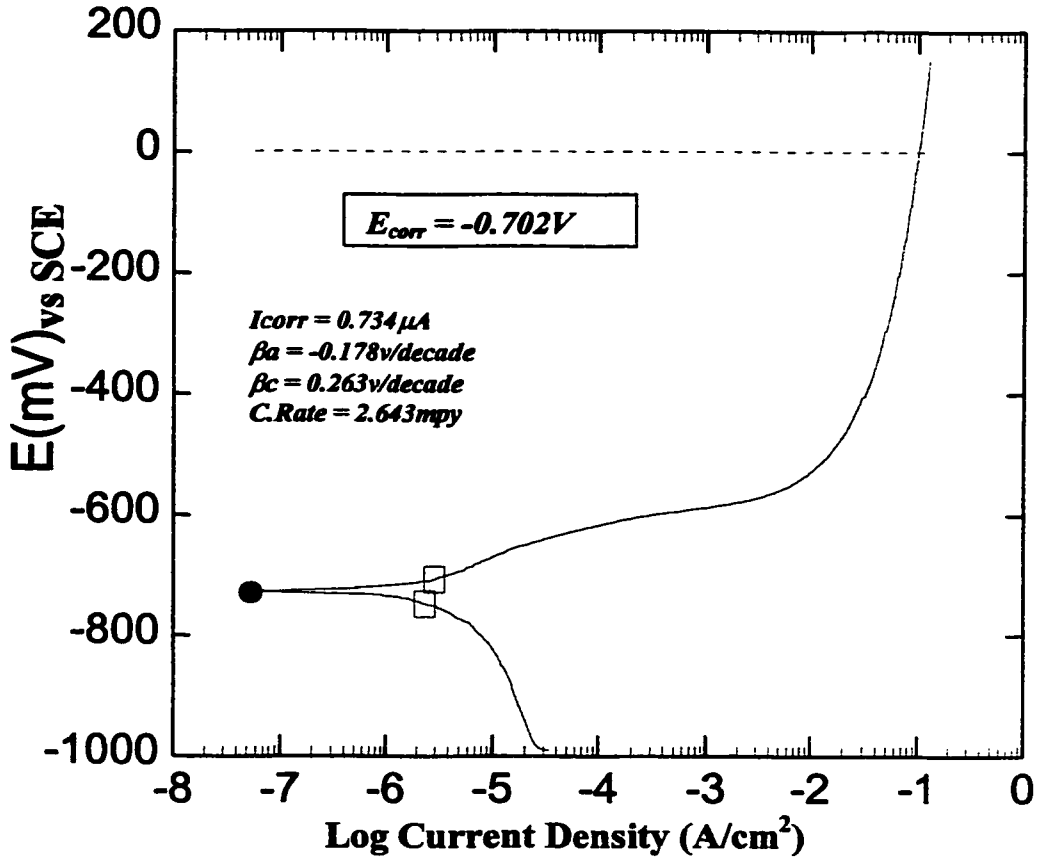

Figure 5.12: Potentiodynamic Curves for F3K.20S Alloy

Table 5.8: Potentiodynamic Result for F3K.00S using Tafel and Polarization Resistance (R_P) Calculations

Sample Identification	Temperature (degree Celcius)	Corrosion Current Icorr (uA)	OCP (Volt)	Beta Anodic (Volt/decade)	Beta Cathodic (Volt/decade)	TAFEL CALCULATIONS: Corrosion Rate	
						(mpy)	(mm/yr)
1B-1	Room Temp.	0.3804	-0.547	117.6E-3	195.5E-3	0.936	0.024
1B-2	Room Temp.	0.6524	-0.537	248.9E-3	546.2E-3	0.541	0.032
1B-3	Room Temp.	0.9735	-0.479	112.8E-3	226.6E-3	0.764	0.019

Sample Identification	Temperature (degree Celcius)	Corrosion Current Icorr (uA)	OCP (Volt)	Beta Anodic (Volt/decade)	Beta Cathodic (Volt/decade)	R_P CALCULATIONS: Corrosion Rate	
						(mpy)	(mm/yr)
1B-1	Room Temp.	2.180	-0.549	0.1	0.1	3.324	0.086
1B-2	Room Temp.	5.222	-0.540	0.1	0.1	2.597	0.067
1B-3	Room Temp.	2.953	-0.483	0.1	0.1	2.667	0.069

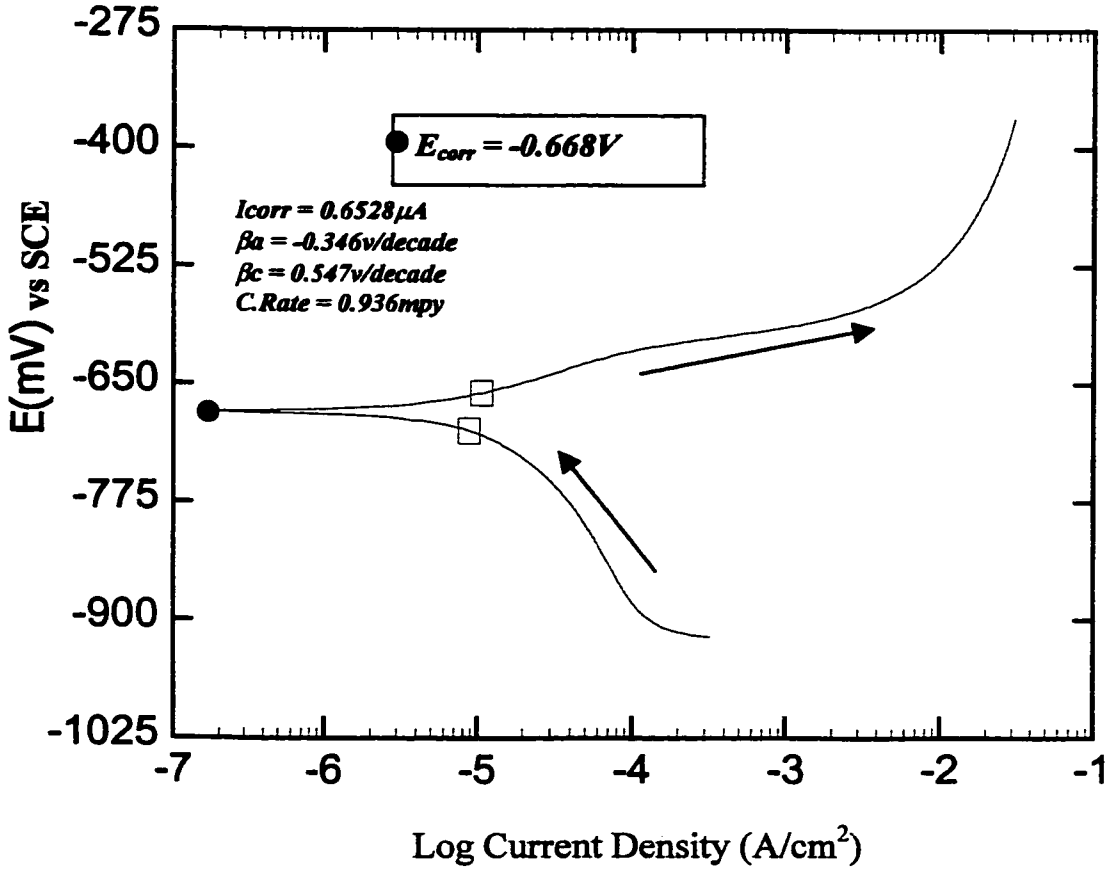

Figure 5.13: Potentiodynamic Curve for F3K.00S Alloy

Table 5.9: Summary of the Results obtained from Cyclic Polarization Experiment

Material	Ep (Volt)	Epp (Volt)	Ecorr (Volt)	E=Ecorr -Ep (Volt)	E=Ecorr -Ep (Avrg)
F3S.20S-1	-0.589	-0.717	-0.476	0.111	
F3S.20S-2	-0.411	-0.622	-0.621	0.21	
F3S.20S-3	-0.424	-0.682	-0.512	0.088	0.1386
F3S.00S-1	-0.488	-0.512	-0.593	0.105	
F3S.00S-2	-0.411	-0.622	-0.620	0.209	
F3S.00S-3	-0.410	-0.502	-0.562	0.151	0.1550
F3K.20S-1	-0.412	-0.612	-0.503	0.091	
F3K.20S-2	-0.396	-0.557	-0.525	0.129	
F3K.20S-3	-0.365	-0.562	-0.476	0.111	0.1236
F3K.00S-1	-0.536	-0.564	-0.636	0.100	
F3K.00S-2	-0.413	-0.604	-0.594	0.181	
F3K.00-3	-0.521	-0.603	-0.698	0.177	0.1527

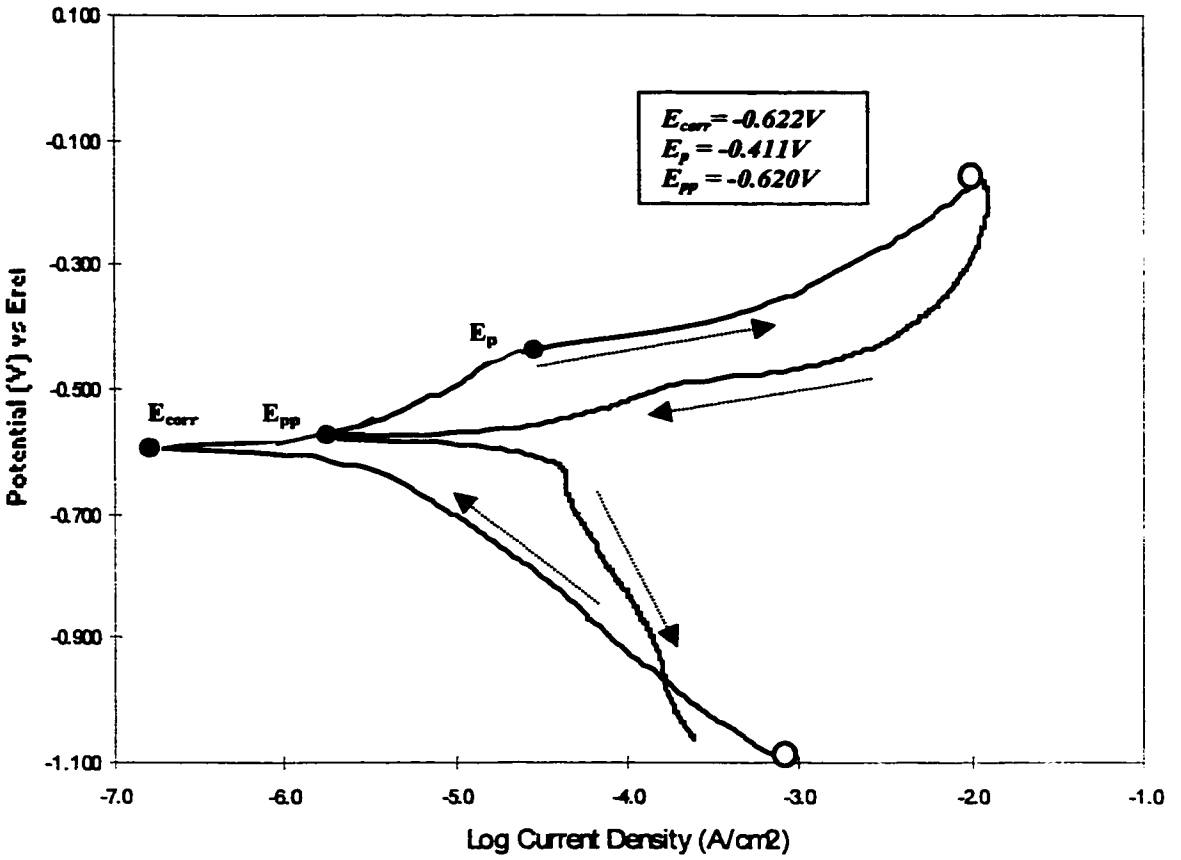

Figure 5.14: Cyclic Polarization Curve for F3S.00S

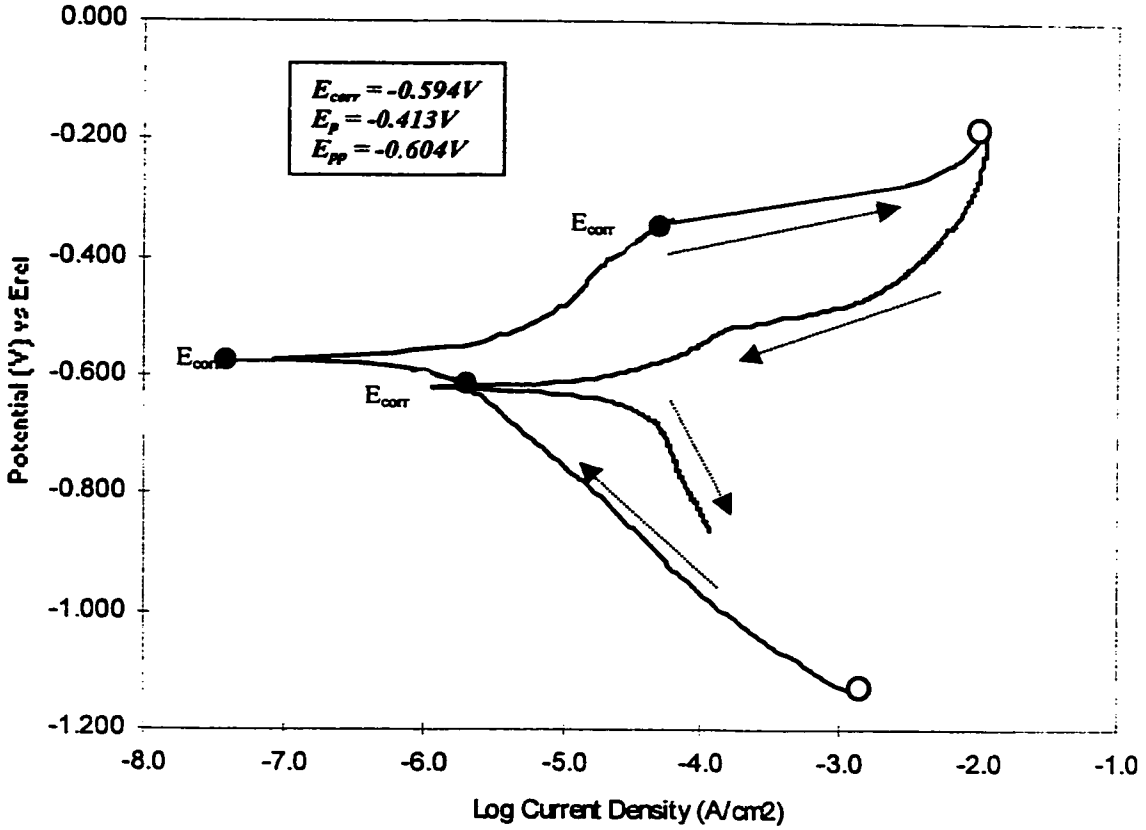

Figure 5.15: Cyclic Polarization Curve for F3K.00S

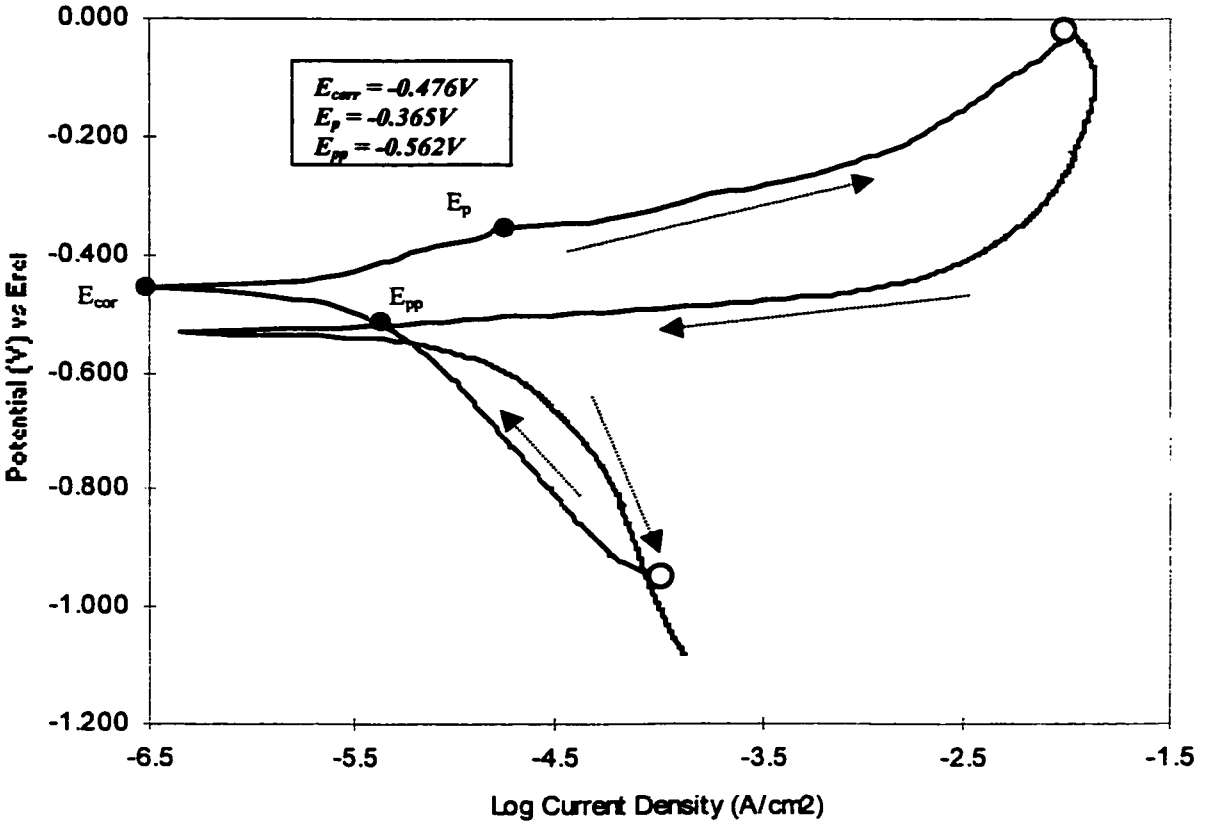

Figure 5.16: Cyclic Polarization Curve for F3K.20S

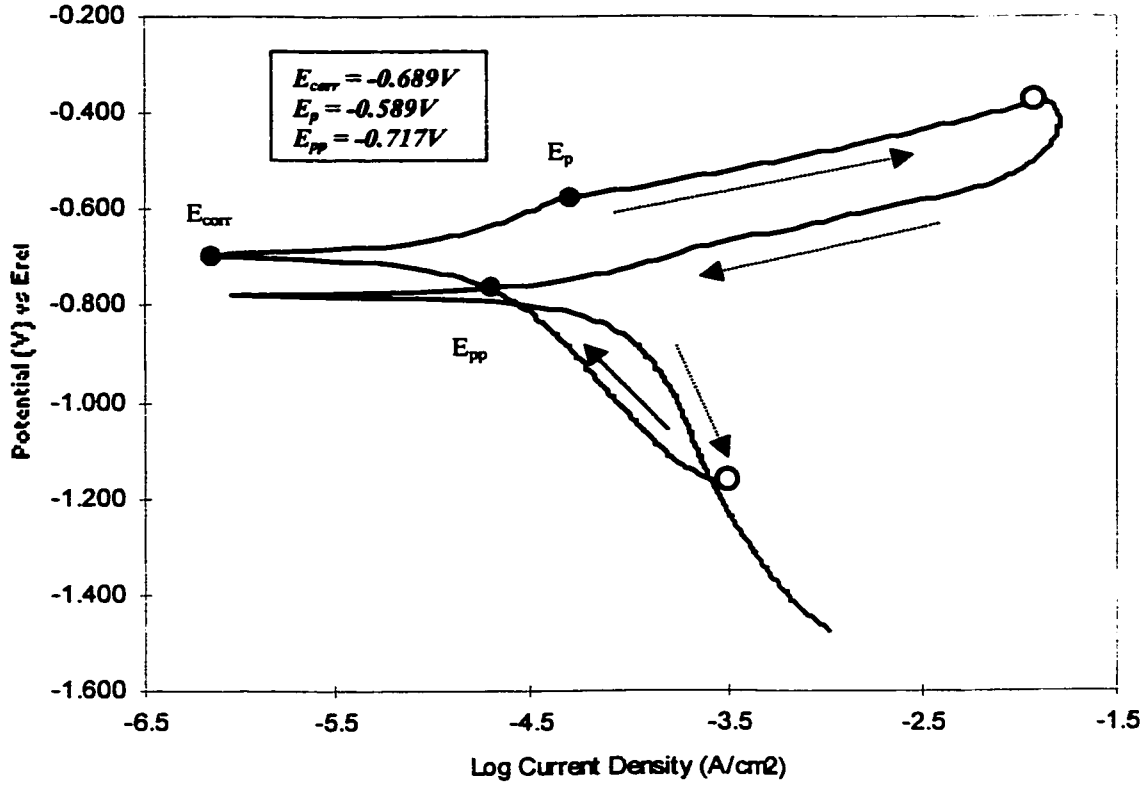

Figure 5.17: Cyclic Polarization Curve for F3S.20S

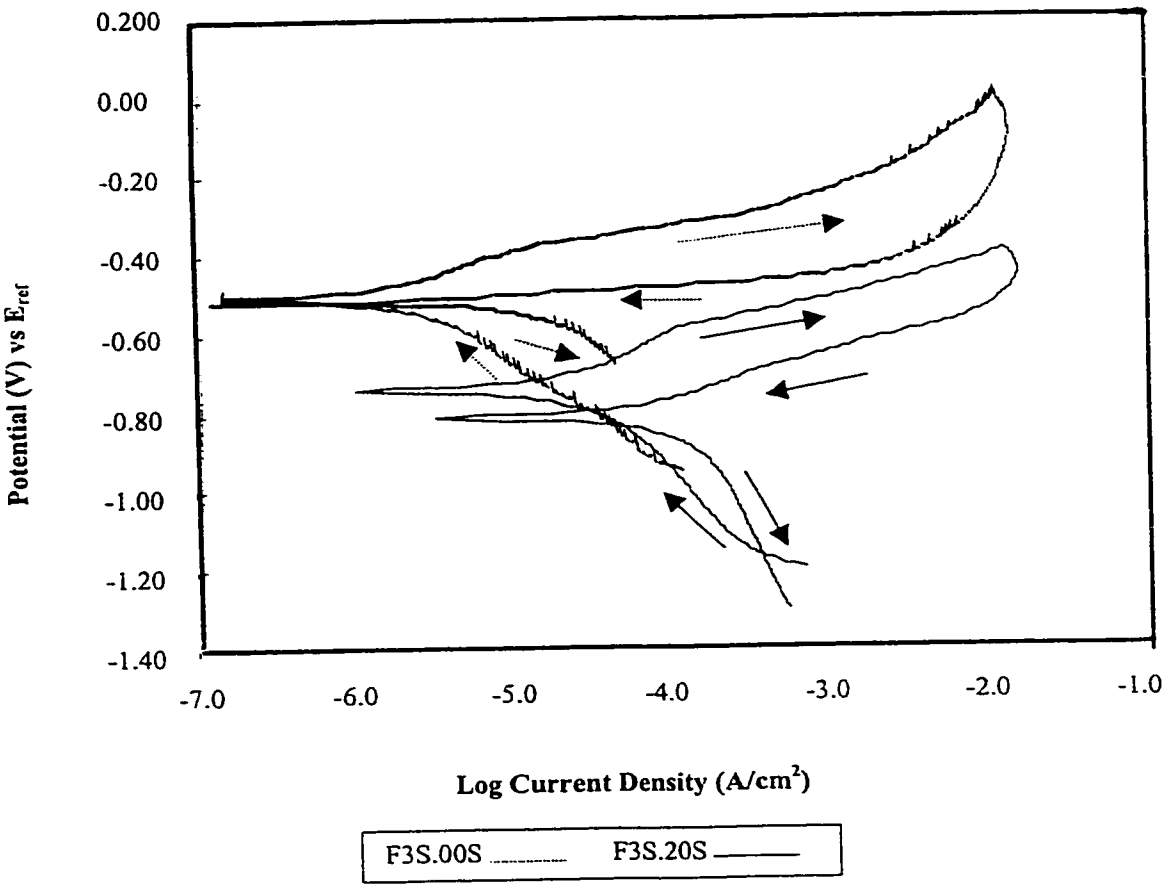

Figure 5.18: Comparison of Cyclic Polarization Curves for F3S.00S and F3S.20S alloys

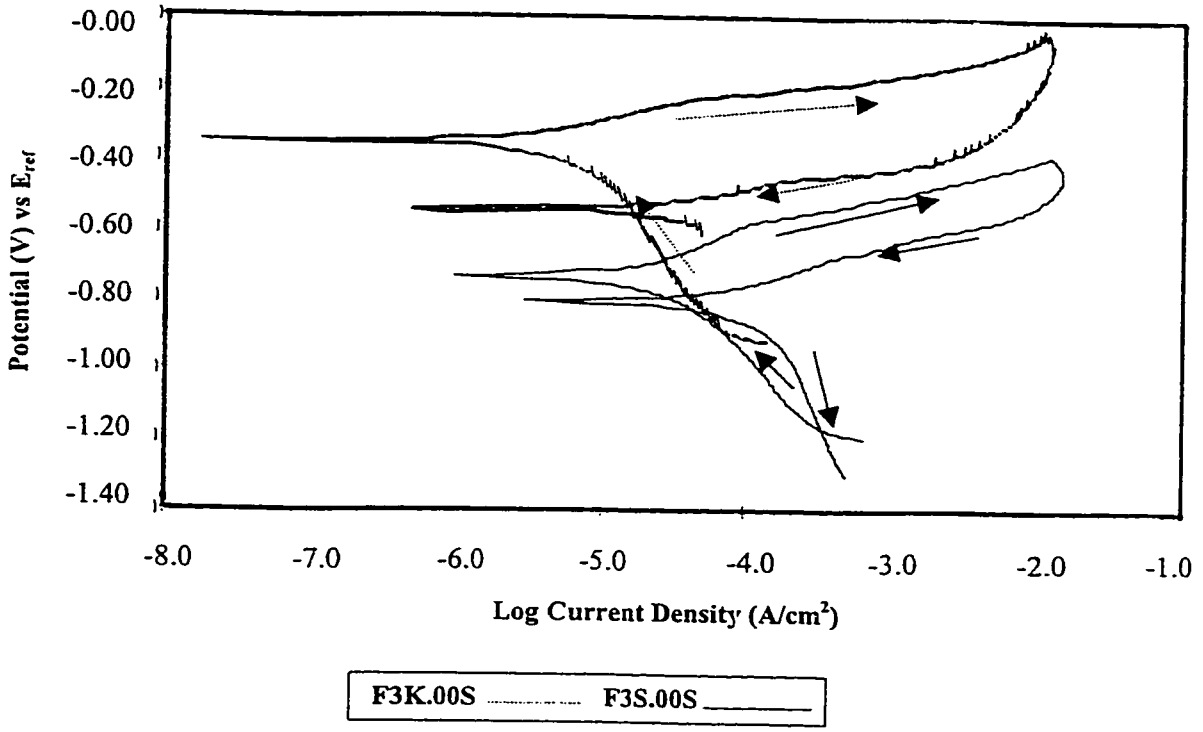

Figure 5.19: Comparison of Cyclic Polarization Curves for F3K.00S and F3S.00S alloys

5.3 Results from Micro-Analytical Studies

Results obtained from both the optical micrography and scanning electron micrography (SEM) are shown from figure 5.20 to figure 5.43. EDS was used to analyze the elemental constituents in the pit's surroundings for all the four alloys.

In F3K.20S alloy, four main elements were indicated by EDS (figure 5.44). These elements are aluminum (Al) with % composition of 52.62, silicon (Si) with % composition of 23.47, nickel (Ni) with % composition of 10.10 and copper (Cu) with % composition of 13.81. Based on the principle guiding the formation of phases in aluminum alloys (Tables 2.2, 2.3, 2.4), these elements found can possibly be Cu_4NiAl_7 and $CuAl_2$ intermetallic phases in the pit region. As a result of this, the region will be anodic with respect to the entire matrix if and only if these elements are responsible for the initiation of dissolution process. In another form of justification, the region which contains these suspected intermetallic phases, might as well be cathodic with respect to entire matrix. Copper is usually added to aluminum alloy deliberately to improve its corrosion resistance. For this reason, phases being formed between copper and other alloying elements are expected to provide suitable protection against corrosion in sodium chloride environment. Hence, other alloying elements or even aluminum matrix might preferentially dissolve into solution of sodium chloride and by doing so, these suspected phases are left unaffected in the pit region.

In F3K.00S alloy, three main elements were observed as shown by EDS result (figure 5.45). These elements are aluminum (Al) with % composition of

about 76.63, silicon (Si) with % composition of 11.18 and copper (Cu) with % composition of about 12.19. Similarly, there is possibility of formation of $CuAl_2$ intermetallic phase in the pit region as previously indicated in its reinforced counterpart, F3K.20S alloy. Improved corrosion resistance obtained in F3K.00S alloy, as compared to F3K.20S alloy, can be attributed to the formation of only one type of intermetallic phase in the pit's surrounding.

In F3S.00S alloy, EDS result showed four main elements in pit's surrounding (figure 5.46). These elements include aluminum (Al) with % composition of 90.47, silicon (Si) with % composition of 3.06, copper (Cu) with % composition of 1.48, and magnesium (Mg) with % composition of 4.99%. Based on this observation, three possible major intermetallic phases can be identified. These phases include $Cu_2Mg_8Si_6Al_5$, Mg_2Si and $CuMg_4Al_6$ (Tables 2.2, 2.3, 2.4). The same justification, as highlighted above, can also be used to explain the possible role of these phases.

Figure 5.47 shows the EDS analysis of surface structure of F3S.20S alloy. Result indicates the presence of four main elements in pit's surrounding. These elements include aluminum with % composition of 54.50, silicon (Si) with % composition of 24.03, Iron with % composition of 21.17 and magnesium with % composition of 0.30. Based on this result, Fe_2SiAl_5 and Mg_2Si intermetallic phases are possibly formed in the pit region.

EDS analysis shows the composition of reinforced particles (Figure 5.51). These particles contain aluminum with % composition of 19.03, silicon with % composition of 70.34% and carbon (C) with % composition of 10.63. In the region of dissolution, predominant coagulation of SiC particles is

formed. This is in support of what Trazaskoma (61) and Ahmad (84) have independently investigated.

In addition to these observations, it was found that the number of pits formed from reinforced alloys (F3S.20S and F3K.20S) is greater when compared with their unreinforced counterparts, F3S.00S and F3K.00S alloys respectively. Approximate counting was achieved by observing $0.6cm^2$-corroded area, under microscope, for each of the alloys. Based on this investigation, improved corrosion resistance obtained in unreinforced alloys can also be attributed to the presence of lesser number of pits as compared to their respective reinforced counterpart.

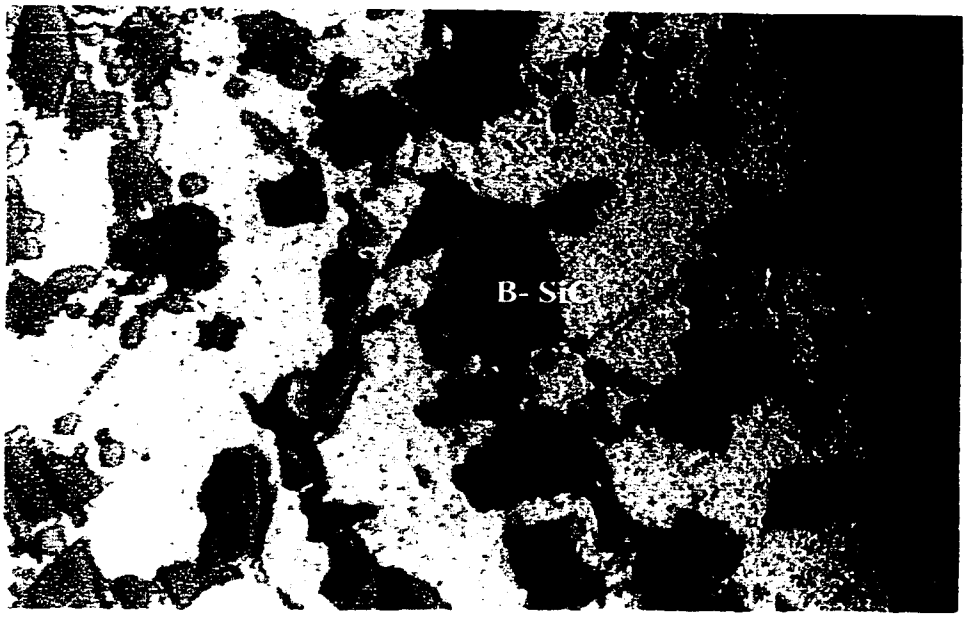

Mag.-x400

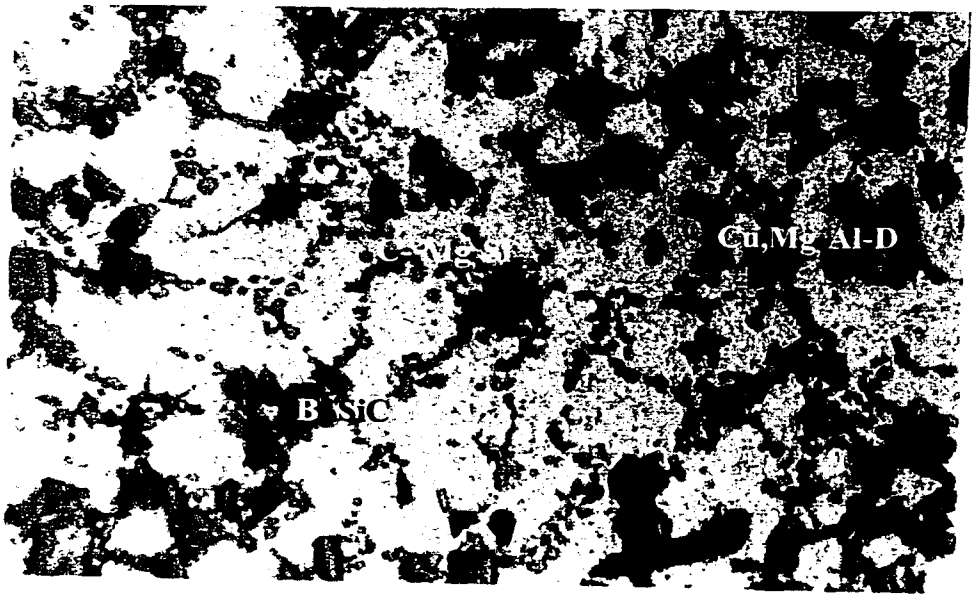

Mag.-x200

Figure 5.20: Optical Micrograph of F3S.20S alloy

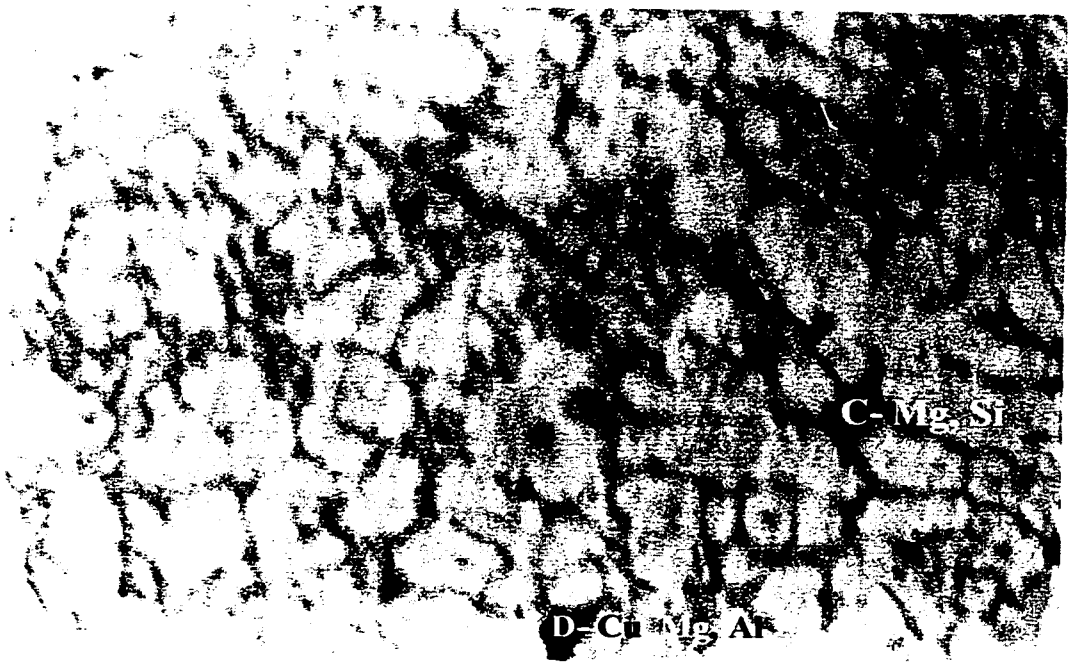

Mag.-x200

Mag.-x400

Figure 5.21: Optical Micrograph of F3S.00S alloy

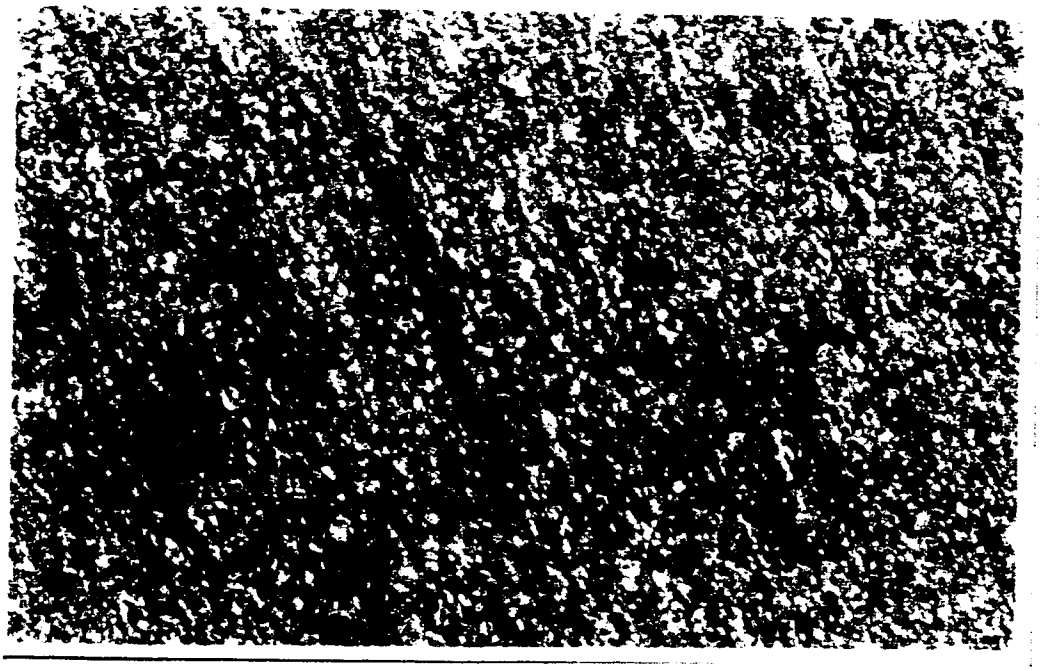

Mag. x100

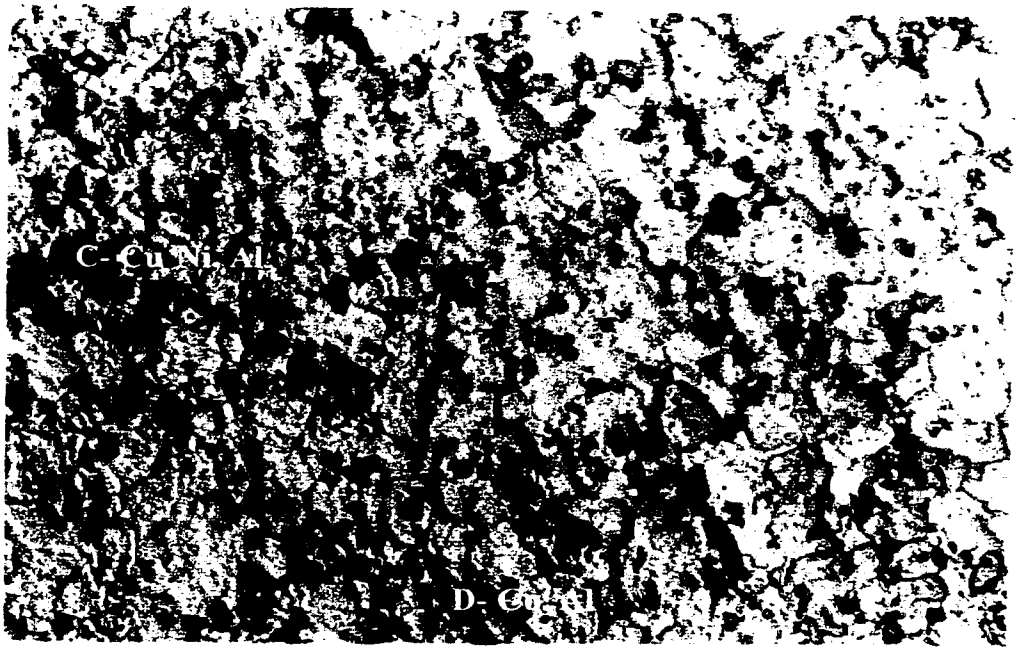

Mag. x400

Figure 5.22: Optical Micrograph of F3K.00S alloy

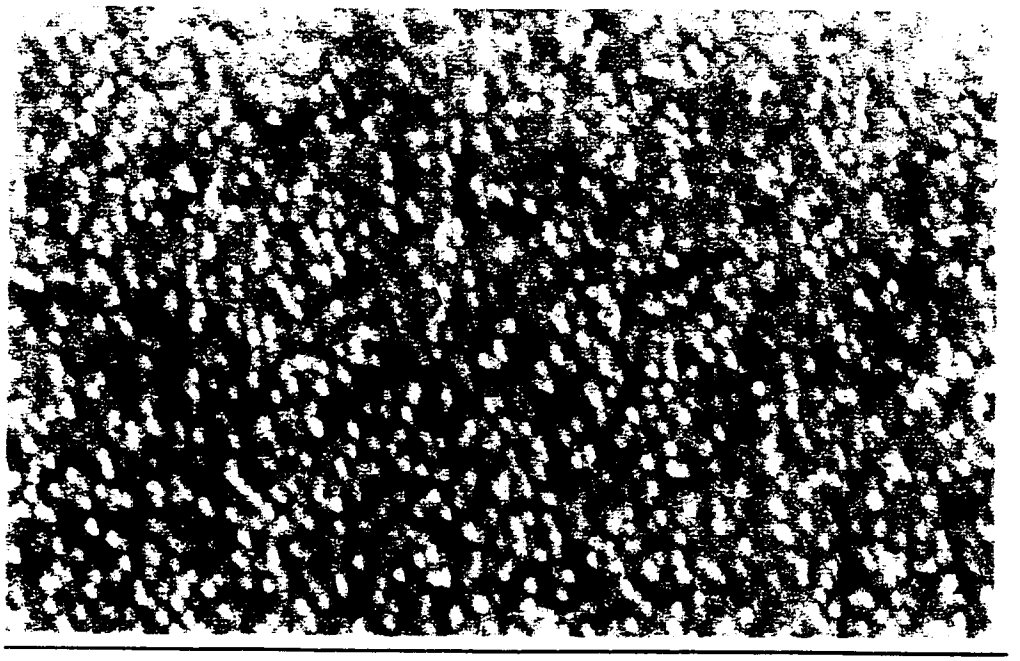

Mag.-x100

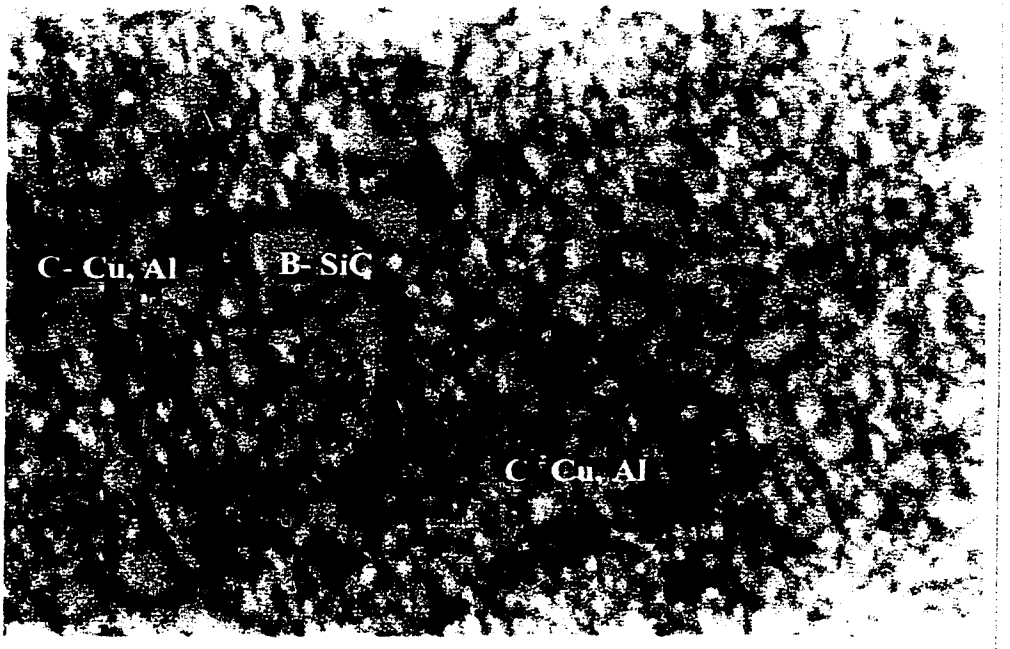

Mag.-x400

Figure 5.23: Optical Micrograph of F3K.20S alloy

(a) *Mag.-x500*

(b) *Mag.-x1000*

Figure 5.24: Micrograph of Non-Corroded Sample for F3S.00S

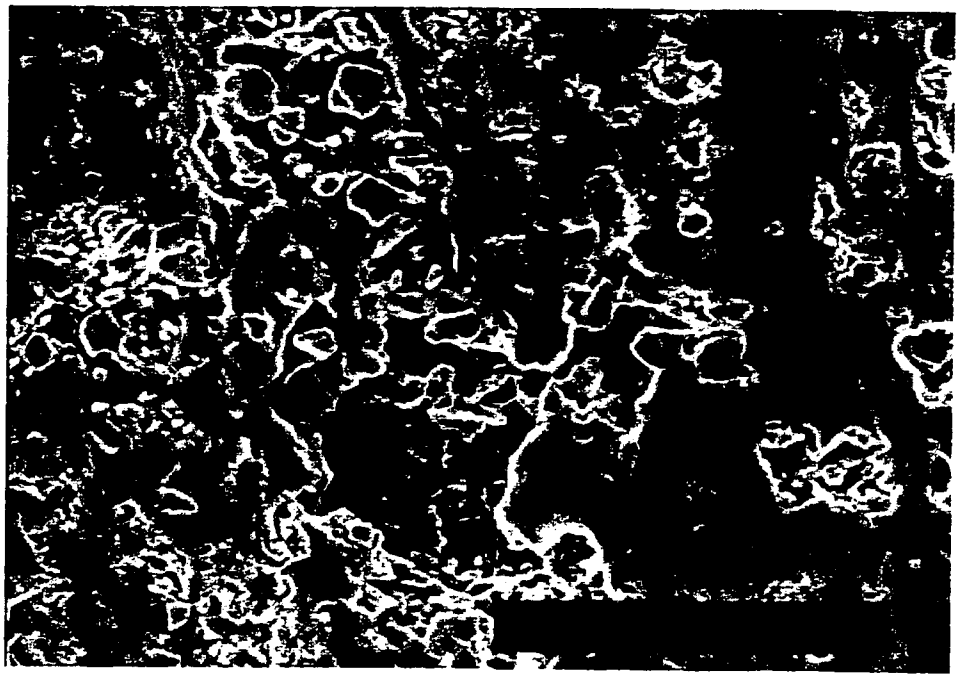

Figure 5.25: Micrograph showing pit in F3S.00S from electrochemical test.

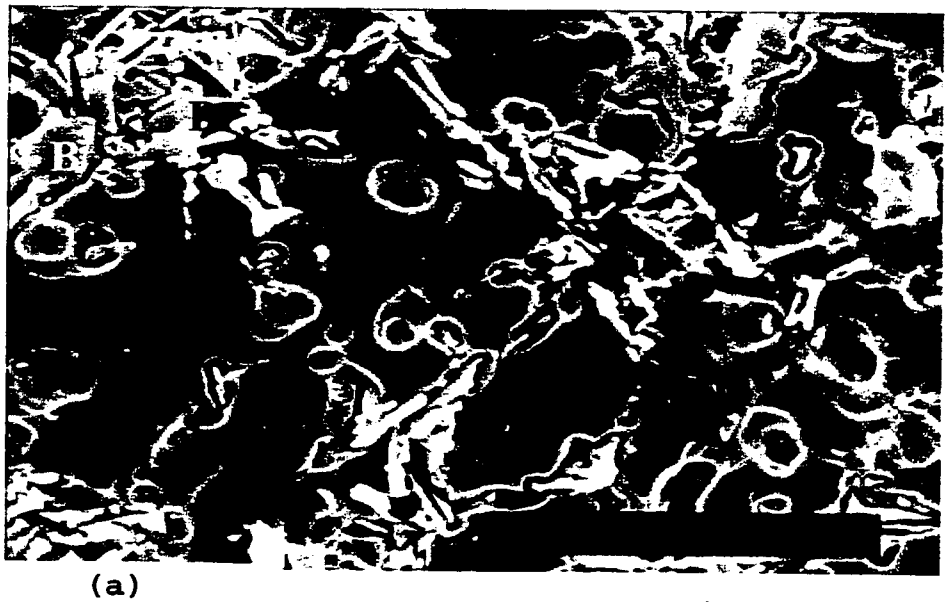

(a)

Mag.-x500

(b)

Mag.-x1000

Figure 5.26: Micrograph of Weight-Loss for F3S.00S (200hrs)

(a) Mag.-x500

(b) Mag.-x1000

Figure 5.27: Micrograph of Weight-Loss Sample for F3S.00S (1000hrs)

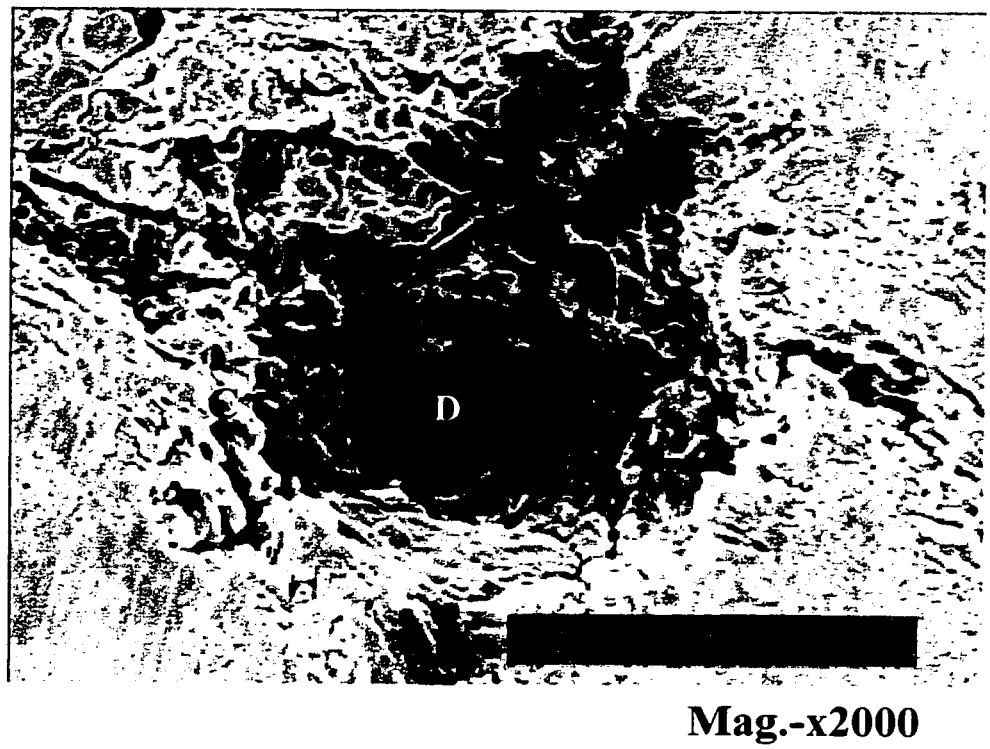

Figure 5.28: Micrograph of Weight-Loss Sample for F3S.00S (1600hrs)

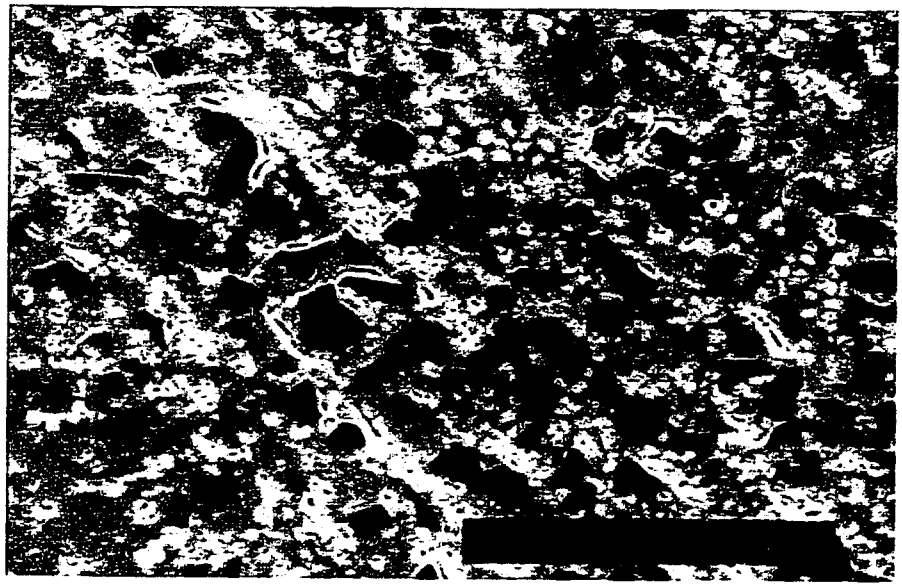

(a) *Mag.-x500*

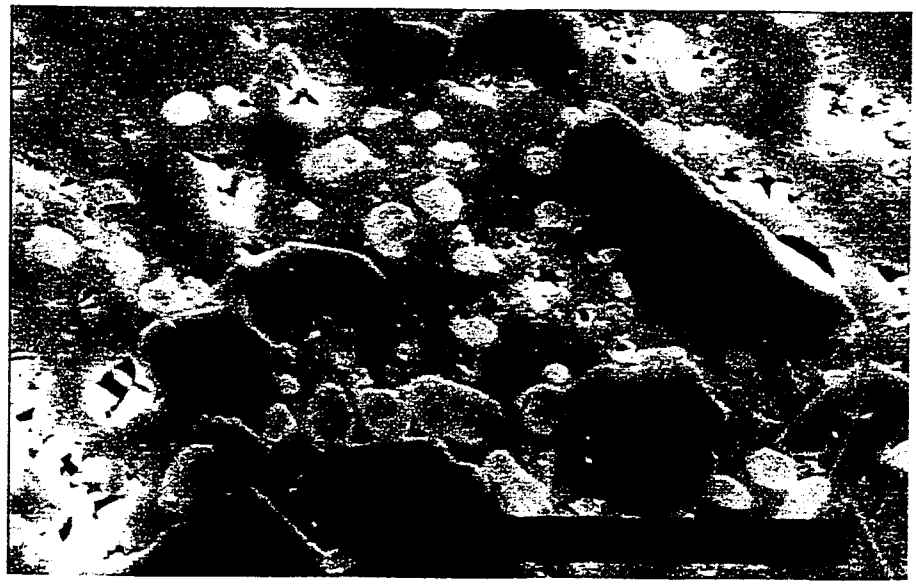

(b) *Mag.-x1500*

Figure 5.29: Micrograph of Non-Corroded Samples for F3S.20S alloy

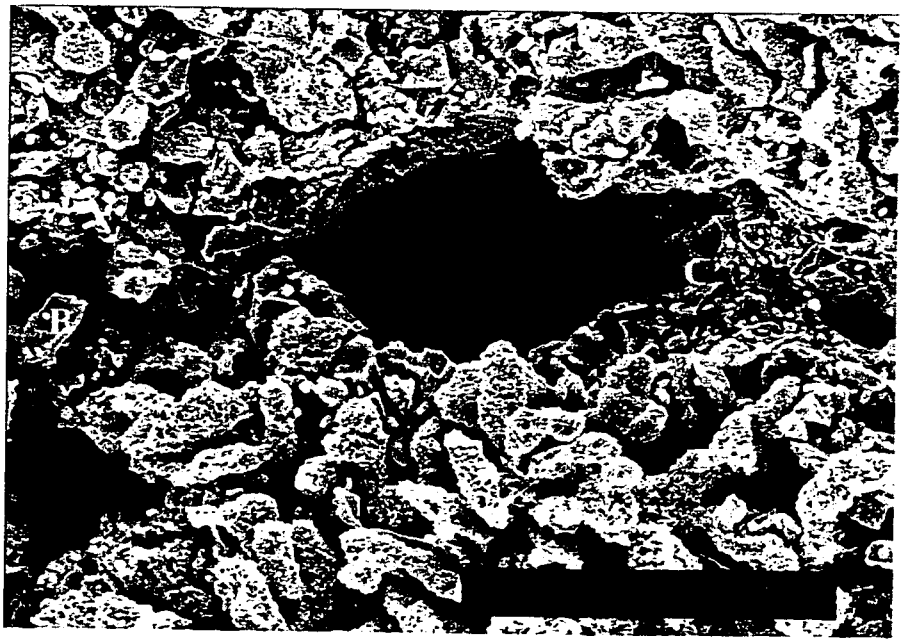

Figure 5.30: Micrograph showing pit in F3S.20S alloy after electrochemical test

(a) ***Mag.-x500***

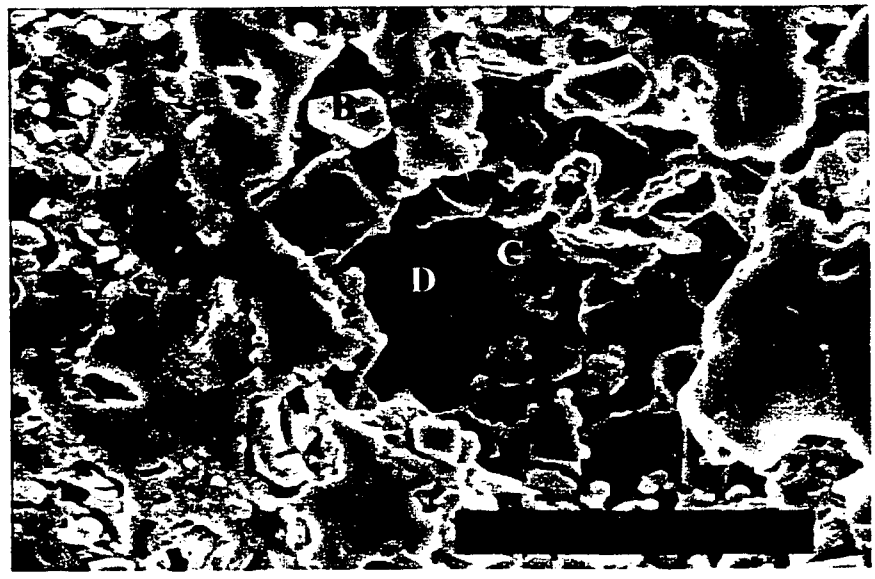

(b) ***Mag.-x1000***

Figure 5.31: Micrograph of Weight-Loss for F3S.20S alloy (200hrs)

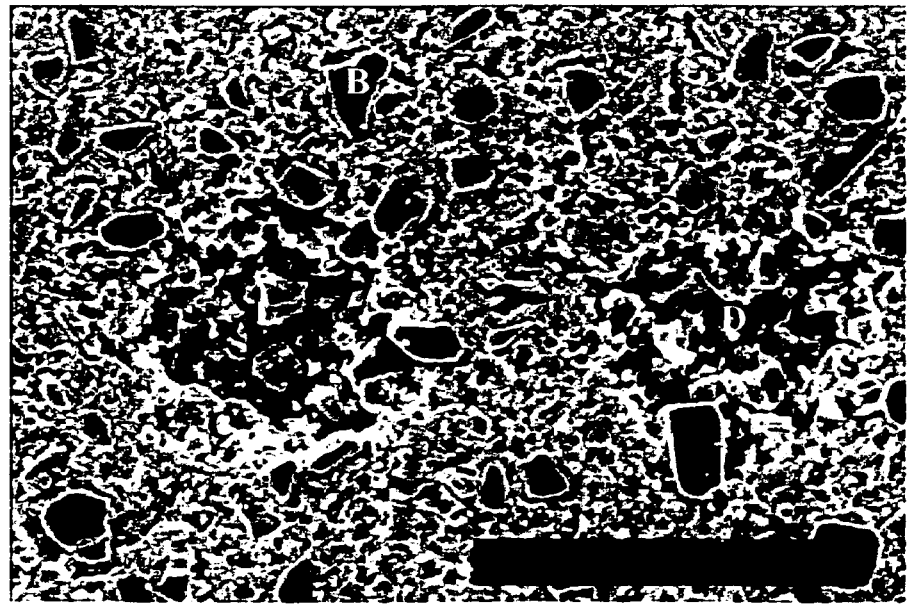

(a) *Mag.-x500*

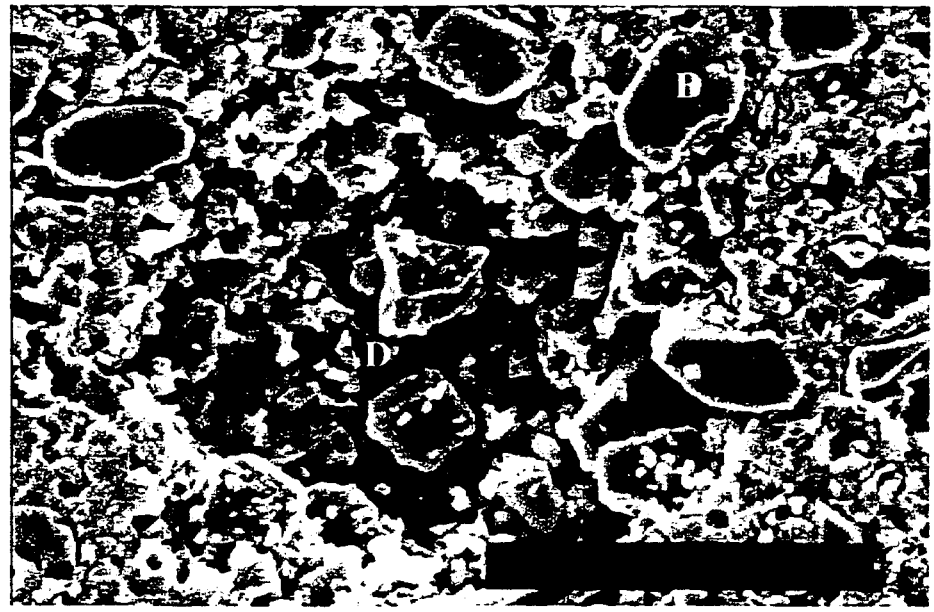

(b) *Mag.-x1000*

Figure 5.32: Micrograph of Weight-Loss Sample (1000hrs) for F3S.20S

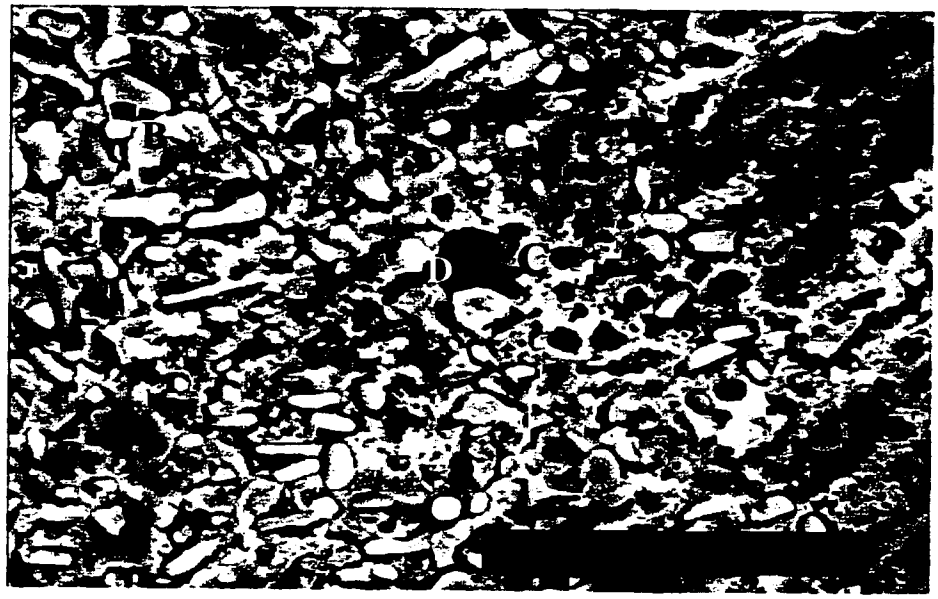

(a) Mag.-x500

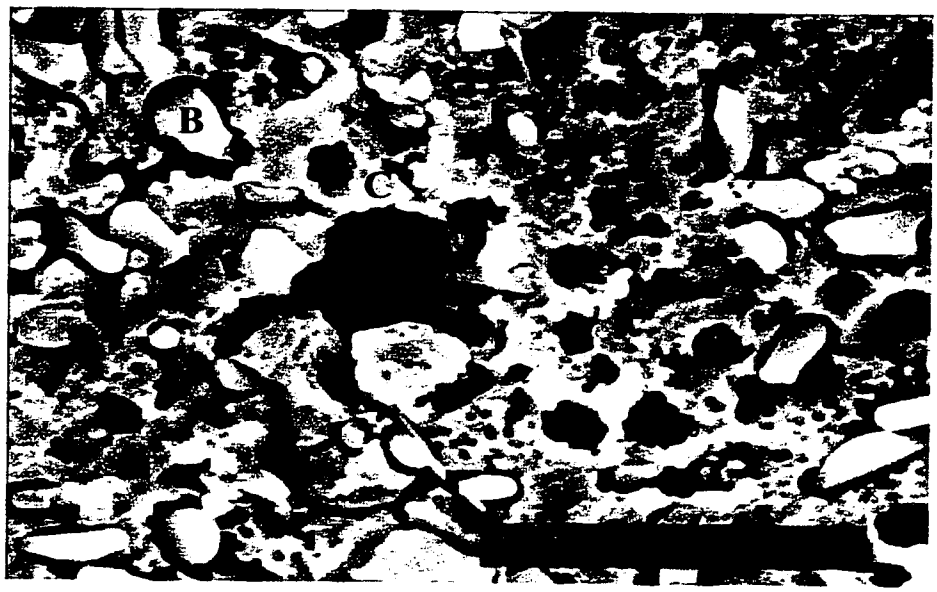

(b) Mag.-x1000

Figure 5.33: Micrograph of Weight-Loss for F3S.20S (1600hrs)

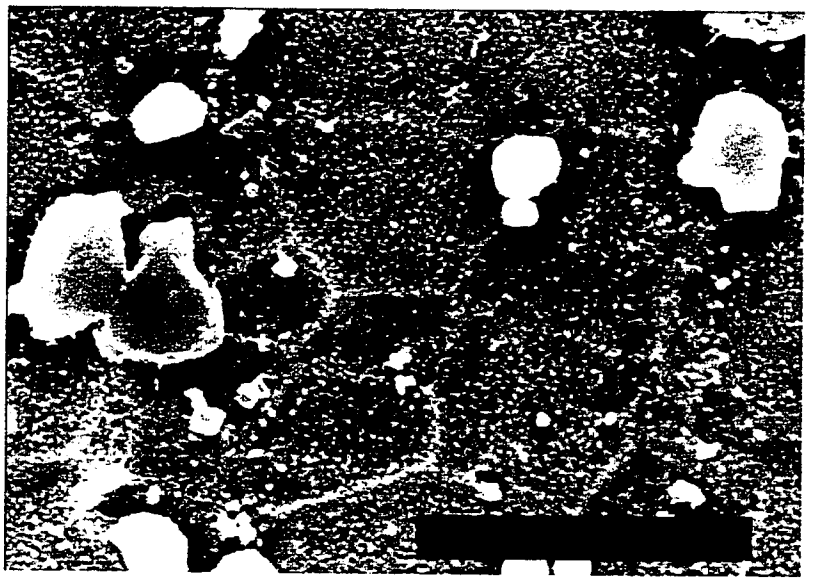

Mag.-x2000

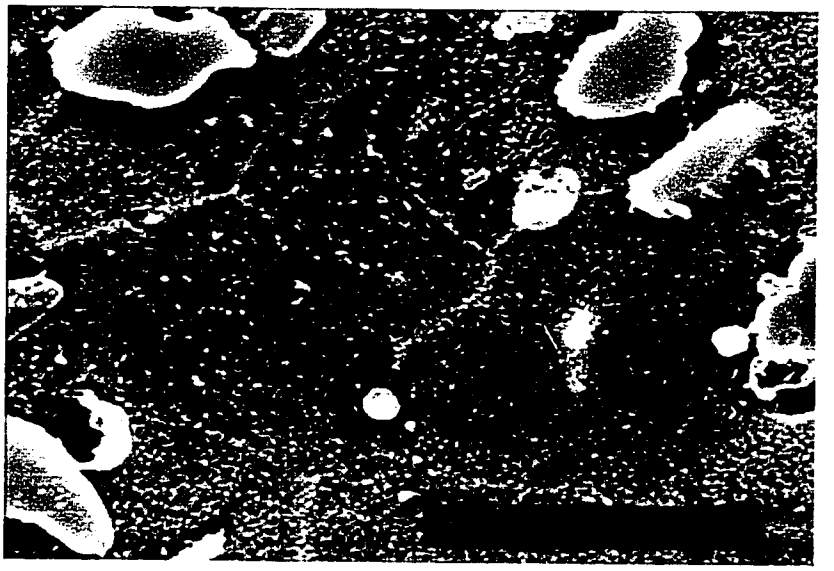

Mag.-x2000

Figure 5.34: Micrograph of Non-corroded sample of F3K.00S

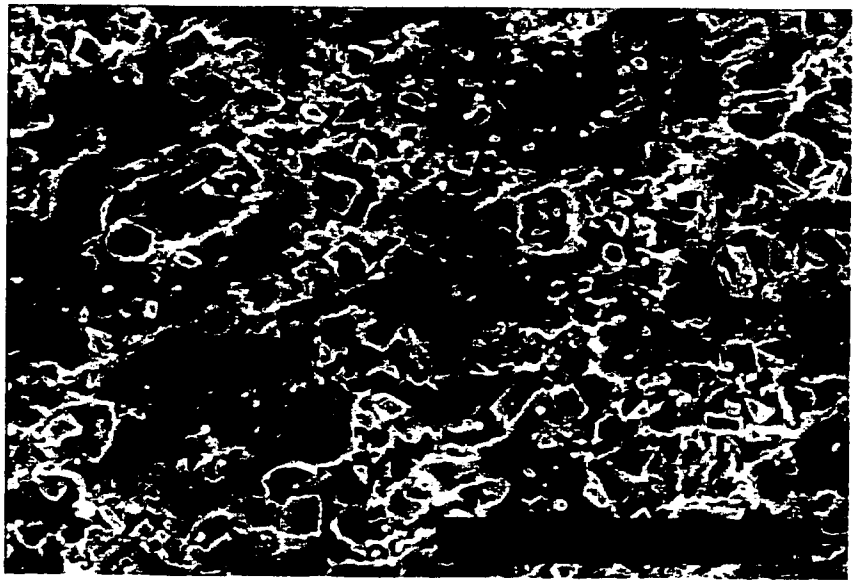

Mag. x500

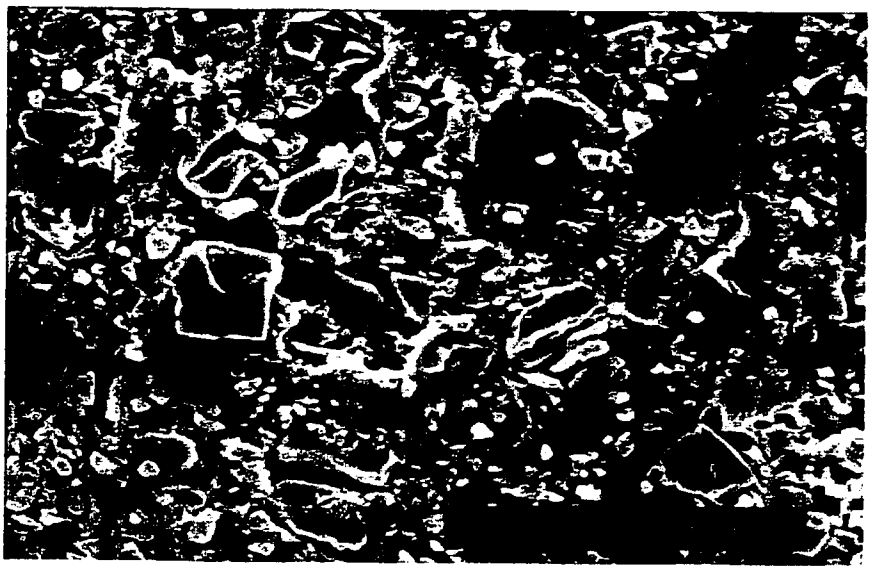

Mag. x1000

Figure 5.35: Micrograph showing pit in F3K.00S from electrochemical test

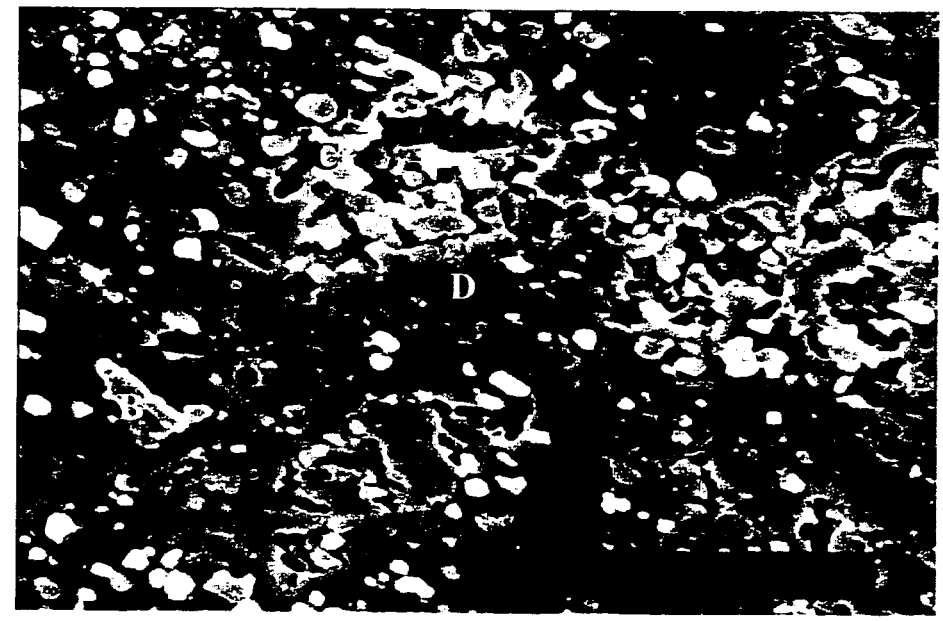

(a) Mag.-x1000

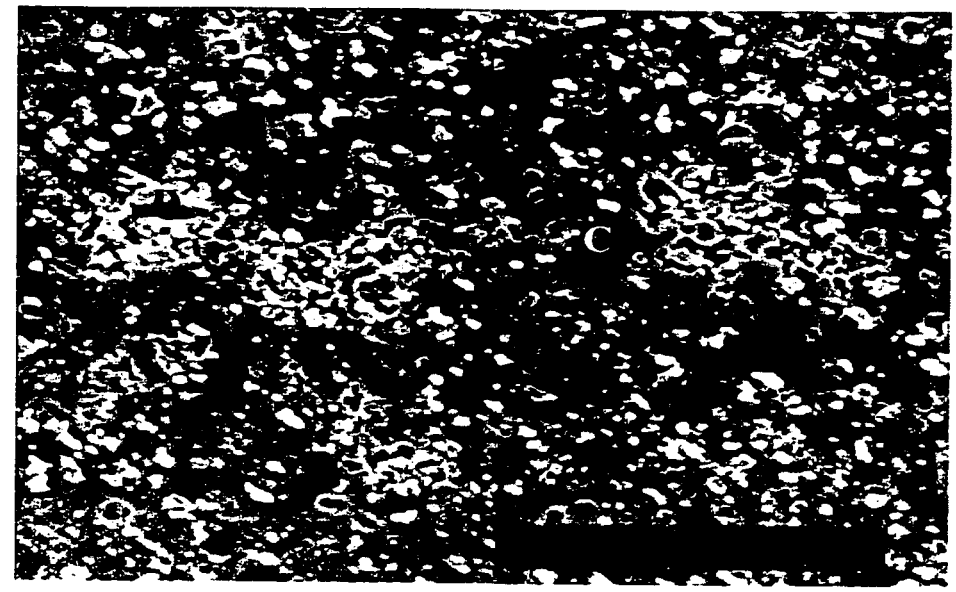

(b) Mag.-x500

Figure 5.36: Micrograph of Weight-Loss for F3K.00S (200hrs)

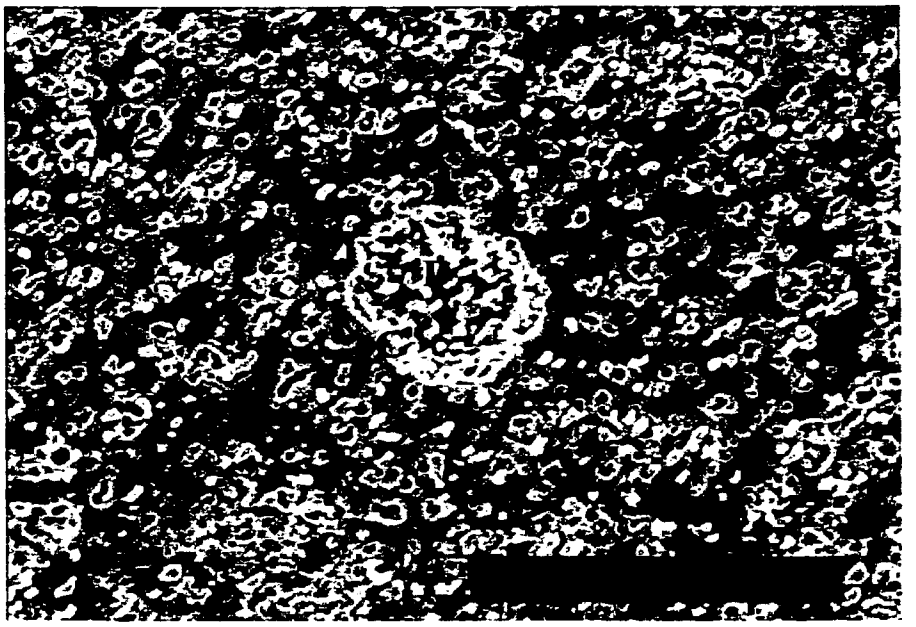

(a) Mag.-x500

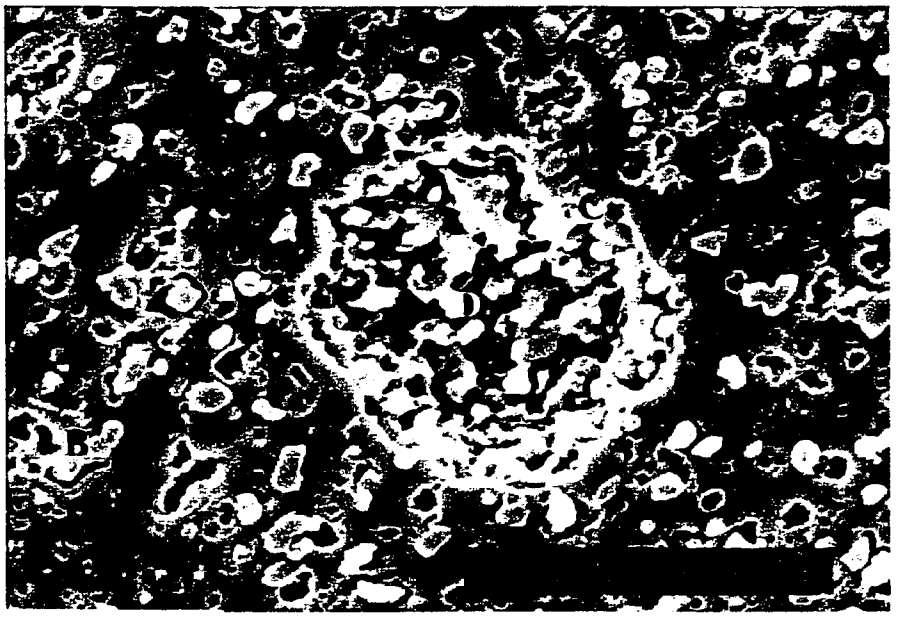

(b) Mag.-x1000

Figure 5.37: Micrograph of Weight-Loss for F3K.00S (1000hrs)

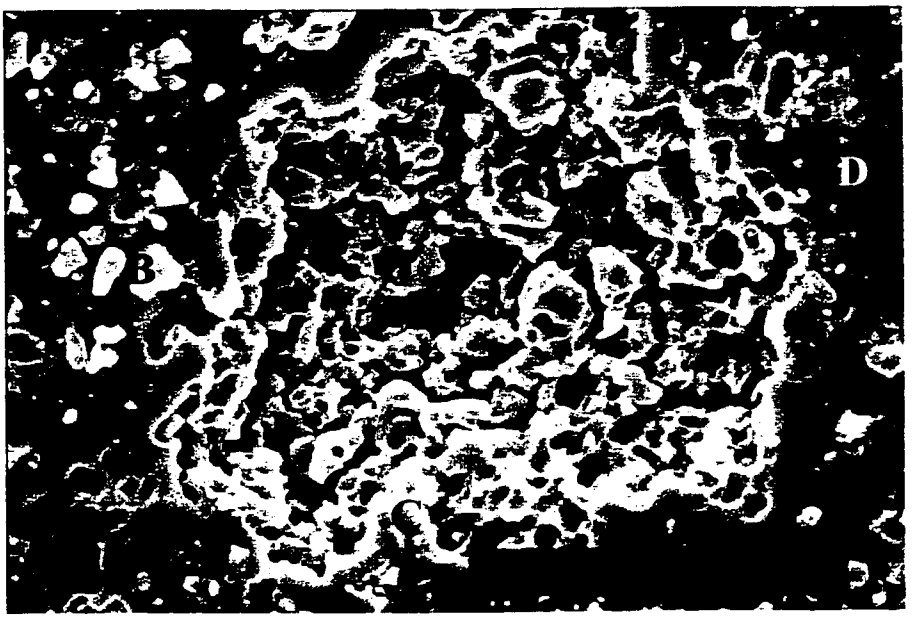

(a) *Mag.-x2000*

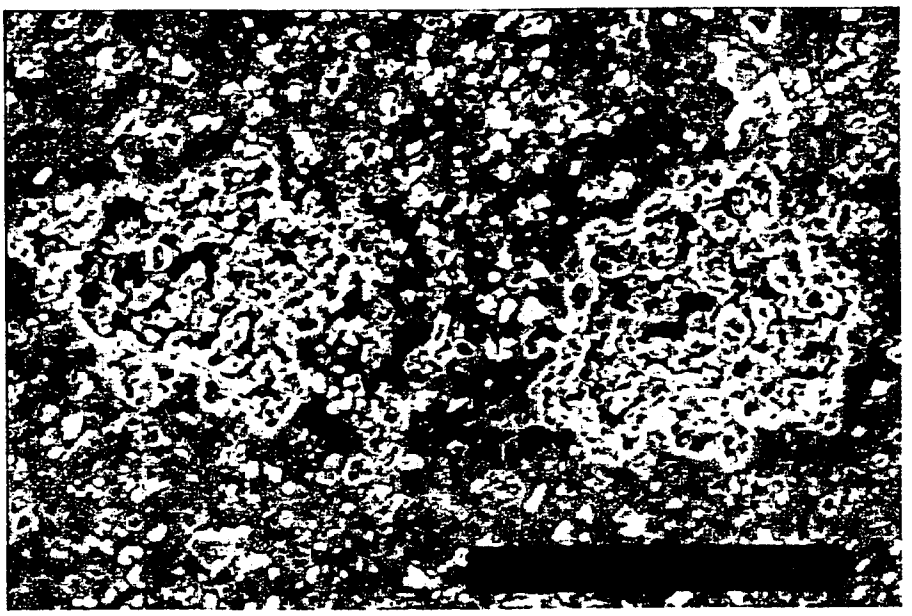

(a) *Mag.-x500*

Figure 5.38: Micrograph of Weight-Loss for F3K.00S (1600hrs)

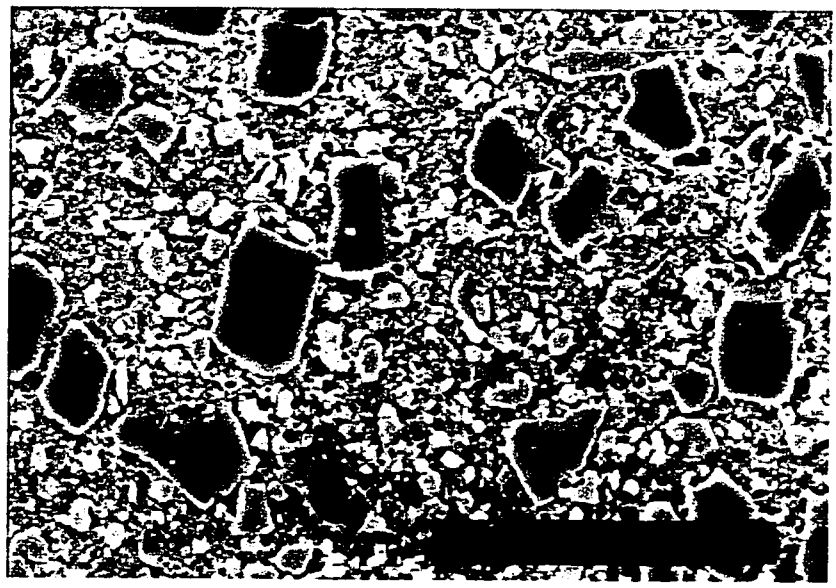

Mag. X 1000

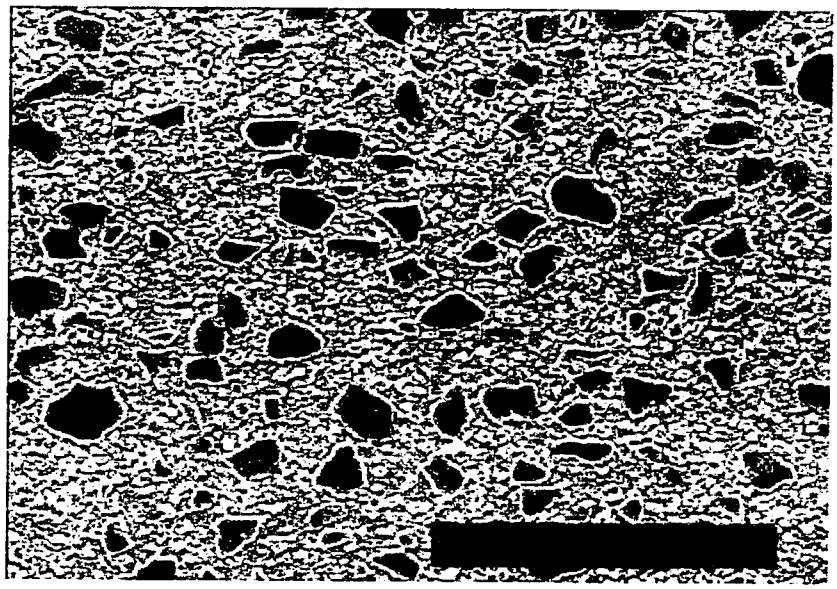

Mag. X 750

Figure 5.39: Micrograph showing Non-corroded sample of F3K.20S

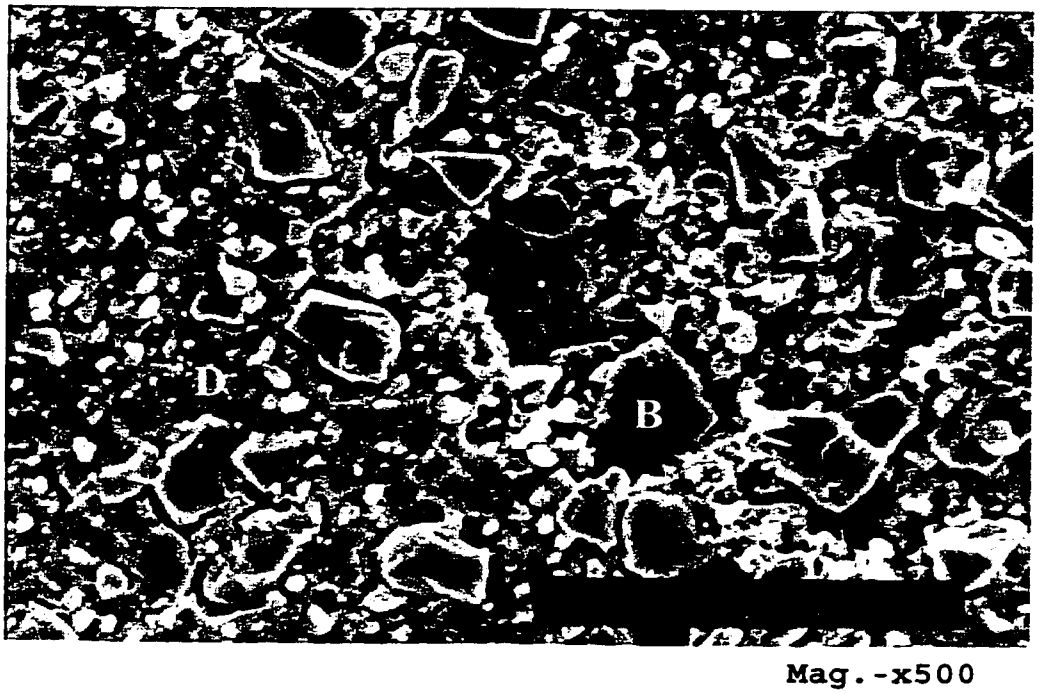

Figure 5.40: Micrograph showing pit in F3K.20S after electrochemical test

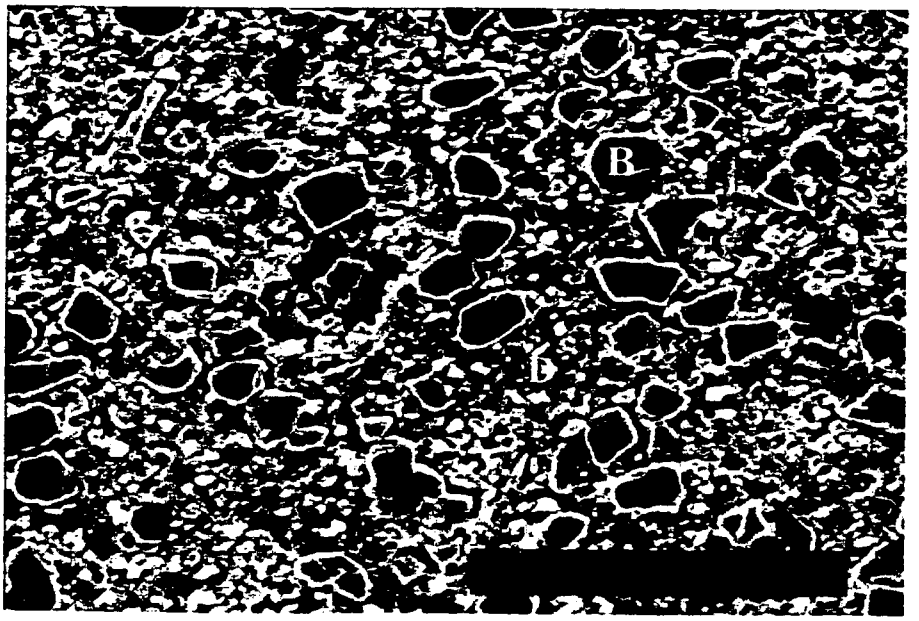

(a) Mag.-x500

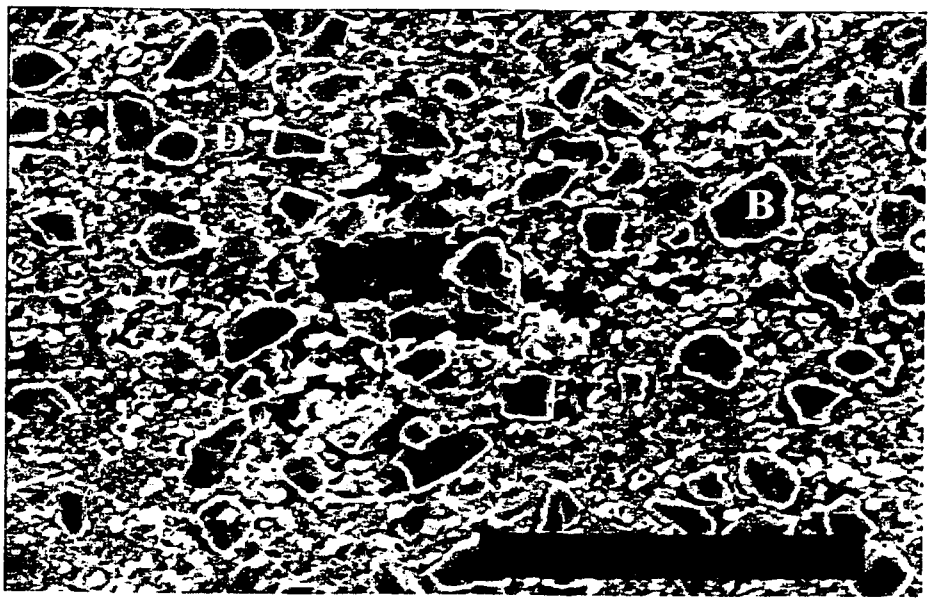

(b) Mag.-x750

Figure 5.41: Micrograph of Weight-Loss for F3K.20S alloy (200hrs)

(a) Mag.-x2000

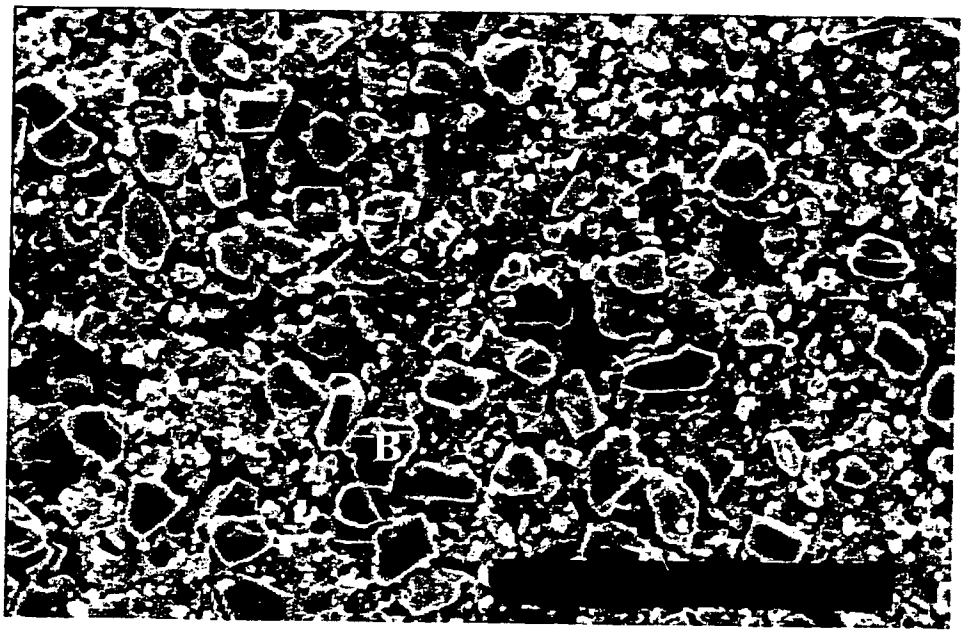

(b) Mag.-x500

Figure 5.42: Micrograph of Weight-Loss Sample for F3K.20S (1000hrs)

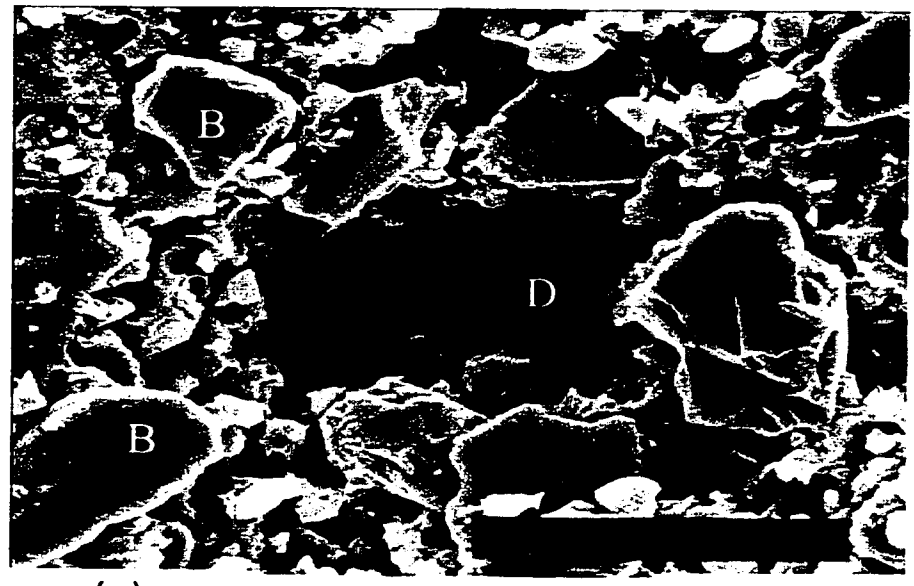

Figure 5.43: Micrograph of Weight-Loss for F3K.20S (1600hrs)

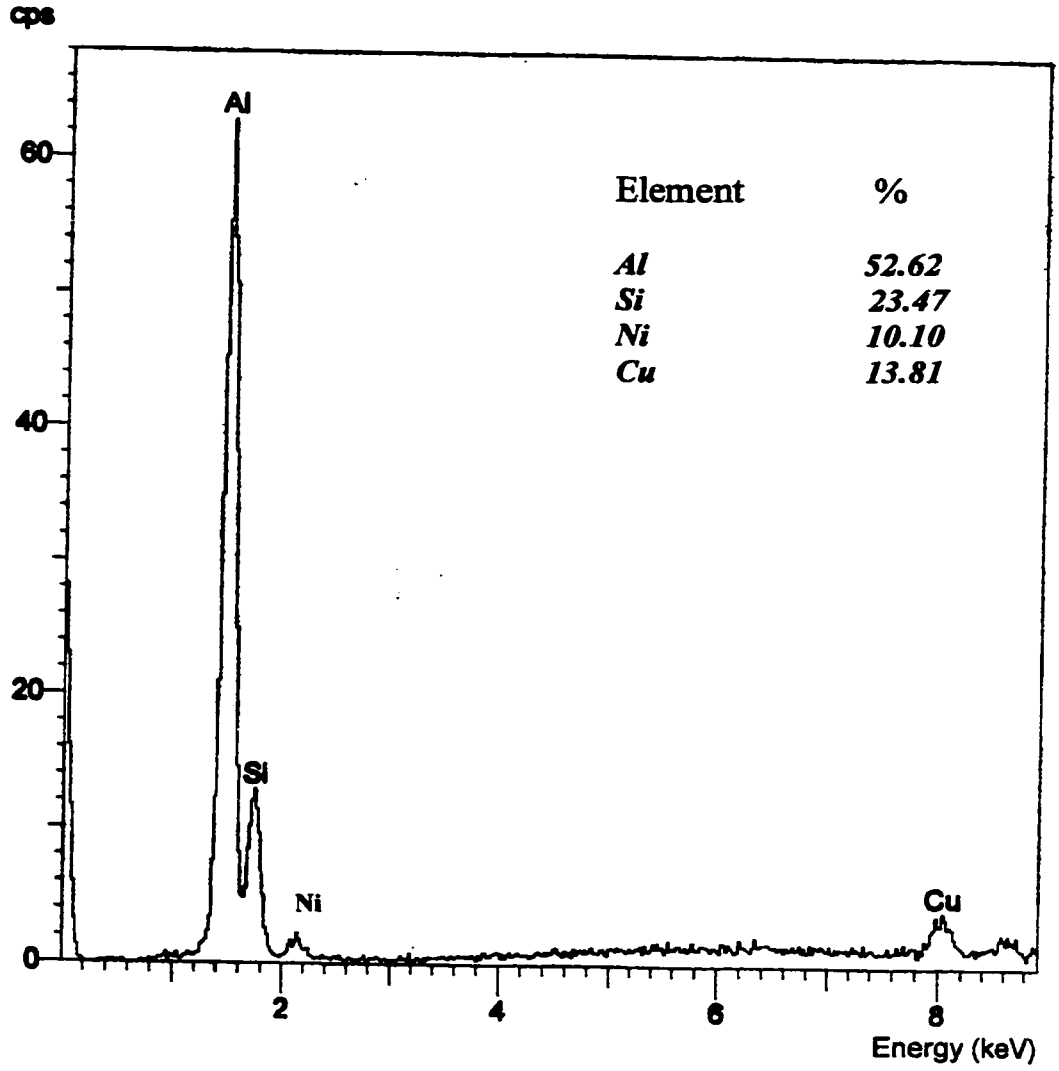

Figure 5.44: EDS analysis of F3K.20S showing elemental constituents in pit's surrounding

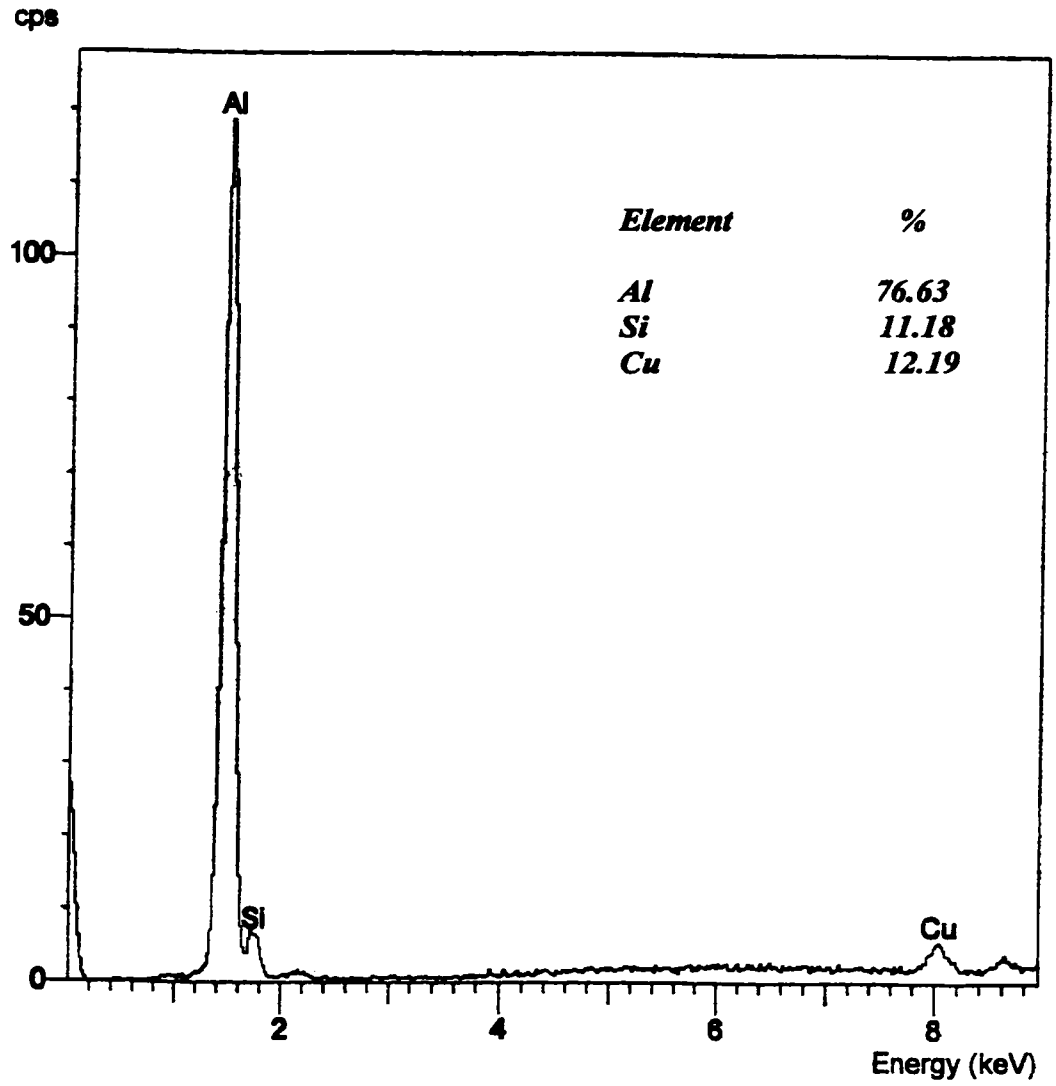

Figure 5.45: EDS analysis of F3K.00S showing elemental constituents in pit's surrounding

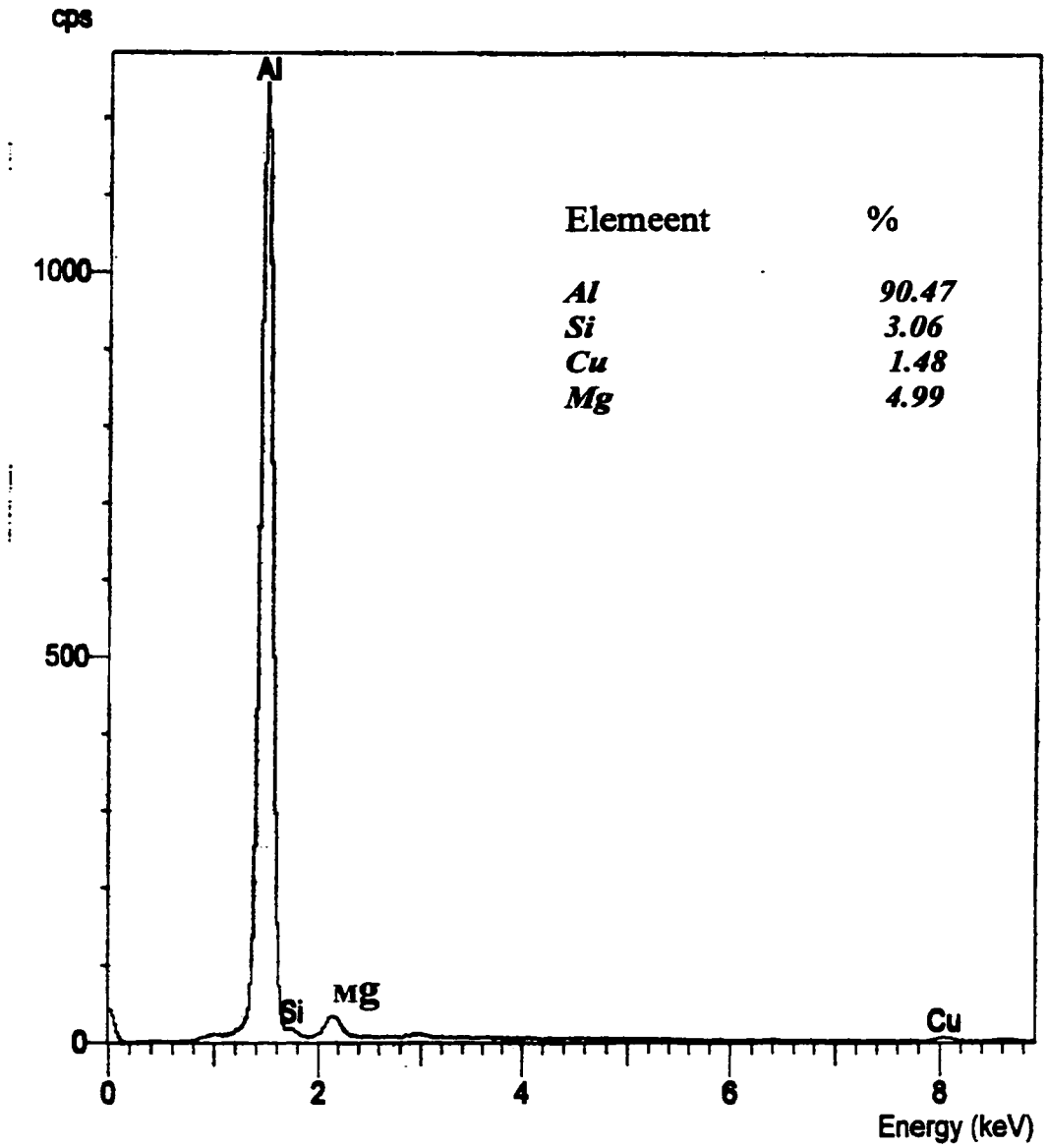

Figure 5.46: EDS analysis of F3S.00S showing elementa constituents in pit's surrounding

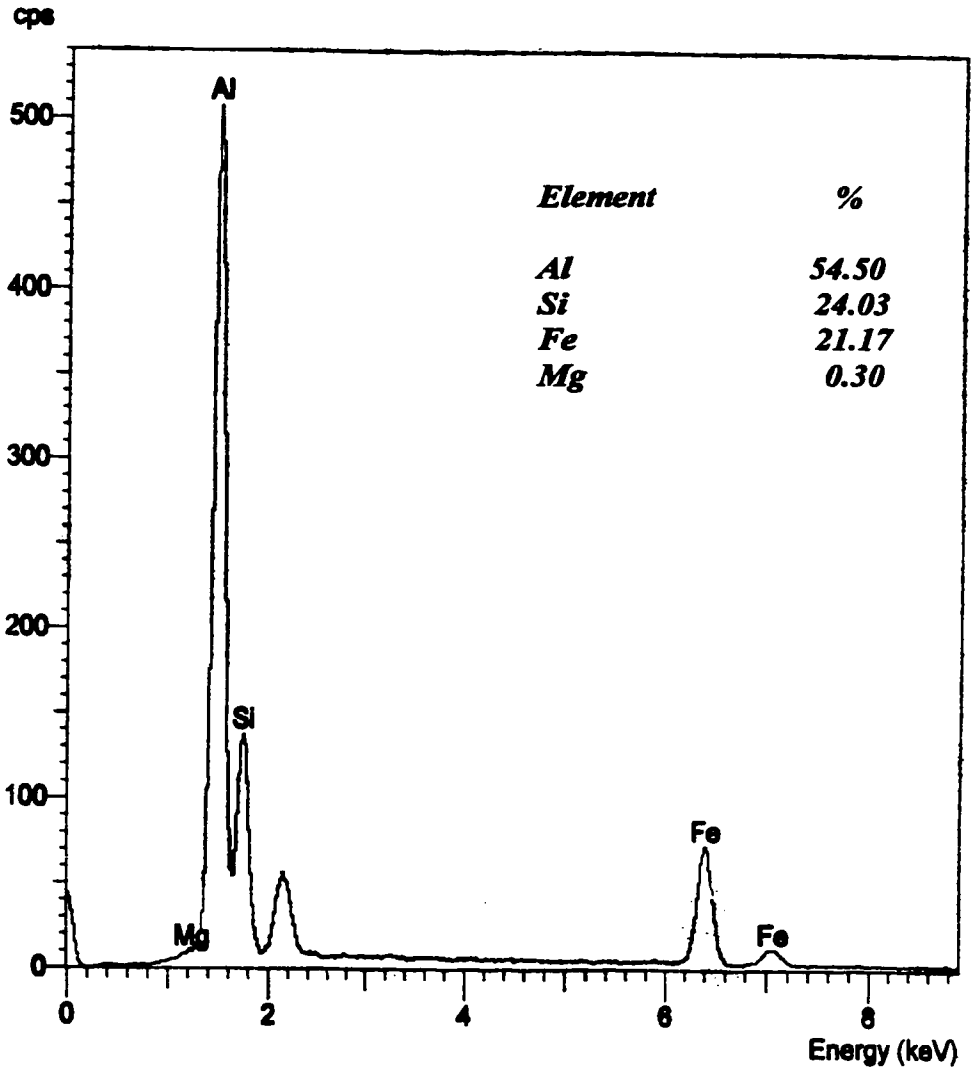

Figure 5.47: EDS analysis of F3S.20S showing elemental constituents in pit's surrounding

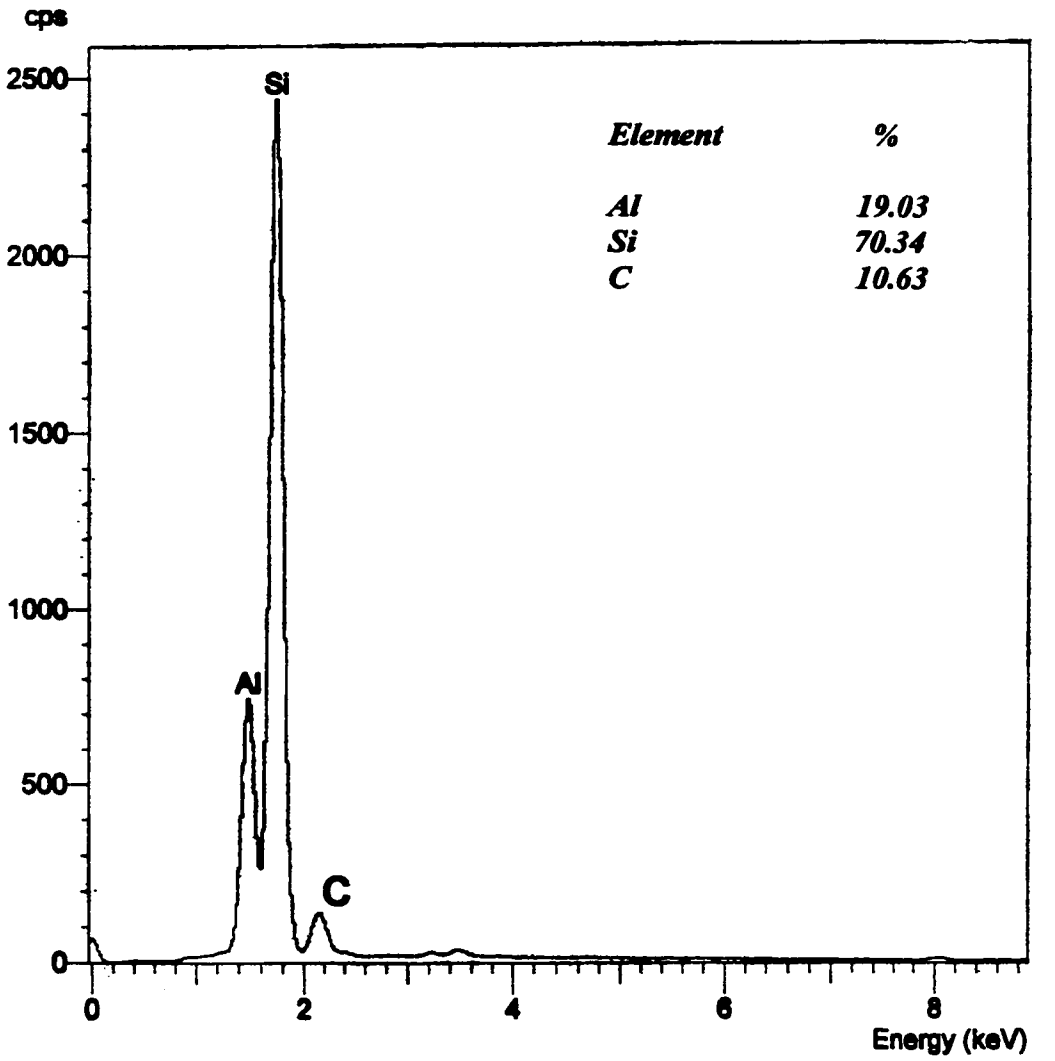

Figure 5.48: EDS analysis of reinforced particles

CHAPTER 6

CONCLUSION AND RECOMMENDATIONS

6.1 Conclusion

Based on the studies made and experiments carried out to investigate the effect of intermetallic phases on the corrosion of aluminum silicon carbide (Al-SiC_p) composites, the following conclusions can be drawn.

- By comparing the corrosion rate of F3S.20S and F3S.00S alloys, it was observed that F3S.20S shows less corrosion rate than F3S.00S in potentiodynamic test and also attains its peak (2.0797mpy) after about 800hrs in weight loss experiment. On the other hand, F3S.00S has a maximum value of 1.4639mpy after about 1200hrs. This result simply shows that, with time, F3S.00S has higher corrosion resistance as compared to F3S.20S.
- Similar trend of result was obtained by comparing the corrosion behavior of F3K.00S and F3K.20S alloys. F3K.00S alloy has higher corrosion resistance as compared to its reinforced counterpart, F3K.20S. Based on these two related observations mentioned above, we can conclude that aluminum alloys reinforced with SiC are more susceptible to corrosion attack in sodium chloride environment than those that are not reinforced.
- From cyclic polarization results, it was found that F3S.00S has the greatest value of difference between E_{corr}, corrosion potential and E_p, pitting potential. This is followed in sequential by values obtained from F3K.00S, F3K.20S, and F3S.20S alloys. This result provides the same conclusion as highlighted above.

- Results obtained from weight loss analysis indicate that as the exposure time increases, the number of pits formed on the surface of corroded samples increases and become shallower in all the alloys used. More pits are observed in F3S.20S and F3K.20S alloys. This shows that these alloys are likely to fail earlier, catastrophically, than F3S.00S and F3K.00S.
- Pits formed, in reinforced alloys appear deeper when examining under microscope. This is believed, with time, will lead to catastrophic failure or serve as an initiation point where other types of mechanical failure can propagate.
- Possible intermetallic phases, Cu_4NiAl_7, $CuAl_2$, and $Cu_2Mg_8Si_6Al_5$, $CuMg_4Al_6$, Mg_2Si, Al_8Fe_2Si observed in F3K.XXX and F3S.XXX alloys respectively appear to represent the weaken regions in the alloys where localized corrosion takes place. This result further shows that these intermetallic phases may directly influence the corrosion behavior of the aluminum alloys used. They are found both in reinforced and unreinforced alloys though more possible phases are observed in the reinforced alloys.
- In addition to the findings just mentioned, secondary phases are clearly observed to have formed in these alloys when compared with the previously investigated 6013 and 6092 alloys [82].
- Silicon-dominating particles were observed to form at the mouth of the pits especially those alloys that are reinforced with SiC particles. This might have contributed significantly to the weakening of pit regions.

RECOMMENDATIONS

In the light of the experiment carried out, the following recommendations are made for future work in this area of research:

- Effect of intermetallic phases on corrosion of aluminum silicon carbide composites were carried out at room temperature, further studies at high temperature are recommended to investigate this behavior.

- Further modification of alloying constituents of these alloys to improve their corrosion resistance is also recommended for future work.

- Where there is relative movement of corrosion environment along the surface of the alloy, it is important to know the corrosion behavior of the alloys in that environment. Thus, effect of velocity on the intermetallic phases is recommended for future studies.

- New processing route for production of these alloys need further exploration in order to achieve better microstructures.

REFERENCES

1. Aylor. D, *Metals Handbook*, 9th edition, Vol. 13, pp. 859-863, A.S.M., Metal Park, Ohio **1984.**

2. Nair S.V, Tien J. K and Bates R. C, *International Metals Review*, 30(6), p. 275, **1981.**

3. Lloyd D. J, *International Metals Review*, 39(1), p. 1,**1994.**

4. Arone R, Botstein O and Shpiglei B,*Isreal Journal of Tech.*, 24, p. 3993, **1988.**

5. Pacej R. C and Agarwala V. S, *Corrosion*, 42, p. 718,**1986**

6. Aylor D. M and Kain R. M, *" Recent advances in composites in the United States and Japan"*, ASTM Spp. Tech. Pub. 8C4, Ed. J. Vinson and M. Taya, ASTM, Philadelphia, PA, p. 632, **1983**

7. Aylor D. M, *DTNSRDC Report No. SME 86-71*(Bathesda, MD., David Taylor Naval Ship Research and Development Center), **1986.**

8. Porter R. C and Wolff E. G, *" Advances in structural composites"*, Paper No. AC14, presented to Society of Aerospace Materials Process Engineering, 12th National Symposium, Exhibit, Western Period, North Hollywood, CA., **1967**

9. Dull D. L, Harring W. C, Jr., and Amateau M. F, in*Proceedings of the 1974 Tri-service Corrosion of Military Equipment Conference*, Ed. F. H. Meyer, 1, (Daytona, OH., Air Force Mat. Lab Report. AMFL, TR-7542, p. 399, **1975.**

10. McCafferty E, Hubler G. K and Natishan PP. M,*Mat. Sc. Eng.*, 87, p.1, **1987.**

11. Natishan PP. M, Mccafferty E, and Hubler G. K, *Journal of Electrochemical Society*, 133, p. 1061, **1986.**

12. Al-Saffar A. H, Ashworth V, Grant W. A, et al.*6th European Cong. Corrosion Sc.*, London, p. 3, **1977.**

13. Latanisson R. M, Saito A, Sandenbergh R, et al.*" Critical Issue in Reducing the Corrosion of Steels, "* Eds. H. Leidheiser, Jr., and S. Haruyama, NACE, p. 182, **1986.**

14. Al-Saffar A. H, Ashworth V, Balimov A. K. O, et al.*Corrosion Sc.*, 20, p. 127, **1980.**

15. Sedriks A. J, Green J. A. S and Novak D. L, *Metals Trans.*, 2, p. 871,**1971.**

16. Bhat M. S. H and Surappa M. K,*Corrosion J. Mat. Sc.*, 26, p. 4991, **1991.**

17. Trzaskoma PP. P, Corrosion, 45(5), p. 402, **1990.**

18. McCafferty E, Trzaskoma PP. P and Natishan P,*Proc. Adv. in Localized Corrosion*, Eds. H. Isacs, and V. Bertocci, p. 181, **1990**

19. Sun H, Koo E. Y and Wheat H. G, *Corrosion*, 47(10), p. 741,**1991.**

20. Paciej R. C and Agarwala V. S, Report No. NDC-86071-80, *Naval Air Development Center*, Westminister, Penn., Oct. **1985**

21. Trzaskoma PP. P, Abstract No. 257, *The Electrochemical Soc. Extended Abstracts*, 86(2), San Diego, CA Meeting, 19-24 Oct. **1986.**

22. Trzaskoma PP. P, *Proc. 10th Congress on Metallic Corrosion*, Madras, India, 5, p. 231, **1987.**

23. Trzaskoma PP. P, McCafferty E and Crane C. R,*J. Electrochemical Soc.*, 130, p. 1804, **1983.**

24. Burleigh T. D, *" Aluminium Alloys, their Physical and Mechanical Properties"*, ICAA-3, 2, p. 435, **1992.**

25. McIntyre J. F, Golledge S and Conrad R,*Naval Surface Warfare Center*, NSWC TR 87-36, **1987.**

26. Trzaskoma PP. P, *" Localized corrosion of metal matrix composites"*, in Environmental Effects in Advanced Materials, by Russell H. Jones and Richard E. Ricker, The Minerals, Metals and Materials Society, p. 249, **1981**

27. Lee A. Jonathan and Mykkanen Donald L, *Metal and Polymer Matrix Composites*, Noyes Data Corporation, Park Ridge, New Jersey, U. S. A, **1987.**

28. Kempster M. H. A, *Materials for Engineers*, Houlder and Stoughton, **1975.**

29. Bertolini L, Brunelia M. F, Candiani S, Corrosion Behavior of a Particulate Metal-Matrix Composite, *Corrosion*, Vol. 55, No 4, pp. 422-431, April **1999**.

30. Styles C. M, Sinclair I, Foster K, and Gregson PP. J, Workhardening effects in SiC particle reinforced aluminium alloys, *Materials Science and Technology*, Vol. 14, pp. 1053-1056, September-October **1998**.

31. Millier C and Surey M, Fabrication and properties of metal matrix composites based on SiC fibre reinforced aluminium alloys, *Materials Science and Technology*, Vol. 4, , pp. 41-51, January **1988**.

32. Divecha A. P, Fishman S. G, and Karmakar S. D, *Journal of Metals*, Vol. 9, pp. 12-17, **1981**.

33. Martineau P, Pailler R, Lahaye M, and Naslain R, *Journal of Materials Science*, Vol. 19, pp. 2749-2770, **1984**.

34. Chou T, Oki T, *Materials Science and Technology*, Vol. 3, pp. 378-385, **1987.**

35. Geiger A. L and Jackson M,*Advanced Materials and Processes*, Vol. 7, pp.

23-28, **1989.**

36. Schuster D. M, Skibo M, and Yep F,*Journal of Metals*, pp. 60-61, **1987.**

37. Surappa M. K and Rohatgi PP. K,*Metals Technology*, Vol. 4, pp.41-43, **1981.**

38. Vasudevan M. and Surappa M. K, Fabrication and properties of Aluminium Matrix composites Reinforced with SiC particles, *Advances in Composite Materials*, pp. 265-280, **1990.**

39. Buhrmaster C. L, Clark D. E and Smartt H. B, Spray Casting Aluminium and Al/SiC Composites, *Journal of Metals*, pp. 44-45, November **1988.**

40. Bronsveld PP. M, Bruinsma P, and De Hossson J. Th, Microstructural analysis of hot isostatically pressed Al-SiC, *Materials Science and Engineering*, pp. 77-81, **1991.**

41. Tweed J. H, Manufacturing of 2014 aluminium reinforced with SiC particulate by vacum hot pressing, *Materials Science and Engineering*, , pp. 73-76, **1991.**

42. Xia X, Sakaris P, and Mcqueen H. J,*Materials Science and Technology*, Vol. 10, pp. 487-496, **1994.**

43. Ko B. C, Park K, and Yoo Y. C,*Materials Science and Technology*, , Vol. 14, pp. 765-769, August **1998.**

44. Rack H. J, Fabrication of High Performance Powder-Metallurgy Aluminium Matrix Composites, *Advanced Materials & Manufacturing Processes*, Vol. 3, pp. 327-358, **1988.**

45. Hollingsworth E. H, Hunsicker H, *Metals Handbook*, Vol. 13, ASM International, p. 583, **1987.**

46. Buchheit R. G, *Journal of Electrochemical Soc.*, Vol. 142, p. 142, **1995.**

47. Szklarska-Smialowska Z, Pitting Corrosion of Aluminium, *Corrosion Science*, Vol. 41, pp. 1743-1767, **1999.**

48. Nisacioglu K,*Journal of Electrochemical Soc.*, Vol. 137, pp. 69, **1990.**

49. Golubev A. J, Ronzhin M. N, *Corrosion of Metals and Alloys*, Olbourne Press, London, p. **48, 1966**

50. Mazurkiewicz B, Piotrowski A, *Corrosion Science*, Vol. 23, p. 697,**1983.**

51. Mazurkiewicz B, *Corrosion Science*, Vol. 23, p. 687,**1983.**

52. Buchheit R. G, Grant R. P, Hlava PP. F, McKenzie B, Zender G. L, *Journal of Electrochemical Soc.*, Vol. 144, p. 2621, **1997.**

53. Buchheit R. G, Moran J. P, Stoner G. E, *Corrosion*, Vol. 46, p. 610,**1990.**

54. Zamin M, *Corrosion*, , Vol. 37, p. 627, **1981.**

55. Blanc C, Mankowski, *Corrosion Science*, Vol. 39, p. 949, **1997.**

56. Mondolfo F, *Aluminium Alloys: Structure and Properties*, London, Butterworth, , pp. 534-774, **1976.**

57. Gustafsson G., Thourvaldsson T, and Dunlop G. L, *Metallurgy Trans*, Vol. 17A, pp. 42-52, **1986.**

58. Tang S. K and Sritharan T, *Materials Science and Technology*, Vol. 14, pp. 738-742, August **1998.**

59. Turnbull A, *British Corrosion Journal*, Vol. 27, p. 27, **1992.**

60. Trzaskoma P. P, McCafferty E, and Crowe C. R, *Journal of*

Electrochemical Soc., Vol. 139, p. 1804, **1983**.

61. Trzaskoma P. P, *Corrosion*, Vol. 46, p. 402, **1990.**

62. Trowsdale A. J, Noble B, Harris S. J, Gibbins I. S. R, Thompson G. E, and Wood G. C, *Corrosion Science*, Vol. 38, No. 2, pp. 177-191, **1996.**

63. Guillaumin Valerie and Mankowski Georges, *Corrosion Science*, Vol. 41, pp. 421-438, **1999.**

64. Blanc C, and Mankowski Georges, *Corrosion Science*, Vol. 39, No. 5, pp. 949-959, **1997.**

65. Blanc Ch, Roques Y,and Mankowski Georges, *Corrosion Science*, Vol. 40, No.6, pp. 1019-1035, **1998**.

66. Grigoris E. Kiourtsidis, Stefanos M. Skolianos, Pavlidou Eleni G, *Corrosion Science*, Vol. 41, pp. 1185-1203, **1999**.

67. Guillaumin Valerie and Mankowski Georges, *Corrosion Science*, Vol. 42, pp. 105-125, **2000**.

68. Modi O. P, Saxena M, Prasad B. K, Jha A. K, Das S, and Yegneswaran, *Corrosion Science*, Vol. 54, No. 2, pp. 129-134, **1998**.

69. Liao, C. M, Olive J. M, Gao M, Wei R. P, *Corrosion*, Vol. 54, No. 6, pp. 451-458, **1998**.

70. Sato F, Asakawa Y, *Corrosion*, Vol. 55, No. 6, pp. 522-529, May **1999.**

71. Chen C. and Mansfeld, *Corrosion Science*, Vol. 39, No. 6, pp. 1075-1082, **1997**.

72. Trzaskoma P, McCafferty E, and Crowe C. R, *Journal of Electrochemical*

Soc., Vol. 130, p. 1804, **1983**

73. Trzaskoma P, *Corrosion*, Vol. 46, p. 402, **1990.**

74. Aylor D. M, Moran PP. J, *Journal of Electrochemical Soc.*, Vol. 132, p.1277, **1985.**

75. Sun H, Koo E. Y, Wheat H. G, *Corrosion*, , Vol. 47, pp. 741, **1991**

76. Buarzaiga M. M and Thorpe S. J, *Corrosion Science*, , Vol. 50, pp.176-185, March **1994.**

77. Griffiths A. J, and Turnbull A, *Corrosion Science*, , Vol. 36, No. 1, pp. 23-35, **1994.**

78. Garrand W. Neil C, *Corrosion Science*, Vol. 36, No. 5, pp. 837-851, **1994.**

79. Mansfeld F, Lin S, Kim S, and Shih H, *Corrosion*, Vol. 45, pp. 615,**1989.**

80. Al-Kharafi F. M, Badawy W. A,*Corrosion*, Vol. 54, No. 5, pp. 377-385, **1998.**

81. Ahmad Z, and Abdul Aleem B.J, *Journal of Materials Engineering and Performance*, Vol. 2, No. 2, pp. 739-744, **1993.**

82. Ahmad Z, and Abdul Aleem B. J,*Corrosion*, Vol. 52, No. 11, pp. 857-864, **1996.**

83. Ahmad Z et al, *Journal of Materials Science*, Vol. 35, pp. 2573-2579, **2000.**

84. Ahmad Z and Abdul Aleem B. J, *British Corrosion Journal*, , Vol. 33, No. 3, pp.230-236, **1998.**

85. American Society for Testing and Materials (ASTM), Vol.2,**1995.**

APPENDIX A: X-RAY FLUORESCENCE (XRF)

Sample Name: F3S.00S

Print 2000/10/31 19:10:48

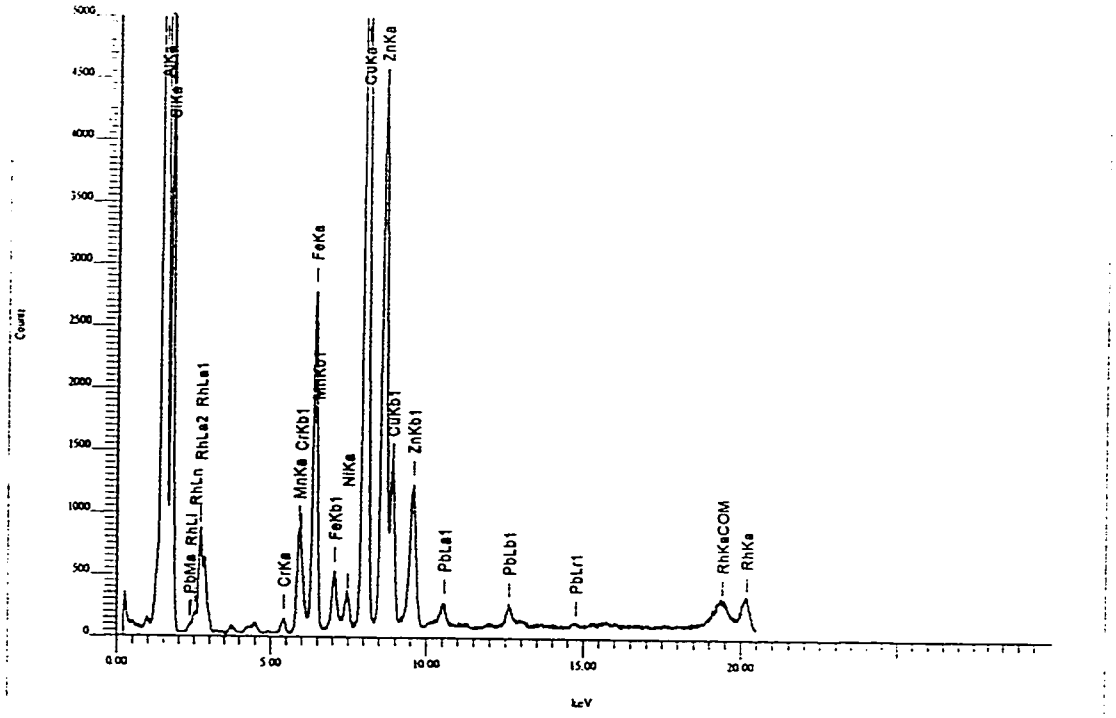

Num	Atom/Chem.Formula	wt(%)	at/mole(%)	K-ratio	Integral Int.	Standard dev.
1	13 Al	80.3111	83.5311	0.4463167	525593	0.0879
2	14 Si	13.8907	13.8797	0.0491685	59910	0.1412
3	24 Cr	0.0716	0.0386	0.0007005	2214	0.0311
4	25 Mn	0.2824	0.1442	0.0031925	10235	0.0278
5	26 Fe	1.1188	0.5622	0.0135403	48128	0.0246
6	28 Ni	0.0749	0.0358	0.0011140	4098	0.0213
7	29 Cu	2.7002	1.1925	0.0422410	158626	0.0211
8	30 Zn	1.3811	0.5929	0.0239842	90394	0.0199
9	82 Pb	0.1693	0.0229	0.0060969	7665	0.0571

Sample Name: F3S.20S

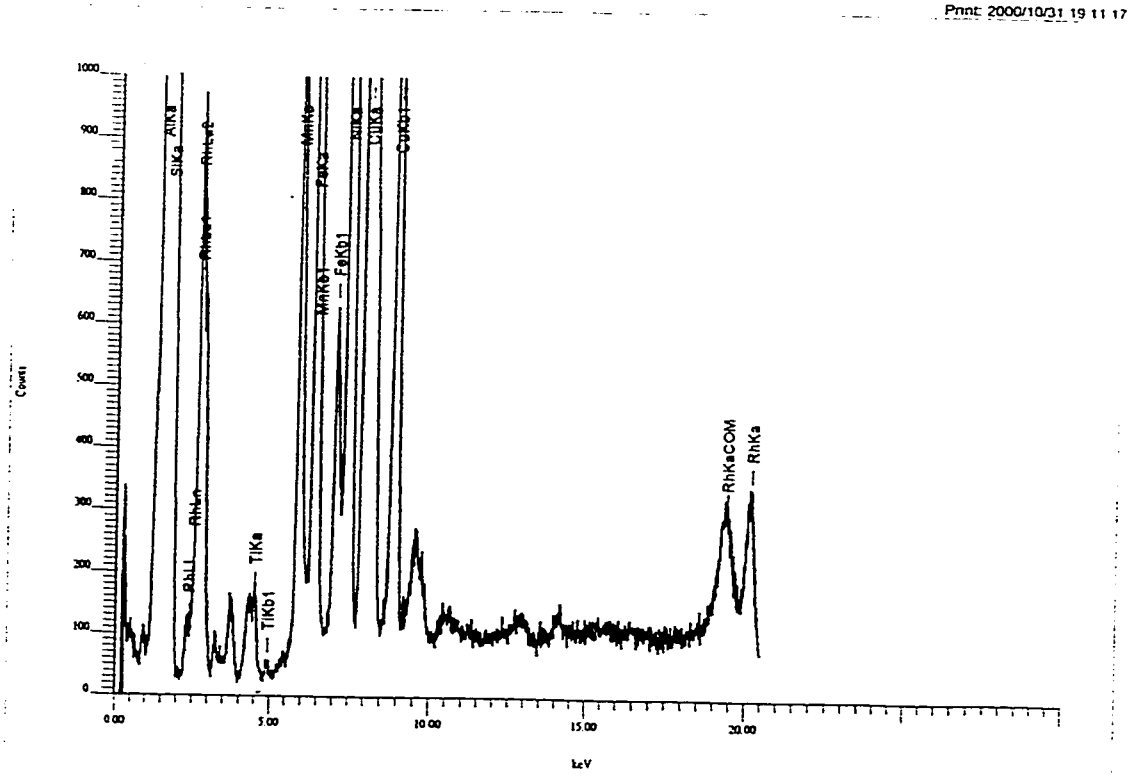

Num	Atom/Chem.Formula	wt(%)	at/mole(%)	K-ratio	Integral Int.	Standard dev.
1	13 Al	55.2235	58.2746	0.3077704	351455	0.0611
2	14 Si	37.9918	38.5150	0.1692767	200007	0.0782
3	22 Ti	0.0636	0.0378	0.0004856	1137	0.0329
4	25 Mn	0.5902	0.3059	0.0064981	20201	0.0198
5	26 Fe	1.0204	0.5202	0.0120388	41494	0.0176
6	28 Ni	1.5353	0.7446	0.0214593	76541	0.0158
7	29 Cu	3.5751	1.6019	0.0534765	194732	0.0154

Sample Name: F3K.20S

Print 2000/10/31 19:14:31

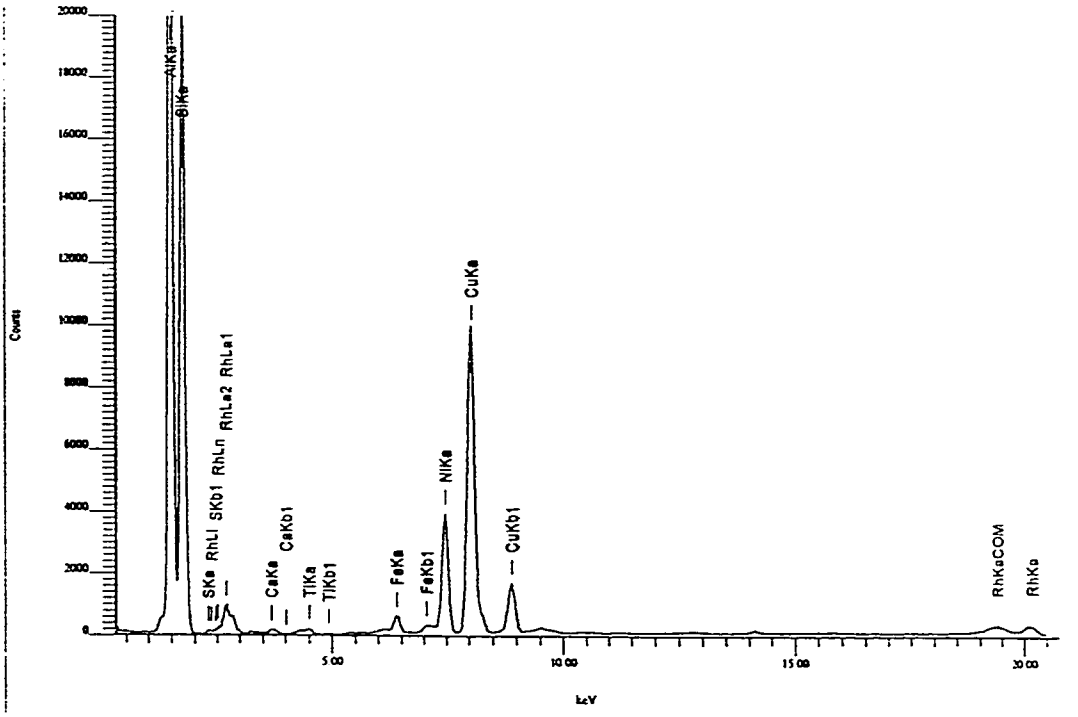

Num	Atom	Chem.Formula	wt(%)	at/mole(%)	K-ratio	Integral Int.	Standard dev.
1	13	Al	54.1264	56.6314	0.3173410	362384	0.0603
2	14	Si	40.7495	40.9594	0.1886919	222946	0.0780
3	16	S	0.0638	0.0562	0.0002507	691	0.0453
4	20	Ca	0.1129	0.0795	0.0009085	1230	0.0510
5	22	Ti	0.0897	0.0528	0.0006874	1609	0.0340
6	26	Fe	0.2291	0.1158	0.0027610	9516	0.0179
7	28	Ni	1.3265	0.6379	0.0198961	70966	0.0153
8	29	Cu	3.3021	1.4670	0.0531134	193410	0.0148

Sample Name: F3K.00S

Print 2000/10/31 19:12:54

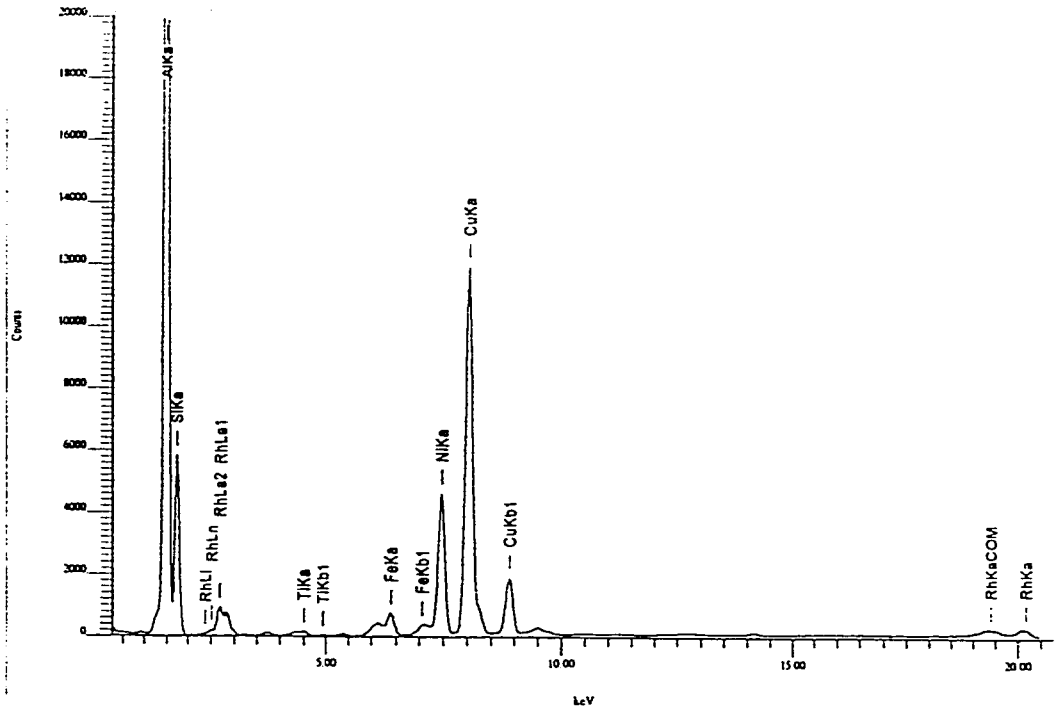

Num	Atom	Chem.Formula	wt(%)	at/mole(%)	K-ratio	Integral Int.	Standard dev.
1	13	Al	78.9053	82.1324	0.4593998	491818	0.0885
2	14	Si	15.1635	15.1633	0.0571247	63277	0.1399
3	22	Ti	0.0679	0.0398	0.0005601	1229	0.0461
4	26	Fe	0.2551	0.1283	0.0033194	10726	0.0241
5	28	Ni	1.5834	0.7575	0.0251562	84120	0.0210
6	29	Cu	4.0248	1.7788	0.0682110	232863	0.0205

APPENDIX B: X-RAY DIFFRATION (XRD) SEARCH-MATCH FOR THE ALLOYS USED

Sample Name: F3K.20S

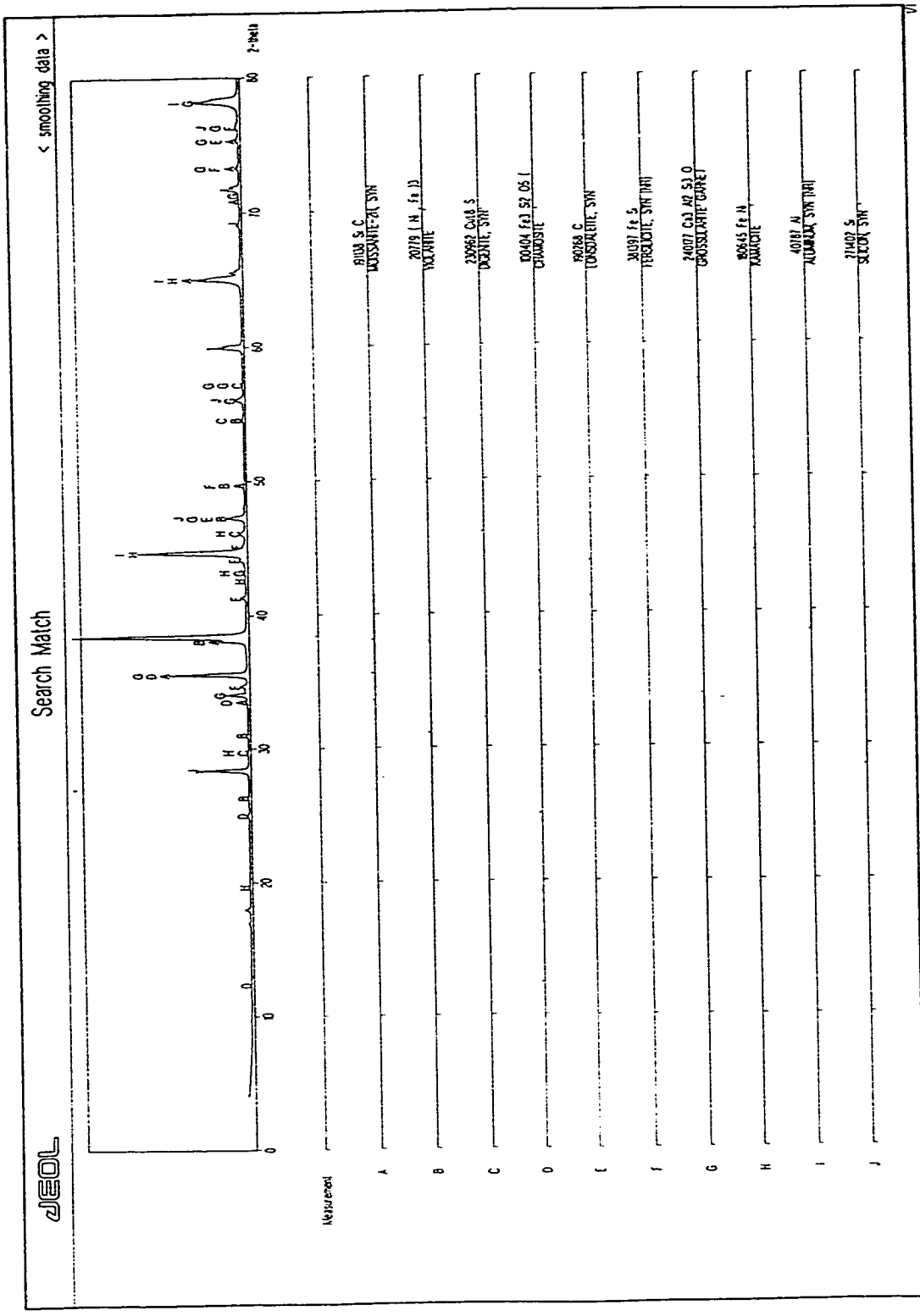

Sample Name: F3K.00S

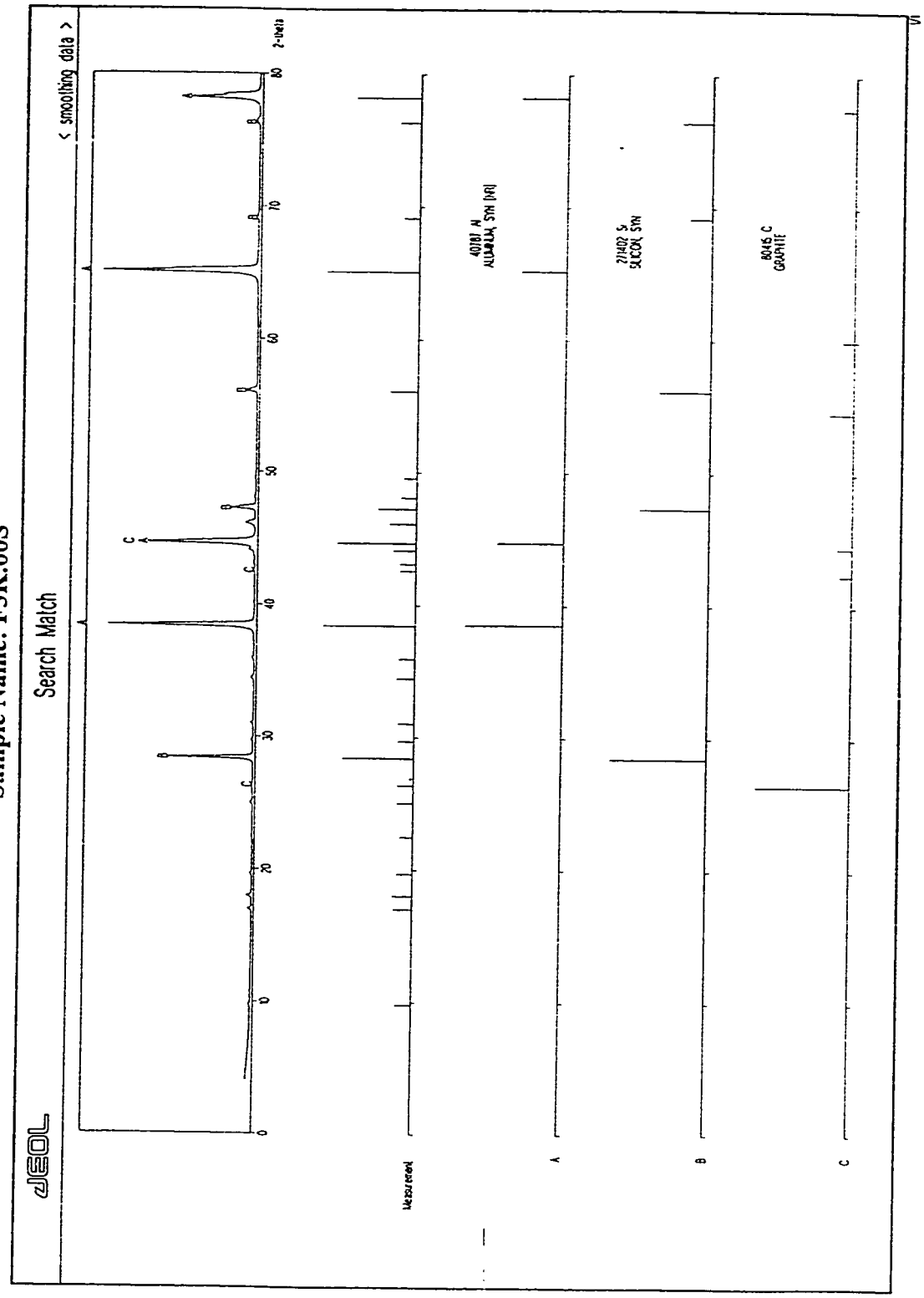

Sample Name: F3S.00S

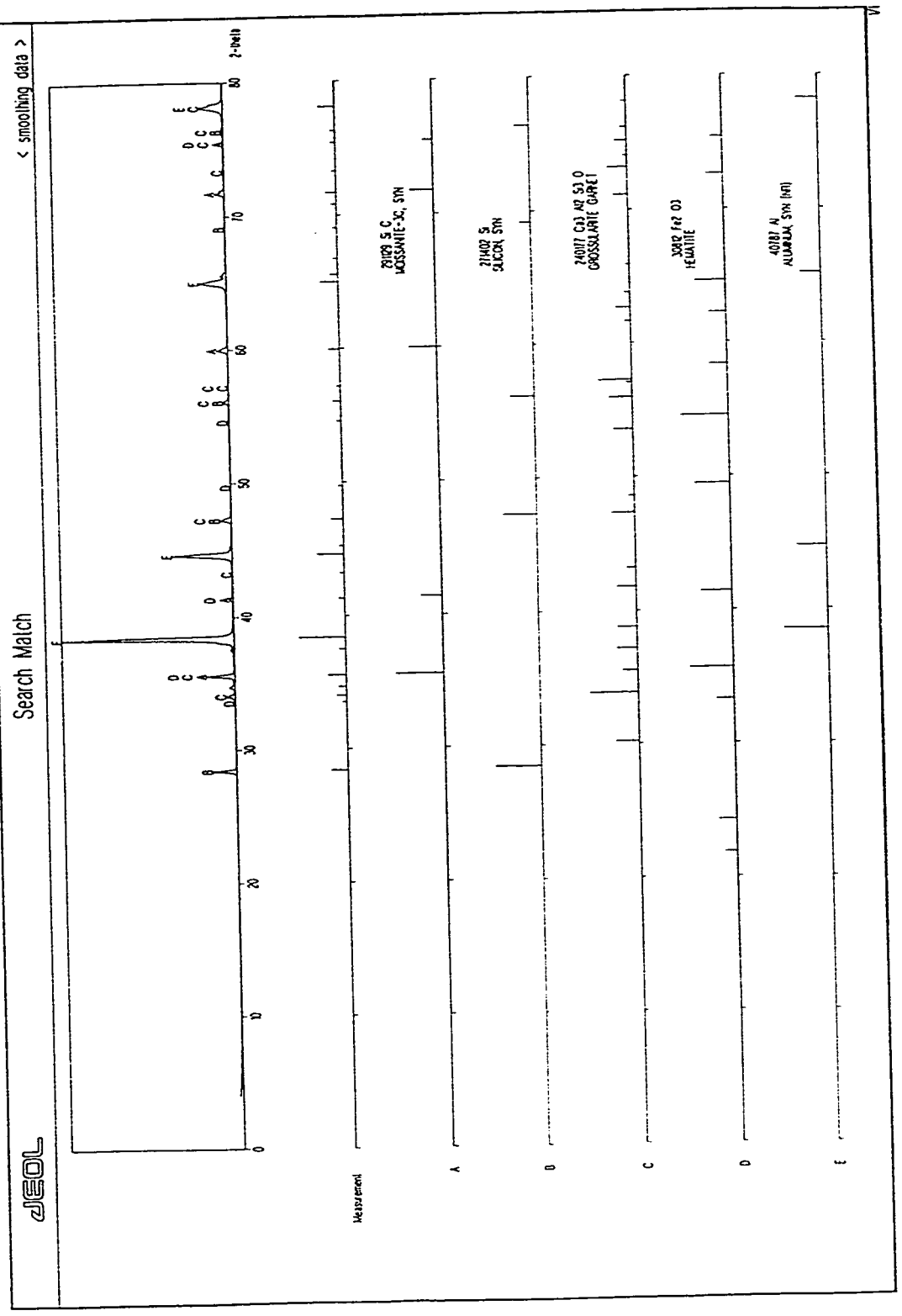

Sample Name: F3S.20S